MODELING AND OFF-LINE CONTROL OF FLUID DISPENSING FOR ELECTRONICS PACKAGING

A Thesis Submitted to the College of

Graduate Studies and Research

in Partial Fulfillment of the Requirements

for the Degree of Doctor of Philosophy

in the Department of Mechanical Engineering

University of Saskatchewan

Saskatoon

By

Daniel Xiongbiao Chen

Spring 2002

© Copyright Daniel Xiongbiao Chen, 2002. All rights reserved.

MODELING AND OFF-LINE CONTROL OF FLUID DISPENSING FOR ELECTRONICS PACKAGING

DANIEL XIONGBIAO CHEN

2002

PERMISSION TO USE

In presenting this thesis in partial fulfilment of the requirements for a Postgraduate degree from the University of Saskatchewan, I agree that the Libraries of this University may make it freely available for inspection. I further agree that permission for copying of this thesis in any manner, in whole or in part, for scholarly purposes may be granted by the professors who supervised my thesis work or, in their absence, by the Head of the Department or the Dean of the College in which my thesis work was done. It is understood that any copying or publication or use of this thesis or parts thereof for financial gain shall not be allowed without my written permission. It is also understood that due recognition shall be given to me and to the University of Saskatchewan in any scholarly use which may be made of any material in my thesis.

Requests for permission to copy or to make other use of material in this thesis in whole or part should be addressed to:

Head of the Department of Mechanical Engineering

University of Saskatchewan

Saskatoon, Saskatchewan, S7N 5A9

ABSTRACT

Fluid dispensing is a method by which fluid materials are delivered to substrates, boards or work-pieces in a controllable manner. This method has been widely used in various packaging processes in the electronics manufacturing industry. In these processes, the flow rate of fluid dispensed and the profile of fluid formed on a board are the two most important performance variables to be controlled consistently.

This research presents a comprehensive study on the modeling and control of the time-pressure dispensing processes. First of all, the characterization of the rheological behaviour of fluids for electronics packaging is addressed from both time-independent and time-dependent perspectives. Under the assumption that the pressure in the dispensing syringe has reached a steady-state status, a model representative of the steady-state flow rate of fluid dispensed is developed. To represent the profile of fluid formed on a board, the spreading of fluid on a board is addressed and a solution to this problem is established.

To consider the influence of time-dependent fluid behaviour in fluid dispensing, a method of applying model updating technique is developed in this study. Based on this method, an off-line control of the dispensing process is developed to improve the consistency in the flow rate of fluid dispensed, which is broken by the time-dependent fluid behaviour.

Taking into account air compressibility and the fluid inertia, a model is developed to represent the dynamics of the flow rate of fluid dispensed, which

shows that the dynamics is sensitive to the air volume in the syringe. Based on the model, the inconsistency in the fluid amount dispensed due to the variation of the air volume in the syringe over a dispensing process is investigated, and an off-line control is developed to alleviate the amount inconsistency.

Experiments on a typical commercial dispensing system are designed and carried out to verify the effectiveness of the models and the off-line control developed in this study. It is shown that the model results have an excellent agreement with the experimental results. Also, with the introduction of the off-line control, the consistency in both the flow rate and the amount of fluid dispensed can be significantly improved.

ACKNOWLEDGEMENTS

I with to express my profound gratitude to my supervisors: Prof. Greg Schoenau and Prof. Chris Zhang. Throughout the completion of the present study, they provided me with the invaluable guidance, criticism, suggestions, and continuous encouragement. Their enthusiasm and expertise were immersed into any little progress in this study. For all of these, I will always be grateful.

Also, I would like to extend my appreciation to the other members of the Advisory Committee: Prof. S. Habibi, Prof. R.T. Burton, and Prof. H. Wood for their examination and advices in the whole process.

Special thanks are due ASM Assembly Automated Ltd., Hong Kong, for providing both the incentive and the working atmosphere in the conduction of the experiments involved in this study. In particular, the support and encouragement from Dr. Peter Liu (Technical Director of ASM) is highly appreciated

Also, it is acknowledged the financial support for the present study from ASM Assembly Automated Ltd. Hong Kong, Department of Mechanical Engineering in the University of Saskatchewan (through the scholarship), and National Science and Engineering Research Council and Atomic Energy Canada Limited (though a cooperative research and development grant).

Finally, I wish to thank my devoted wife Qi Huang for her continuous moral support.

TABLE OF CONTENTS

LIST OF TABLES

LIST OF FIGURES

NOMENCLATURE

a : position of the equilibrium contact line, m.

A : cross-section area, m^2.

A_l : cross-section area of the transmission line, m^2.

C_m : mass flow parameter, dimensionless.

C_d : discharge coefficient, dimensionless.

D_n : internal diameter of the needle, m.

g : gravitational acceleration, m/s^2.

h : interface between the fluid and the ambient air, m.

H : width of the shape of fluid formed on a board, m.

k : sum of the rates of the build-up and break-down structures, s^{-1}.

k_c : rate of the build-up structure, s^{-1}.

k_d : rate of the break-down structure, s^{-1}.

K : consistency index, $Pa \cdot s^n$.

K_c : entrance loss correction factor, dimensionless.

L : length, m.

L_n : length of the needle, m.

m : thixotropic index, dimensionless.

$\dot{m}$: mass flow rate of air, Kg/s.

$\dot{m}_1$: mass flow rate of air into the transmission line, Kg/s.

$\dot{m}_2$: mass flow rate of air into the syringe, Kg/s.

n : flow behaviour index, dimensionless.

p : pressure, Pa.

p_0 : fluid pressure at h=0, Pa.

p_a : air pressure, Pa.

P: manipulated parameter vector.

P_{as} : pressure of the air supply, Pa.

P_d : downstream pressure, Pa.

P_e : pressure at the exit of the needle, Pa.

P_g : pressure at the air-fluid interface, Pa.

P_l : pressure in the transmission line, Pa.

P_s : pressure in the syringe, Pa.

P_u : upstream pressure, Pa.

Q : flow rate of fluid dispensed, m^3/s.

R : radial of the needle, m.

S: sensitivity or sensitivity matrix, dimensionless.

t : time, s.

T : fluid temperature, °C.

T_l : temperature of the transmission line, °C.

T_s : temperature of the syringe, °C.

T_u : upstream air temperature, °C.

T_w : board temperature, °C.

u: fluid flow velocity, m/s.

u_1 : average velocity at the air-fluid interface, m/s.

u_2 : average velocity at the exit of the needle, m/s.

v : speed of the needle movement, m/s.

V : volume of fluid dispensed, m^3.

V_s : air volume in the syringe, m^3.

W : width of the shape of fluid formed on a board, m.

α_1: kinetic energy correction factor at the air-fluid interface, dimensionless.

α_2: kinetic energy correction factor at the exit of the needle, dimensionless.

ΔP: pressure drop in the needle, Pa.

Δt: time period of viscosity-recovery process, s.

$\dot{\gamma}$: shear rate, s^{-1}.

η: fluid viscosity, Pa·s.

η_i: fluid viscosity at the zero shear time, Pa·s.

η_e: fluid viscosity at the equilibrium state, Pa·s.

η_1: fluid viscosity at the beginning of the viscosity-recovery process, Pa·s.

η_2: fluid viscosity at the end of the viscosity-recovery process, Pa·s.

λ: structural parameter, dimensionless.

λ_i: initial value of the structural parameter, dimensionless.

λ_e: equilibrium value of the structural parameter, dimensionless.

λ_1: structural parameter value at the beginning of the viscosity-recovery process, dimensionless.

θ: contact angle, degree.

ρ: fluid density, Kg/m^3.

σ: surface tension, N/m.

τ_0: yield values, N/m^2.

τ: shear stress, N/m^2.

τ_w: shear stress at the needle wall, N/m^2.

1. INTRODUCTION

1.1 Fluid Dispensing in the Electronics Manufacturing Industry

Fluid dispensing is a method by which fluid materials are delivered to substrates, boards or workpieces in a controlled manner. It has been widely used in various processes in the electronics manufacturing industry; such as advanced integrated circuit encapsulation (AICE), surface mount technology (SMT), etc. as well as in other industries.

In AICE, one of the typical processes is die encapsulation. In this process, a die and wires bonding between the die and a substrate need to be enclosed in an encapsulant, which has low ionic, moisture absorbent and thermal-expansion coefficient properties, in order to protect the die and wires from any environmental attacks [Babiarz 1997, Babiarz and Huysmans 1997, Quinones *et al.* 2000]. Usually, the encapsulant is delivered by means of dispensing. Figure 1.1 (a) shows a typical encapsulation configuration, called *Dam and Fill*, in which an encapsulant with high viscosity is first dispensed on the substrate, forming a dam or border surrounding the die and wires, and then another encapsulant with a low viscosity is dispensed to fill the inside of the dam for the protection. In such a configuration, the profile of the dam is critical because it not only determines the encapsulant volume needed for

filling, but also significantly contributes to the aesthetics of the final packaging. Thus, the dispensing process needs to be controlled precisely for achieving the desired profile.

Another typical application of dispensing in AICE is underfill encapsulation, which is shown in Figure 1.1 (b), in which the flip chip provides an area array that interconnects the chip and substrate. To prevent the corrosion of the connections and to relieve the stress resulting from the thermal-expansion coefficient differences between the chip and the substrate, the gap between them must be filled with an encapsulant [Tummala and Rymaszewski 1989, Stokes 1996, Babiarz 1997, Babiarz and Huysmans 1997, Han and Wang 1997, Carbin 1998, Wun and Margaritis 1998, Lewis *et al.* 1998, Quinones *et al.* 2000]. For this purpose, encapsulant is dispensed along at least one side edge of the flip chip, and then, under capillary action or surface tension), the encapsulant flows and evenly fills the gap between the chip and the substrate. In this process, the dispensing amount of encapsulant (the desired amount depends upon the geometry of the flip chip) is of importance and also needs to be controlled.

In SMT, as shown in Figure 1.1 (c), a small quantity of surface mount adhesive (SMA) is required to secure surface components to a board prior to wave soldering [Prasad 1989, Chandraker 1990, Cavallaro 1991, West *et al.* 1993 and 1995, Norris 1996, Gilleo 1996, Dixon *et al.* 1997, Murch *et al.* 1997, Byers and Reighard 1998, Ness and Lewis 1997 and 1998, Bush 1997 8]. By means of dispensing, the required amount of SMA needs to be delivered between the two conductive pads with a typical distance of 0.5 mm ~ 1.2 mm [Ness and Lewis 1997]. The dispensing

process in this application is generally required to run continuously for a high throughput, while achieving a high degree of repeatability in the amount dispensed.

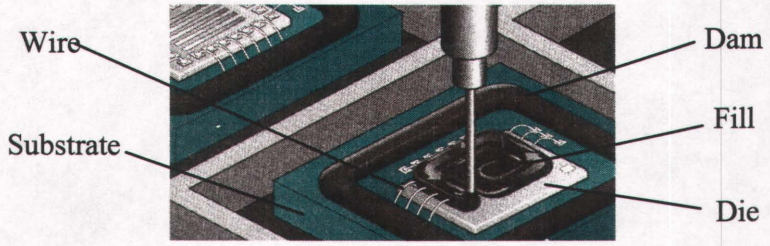

(a)

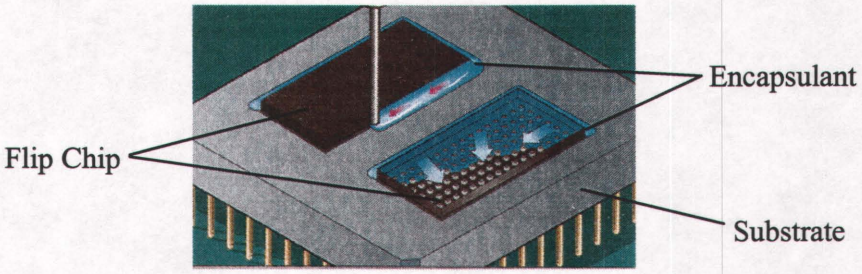

(b)

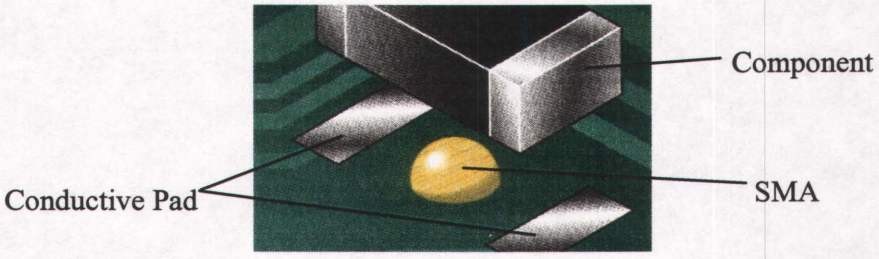

(c)

Figure 1.1 Applications of dispensing in the electronics industry;

(a) die encapsulation, (b) underfill encapsulation, and (c) surface mount technology.

In addition, the need to have structurally bonded joints in the automotive and aerospace industries has considerably extended the applications of fluid dispensing. To achieve such joints, a continuous bead of fluid (such as adhesive, sealant) must be dispensed consistently along a path on a workpiece [Razban 1993, Razban and Davies 1995, Davies *et al.* 1996].

In all these applications, besides the accuracy of location where the fluid is delivered, the other important measurements are the amount dispensed (i.e., an integration of flow rate over the dispensing time period) or directly the flow rate, and the profile of fluid formed on boards. As a general requirement, they must be achieved with an accepted precision, which depends on the application.

1.2 Fluid Dispensing Approaches

There are currently a variety of dispensing approaches employed in industry [Murch *et al.* 1997, Babiarz and Huysmans 1997, Ness 1997, Krieger and Behler 1998, Chen *et al.* 1999]. Depending on the ways of driving fluid out of the needle, the dispensing approaches can be classified into four categories; time-pressure, shut-off valve, rotary screw, and positive displacement. They are shown schematically in Figure 1.2, respectively.

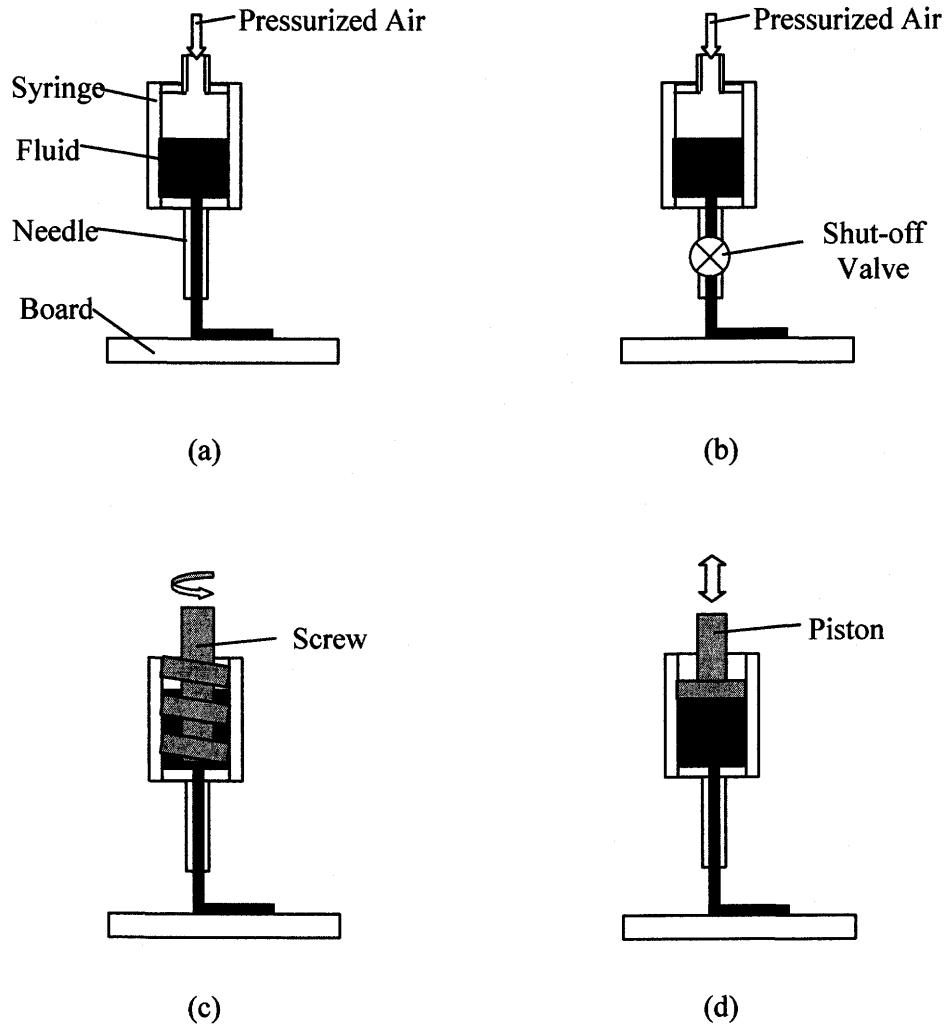

Figure 1.2 Schematic diagrams of fluid dispensing approaches;
(a) time-pressure, (b) shut-off valve, (c) rotary screw, and (d) positive displacement.

- Time-pressure

Time-pressure dispensing utilizes pressurized air to drive fluid out of the needle. The amount of fluid dispensed is controlled by regulating the magnitude and duration of pressurized air. The advantages of this approach mainly include a flexible adaptation to application situations, simple operation, ease of maintenance,

and the ability to dispense very small volumes. The main disadvantage is that the amount of fluid dispensed is significantly affected by fluid viscosity and the air volume in the syringe [Dixon *at al.* 1997, Chen *et al.* 2001 and 2002].

- Shut-off valve

Dispensing very low viscosity fluid may be very difficult using the time-pressure approach because of the open end of the needle. One way to eliminate unexpected dripping of fluid from the needle end is to use a shut-off valve at the end of the needle. This valve is opened only during the dispensing process, and the amount of fluid dispensed can be regulated by controlling the valve opening and closing. However, the filler particles in the fluid may clog the valve and maintaining a clean valve is very difficult. Also the relatively short lifetime of such a rapidly moving valve may also be a problem [Krieger and Behler 1998].

- Rotary screw

Rotary screw dispensing utilizes the rotation of a motor-driven screw to move fluid down a syringe and then out of a needle. This approach is a major improvement in control over the time-pressure approach. In this dispensing approach, a large pressure can be developed in the fluid at the syringe bottom, which forces fluid to flow upwards past the screw. As a result, the amount of fluid dispensed is still affected by fluid viscosity [Babiarz 1997, Ness and Lewis 1997, Li and Hsieh 1996], though less sensitive than time-pressure dispensing.

- Positive displacement

In positive displacement dispensing, the linear movement of a piston is employed to force fluid out of the needle. The distinct advantage is that the volume of fluid dispensed is dependent only on the mechanical movement of the piston. This is true for dispensing a large amount of fluid with a continuous movement of the piston. However, for dispensing a small amount, the advantage is lost because of the effects of fluid compressibility as well as the inertia of both the piston and the mechanism used to drive the piston.

Although all of the dispensing approaches discussed above can theoretically dispense all fluids, each excels when used with a certain fluid and/or in specific applications [Bush 1997]. As a matter of fact, the time-pressure approach is the most widely used among all dispensing approaches due to the distinct advantages aforementioned as well as comparatively low-cost. It is estimated that about 70% of all dispensers on the market today use the time-pressure approach [Dixon *at al.* 1997]. Unfortunately, the fluid dispensing process using the time-pressure approach (or the time-pressure dispensing process for short) is the most difficult to control because of the sensitivity of the amount of fluid dispensed to such factors as fluid viscosity, the air volume in the syringe, etc. The study presented in this thesis will concentrate on the time-pressure dispensing process, with an emphasis on application to electronics packaging. However this study is also applicable in dealing with the issues encountered in the dispensing process employing the other three dispensing approaches.

1.3 Modelling and Control of Dispensing Processes - A Critical Review

1.3.1 The Time-Pressure Dispensing Process

Figure 1.3 is a schematic diagram of a typical time-pressure dispensing process. An air supply is used to provide pressurized air in combination with a valve to control the duration of the pressurized air. Through a transmission line, pressurized air is applied to a syringe. Under this action, fluid in the syringe is forced through and out of the needle. Once the fluid is extruded from the needle, it drops onto a board, and then flows or spreads on the board until an equilibrium profile is formed. For such a process, the flow rate or amount of fluid dispensed and the profile of fluid formed on the board are two important measurements of the process performance.

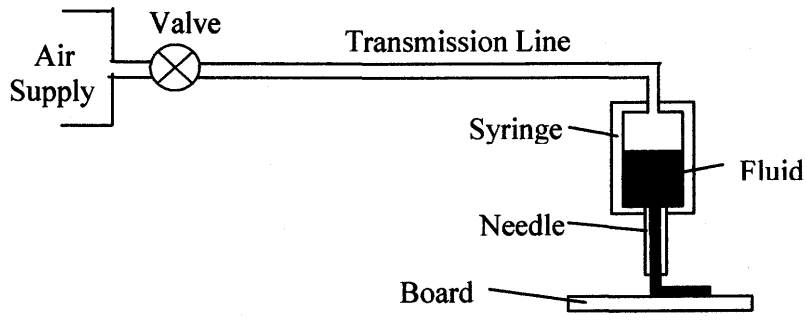

Figure 1.3 Schematic of a typical time-pressure dispensing process.

From Figure 1.3, it is seen that the time-pressure dispensing process is very complex by involving air flow and fluid flow in cylindrical tubes (e.g. transmission line, syringe, and needle) as well as the spreading of fluid on a board. As a result, air

compressibility and fluid behaviour can significantly contribute to the flow rate or the amount of fluid dispensed, thereby the profile of fluid formed on the board.

When dispensing small amounts of fluid (typically 0.002 grams in SMT) using short-time pressure pulses from the air supply, the influence of air compressibility on the flow rate (thus the amount of fluid) is particularly significant. One of the serious problems observed in this process is the inconsistency in the amount dispensed under identical pressure pulses [Dixon *et al.* 1997, West and Williams 1995, Cavallaro *at al.* 1998, Chen *at al.* 2001 and 2002]. This is due to the fact that the air volume in the syringe gradually increases as the process proceeds, causing a corresponding change in the dynamics of flow rate and thus the amount dispensed. As an example, it was observed by Dixon *et al.* [1997] that the amount of the fluid dispensed could be reduced by 30% with increasing in air volume in the syringe from nil to full. When continuously dispensing fluid (e.g. AICE) with a constant pressure from the air supply, the stability of fluid behaviour dominates the process performance. One of the serious problems occurring in this situation is that the flow rate changes with respect to time due to the fact that the fluid exhibits time dependent behaviour [Kolcun *at al.*, 1997, Box 1998, Bretmersky *at al.* 1999, Reighard *at al.* 2001, Baron *at al.* 2000, Bouras *at al.* 1999].

To alleviate these problems, many efforts have been made in industry and some of the techniques resulted have been patented [Kolcun *at al.*, 1997, Box 1998, Cavallaro *at al.* 1998, Bouras *at al.* 1999, Bretmersky *at al.* 1999, Baron *at al.* 2000, Kay 2001, Goodin *at al.* 2001, Reighard *at al.* 2001]. Meanwhile, with the dies, chips, and components becoming smaller and smaller, increasing demand for a more

precise fluid dispensing has greatly raised the need for modeling and control of the dispensing process for improved process performance. In recent years, various methods have been developed for this purpose and evaluated with varying degrees of success; however, much work remains to be done. In the rest of this section, a critical review of these methods and those patented techniques is presented, along with the identified key issues involved in this research area.

1.3.2 Modelling of Fluid Dispensing Processes

To represent the flow rate of fluid dispensed, one of the modeling approaches utilized treats the flow in the needle as a fully developed laminar flow of Newtonian fluid [Babiarz 1997, Krieger and Behler 1998]. So the well-known Poiseuille equation can be used to establish the flow rate, Q, which is given by

$$Q = \frac{\pi D_n^4 \Delta P}{128 \eta L_n} \tag{1.1}$$

where ΔP is the pressure drop in the needle, η is the fluid viscosity, and D_n and L_n are the internal diameter and length of the needle. This model is simplified due to the assumption of Newtonian fluid. Unfortunately, most fluids used in the electronics packaging usually exhibit non-Newtonian or rheological behaviour, so the Newtonian fluid assumption greatly limits the application of the model.

Considering fluids as non-Newtonian, Razban and Davies [1993 and 1995] developed a more complicated model. In their studies, the fluid behaviour is characterized by using the Power Law equation, i.e.,

$$\tau = K\dot{\gamma}^n \tag{1.2}$$

where τ and $\dot{\gamma}$ are the shear stress and shear rate, respectively; K is the consistency index, and n is the flow behaviour index ($n = 1$ for Newtonian fluids). The flow rate is then established under the assumption of laminar flow, which is given by

$$Q = \frac{n\pi D_n^3}{8(3n+1)}\left(\frac{D_n \Delta P}{4L_n K}\right)^{1/n} \tag{1.3}$$

It is noted in the above models that the flow rate represented is steady-state. However, the dynamics of the flow rate is very important in the fluid dispensing process, especially when small amounts of fluid are required to dispense. Unfortunately, little attention has been paid to the dynamics and only a few empirical dynamic models have been reported in the literature. These models have been derived using system identification methods.

One such model was developed by Razban [1993]. Based on an experimental investigation relating the output, which was the size of the profile of fluid formed, to the input, which was the voltage applied to a dispensing valve, it was found that the dynamics could be modeled as a second order system with a pure time delay. The following transfer function was developed:

$$G(S) = \frac{332.13\,K_p}{S^2 + 21.18S + 322.13} e^{-T_l S} \tag{1.4}$$

where K_p is the process gain and T_l is the lumped time delay. Both of them are dependent upon the operational conditions.

Another empirical dynamic model is the auto regressive with external input (ARX) model developed by West *et. al.* [1995]. It is given by

$$\begin{aligned} &y(nT) + a_1 y(nT - T) + \cdots + a_n y(0) = \\ &\quad b_0 u(nT) + b_1 u(nT - T) + \cdots + b_m y(nT - mT) + e(nT) \end{aligned} \tag{1.5}$$

where T is the sampling interval, y is the blob area of the adhesive dispensed that is proportional to the amount dispensed, u is the air pressure, and e is the error term. Auto-regression techniques were employed to determine the coefficients: a_i (i = 1, 2, ... n) and b_j (j = 1, 2, ... m).

These models did facilitate the design of process controllers because of the linear dynamics of the input-output relationship but could not provide information related to the influence on the flow rate of such parameters as the transmission-line length, syringe and needle sizes, etc., which need to be known in the primary stage of designing a dispensing process. Also, any change in these parameters requires a new system identification process and consequently a new empirical model must be generated. Obviously, this strategy is very costly and may be difficult to implement in practice. Moreover, as discussed previously, one serious problem occurring in the

dispensing process is the inconsistency in the amount of fluid dispensed under the same operational conditions. Using these empirical models, it could be an extremely difficult task to gain insight into the problem. Thus, a physical model representative of the flow rate dynamics is obviously desirable and advantageous.

Besides the flow rate of fluid dispensed, the profile of fluid formed on boards is also an important measurement of the dispensing process. It is known that, once extruded from the needle, the fluid drops onto a board and starts to spread on the board until an equilibrium profile is formed. Depending on whether the needle moves horizontally or not, two kinds of profiles are usually formed on the board: a line and a dot, as shown in Figure 1.4. The cross-section sizes are measured by the width and height (denoted by *W* and *H*) for a line, and diameter and height (denoted by *D* and *H*) for a dot. These are important indexes in electronics packaging.

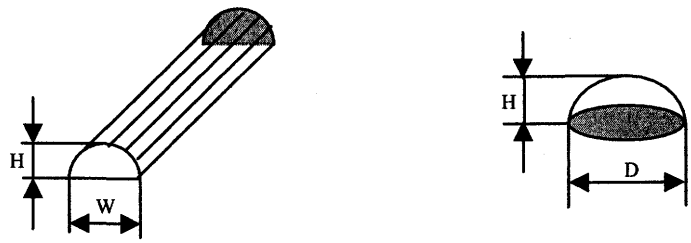

(a) (b)

Figure 1.4 Profiles of fluid formed on a board; (a) a line and (b) a dot.

To determine the cross-section size, it was assumed by Razban and Davies [1995] that the line was cylindrical in shape. The cylinder diameter, D, is then established using the volume conservation as

$$D = \sqrt{\frac{4Q}{\pi v}} \tag{1.6}$$

where Q is the flow rate of fluid dispensed, and v the speed of the needle movement. Obviously, this is an approximation because it does not consider the further spreading of fluid on a board.

When the spreading of fluid on a board is taken into account, the surface tension (i.e., the force exerted on the surface due to intermolecular interactions) must be considered. Tummala and Rymaszewski [1989] gave the height of an equilibrium dot formed on a board, including surface tension effects, as

$$H = \sqrt{\frac{2\sigma(1-\cos\alpha)}{\rho g}} \tag{1.7}$$

where σ is the surface tension, α the angle at the contact line between the fluid and the board, ρ the fluid density, and g the gravitational acceleration.

In general, whether a line or a dot is formed on a board in the dispensing process, both of them are related to the spreading of fluid on a smooth board. This is a fundamental problem in fluid mechanics, in which bulk, surface and line forces are

coupled through a free boundary [Schonhorn *et al.* 1966, Newman 1968, Greenspan 1978, Dussan V 1979, Hocking and Rivers 1982, Ehrhard and Davis 1991, Haley and Miksis 1991]. Obviously, it would be of great advantage to incorporate the knowledge and results from this research area into the development of a model to represent the fluid profile in the fluid dispensing process.

1.3.3 Control of Fluid Dispensing Processes

As discussed previously, it is known that the fluid dispensing for electronics packaging applications has two types: dispensing of dots and dispensing of lines. In the process of dispensing dots, the amount is of importance, which is an integration of flow rate within the dispensing time periods, and the control of this process is considered as a discrete problem. While in the process of dispensing lines, the concern is the flow rate, and the control is considered as a continuous one. It does not matter if it is a discrete or continuous process; the fundamental requirement of the process control is to maintain performance consistency. To fulfill this requirement, some valuable studies have been conducted and reported in the literature which led to the implementation of a number of controllers on the process control as well as approaches for feedback measurements.

For the control of dispensing dots, several studies were conducted by West [West *et al.* 1993 and 1995]. The background of the studies is to dispense dots of adhesive onto boards in SMT with the testbed shown in Figure 1.5. Through a voltage-controlled pressure regulator and solenoid valve, the height and width of the pressure pulse can be controlled, respectively, thus regulating the amount of

adhesive dispensed. Vision feedback on the planar area of the dispensed dot is obtained using a charge-coupled-device (CCD) camera mounted on the dispensing head, and the planar area is adopted as a measure of the dispensed amount. In addition, the testbed also includes a pressure sensor and a temperature sensor for the fault detection. In these studies, the system identification was used to determine a model of the system, which was reviewed in the preceding section. Based on the identified model, an incremental proportional controller was applied to maintain consistency in the dot amounts. In addition, these studies also show that intelligent methods (knowledge-based, fuzzy logic and neural network) could be included in the control system for fault detection (e.g. failure of pressure pulse).

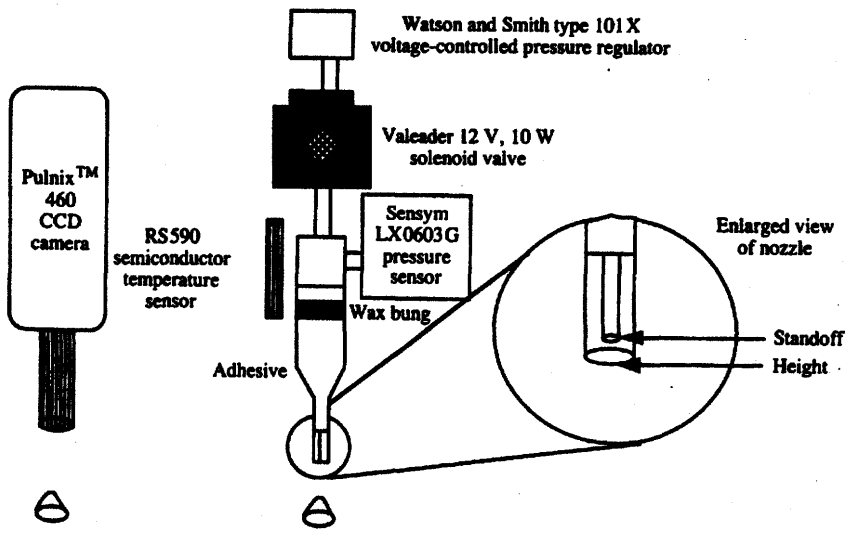

Figure 1.5 Adhesive dispensing system developed by West *et al.* [1993 and 1995].

The main disadvantage of the above control system is having to use camera vision to feedback the dot amount, which complicates the control system and

dramatically increases the cost of control. To overcome this disadvantage, some other devices were developed to directly measure the dot amount or dot size. In the patent [Reighard *at al.* 2001], a scale was used in a feedback control system to weigh the dot amount. As the desired dot amount is typically in the order of 0.002 grams, scales used to accurately measure such a small amount are also rather expensive. In addition, the measured weight is very sensitive to the temperatures of the ambient air and the sample. Thus, weighing of the dot amount was not considered as a very effective method for measurement [Cavallaro *et al.* 1998]. An improved method is to measure the dot size. For this purpose, Cavallaro *et al.* [1998] developed a device or apparatus, in which the sample of a dot dispensed is compressed between two plates such that the dot becomes substantially cylindrical in shape, and then the dot size is determined by the cylindrical diameter and height. Once the dot amount or dot size was measured, some controllers, such as an incremental controller, or Bang-Bang controller were used to regulate the manipulating parameters.

For control in dispensing lines, several studies were conducted by Razban *at el.* [1991, 1992, 1993, 1995]. The background of this work is to dispense lines of adhesive or sealant onto workpieces to have structurally bonded joints in the automotive and aerospace industries in which the consistency is also a crucial issue. In this study, a customer-made vision system, which included a CCD camera and a laser diode, was used for measuring the line size. Based on the system identification method, a model for the process dynamics was developed, which is described in the preceding section. Based on the model, various conventional and predictive controllers were evaluated using either simulation or experimental investigations. It

was found that proportional (P) control was not applicable because of the presence of steady state error. For the proportional-integral (PI) control, the integral component has a considerable effect on forcing the steady state error to be zero. However, due to the relatively long time delay in the dispensing process (typically 50 ~ 200 ms [Razban 1993, Davies *et al.* 1996]), PI control does not work as effectively as it does in a process without a time delay, due to the destabilizing effect of the time delay. Predictive control is relatively effective in the control of the processes with long time delay. However, it should be noted that a process model is an essential part of the predictive control. Due to the difficulty in the model development for the fluid dispensing process, the predictive control scheme can also only achieve a limited performance improvement.

In addition, for dispensing lines in underfill encapsulation, Bouras *et al.* [1999] patented a technique for the process control, called mass-flow calibration. The general idea of the technique is that the flow rate is measured periodically by weighing the fluid dispensed over a determined time interval, and using this measurement the change in fluid viscosity is identified. The manipulated parameters are then adjusted, based on a correction table, in order to compensate for the change in viscosity. For this technique, one of the limitations is that the use of only viscosity is not sufficient to represent the behaviour of the fluid used for electronics packaging. The fluid behaviour considered here is usually featured by a nonlinear relationship between shear stress and shear rate, which is dependent on the shear rate, temperature, and even on time (this issue will be addressed in this thesis). The other limitation is the extent of the performance improvement being dependent on the correction table, including the accuracy of obtaining the table as well as the size

of the table (i.e., whether or not it contains all possible situations with different operational conditions).

Based on the review of fluid dispensing control systems, it can be seen that the design of the controller is actually a relatively small part of this particular control problem. One of the key issues is how to determine the variation in the process performance. From this perspective, if there are models or methods that can accurately predict the performance variation, the integration of them into control systems could significantly improve the control performance.

1.3.4 Issues in Modeling and Control

Fluid dispensing is a very complex process. It is in an interdisciplinary area involving electronics packaging, fluid mechanics, pneumatics, materials engineering, control systems, and manufacturing. The modeling and control of such a process has proven to be a very challenging task. The key issues involved in modeling include:

(1) The fluid flow considered is a time-dependent non-Newtonian one. Some fundamentals of time-independent Non-Newtonian flow have been well defined in the literature; however, research on time-dependent non-Newtonian flow is lacking. In such a flow, the characterization of non-Newtonian fluid behavior and its influence on fluid flow are very difficult, yet essential to modeling of the fluid dispensing process.

(2) The spreading of fluid on a board is a complex process. This process is governed by a set of partial differential equations with moving-boundary conditions. As indicated in the literature [Greenspan 1978, Ehrhard and Davis 1991, Haley and Miksis 1991], these equations cannot be solved unless several simplifying assumptions are made. Unfortunately, these assumptions given in literature are not applicable to the fluid dispensing process considered in this study.

(3) Air compressibility makes the dispensing process more complicated to represent. In time-pressure dispensing, pressurized air is used. As a result, air compressibility can significantly change the dynamics of the dispensing system affecting the overall performance of the dispensing process. This is particularly true when dispensing a small amount of fluid [Chen *et al.* 2001 and 2002].

As a result, modeling of the fluid process is a challenging task and only some very approximate or empirical models have been reported in the literature to date. This situation, without a suitable model, can greatly degrade the control performance of the fluid dispensing process, as discussed previously. Other issues of the dispensing control include:

(1) The fluid dispensing process has a long-time delay. This delay is mainly caused by both the pressure transportations in the pressurized air and the spreading of fluid on a board, and the typical delay time is 50-200 msec [Razban 1993, Davies *et al.* 1996]. Due to the long-time delay, conventional control schemes cannot work well as discussed previously.

(2) Measurements of the process performance are difficult to make accurately, especially when on-line real time measurements are required. This is due to the fact the fluid dispensed on a board is still in a spreading state (note that the spreading of fluid on a board is an extremely temperature-sensitive process). In such a spreading state, measurements are not stable and repeatable. Therefore, the improvement of the process performance using the feedback control based on those measurements is limited.

1.4 Research Objectives

This aim of this research is to carry out a comprehensive study on the modeling and control of time-pressure dispensing for improved process performance, in which the aforementioned issues can be effectively addressed. In particular, two main objectives are established to achieve in this research.

The first objective is *to develop models to represent the process performance, i.e., the amount or flow rate of fluid dispensed and the profile of fluid formed on a board, while taking into account the influence of both the time-dependent fluid behavior and air compressibility.*

It is important to note here that time-dependent fluid non-Newtonian behavior and its influence on the dispensing process are very complex. The current state of the art in fluid mechanics does not provide a satisfactory solution to this problem. This research will look into solutions to this problem from a different perspective,

i.e., model updating, which is a method to update a model by means of experimental data and has been widely used in the improvement of models for structural dynamics in the last decades [Friswell and Mottershead 1995].

The second objective is *to develop an off-line control strategy to improve the dispensing process performance, based on the models developed.*

As discussed previously, feedback control of the dispensing process can only achieve a limited improvement due to the simultaneous presence of the long-time delay and the difficulties in on-line measurements. On the basis of the models developed, the second objective of this study is to develop an off-line control strategy to improve the consistency in the performance of the dispensing process for electronics packaging.

1.5 Organization of the Thesis

In all, there are eight chapters in the dissertation, including this chapter. Other chapters are briefly described as follows.

Chapter 2 deals with the characterization of the rheological behavior of fluid for electronics packaging from both time-independent and time-dependent perspectives. Some models reported in literature are reviewed and examined, and the model using structural theory is extensively addressed to account for the influence of time on the fluid rheological behavior. An experimental investigation of the rheological

behavior of a typical fluid used in electronics packaging is also presented in this chapter.

Chapter 3 addresses the development of a model for the steady-state flow rate of fluid dispensed in the dispensing process, under the assumption that the pressure in the dispensing syringe has reached a steady-state value. For model verification, experimental results are also included in this chapter.

Chapter 4 deals with the spreading of fluid on a board and presents the development of a model to represent the equilibrium profile of fluid formed on a board, along with the experimental verification. In addition, the concepts of surface tension and contact angle are introduced

Time-dependent fluid rheological behaviour has a significant influence on the performance of the fluid dispensing process. In **Chapter 5**, a method, based on model updating, is developed to track and represent this influence and the effectiveness of the method is illustrated experimentally.

Taking into account both air compressibility and fluid inertia, in **Chapter 6** a model is developed to represent the flow rate dynamics in the fluid dispensing process. Experimental verification of the model is also included in this chapter.

Based on the models developed in previous chapters, **Chapter 7** presents the development of an off-line control strategy. Case studies are conducted by applying the strategy in the control of the processes for both dispensing lines and dispensing

dots. The experiments and the results verifying the effectiveness of the off-line control are also included in this chapter.

Chapter 8 presents the conclusions drawn from this research. This is followed by suggestions and recommendations for possible future work.

2. CHARACTERIZATION OF THE RHEOLOGICAL BEHAVIOR OF FLUIDS FOR ELECTRONICS PACKAGING

For modeling the fluid dispensing process, one of the key issues is to understand and characterize the flow behavior of the fluid dispensed. Note that characterization of the fluid behavior is a demanding task, especially when it exhibits rheological behaviour that is not well documented in literature [Irvine Jr. and Capobianchi 1998]. In this chapter, the rheological behavior of fluids for electronics packaging is addressed theoretically and experimentally.

2.1 Introduction to Rheological Fluid

The fluids employed in electronics packing, such as adhesives, epoxy, encapsulant, etc., are usually rheological or non-Newtonian fluids. One of the characteristics that distinguishes rheological fluids from Newtonian fluids is the nonlinear relationship between shear stress and shear rate. Such materials are commonly divided into three categories; purely viscous time-independent fluids, purely viscous time-dependent fluids, and viscoelastic fluids, as shown in Figure 2.1 [Skelland 1967, Barnes *et al.* 1989, Irvine Capobianchi 1998, Chhabra and Richardson 1999].

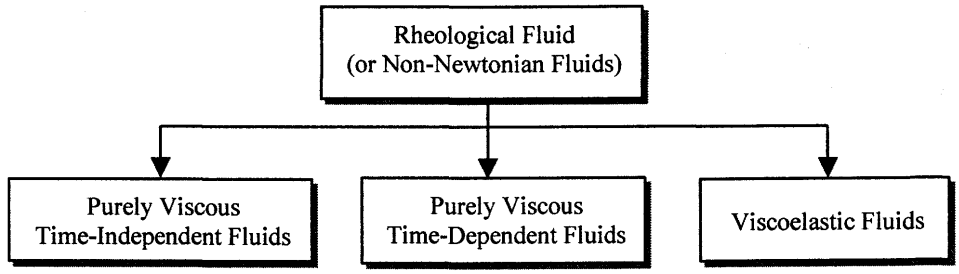

Figure 2.1 Classification of rheological fluids.

Purely viscous time-independent fluids (or time-independent fluids for short) are those for which the shear rate at a given point is solely dependent upon the instantaneous shear stress at that point. Figure 2.2 (a) illustrates the characteristics of flow curves of various time-independent fluids, in which τ_0 denotes the yield stress. The physical behaviour of fluids with a yield stress is usually explained in terms of an internal structure that is capable of preventing movement for values of shear stress less than the yield values, τ_0 [Skelland 1967].

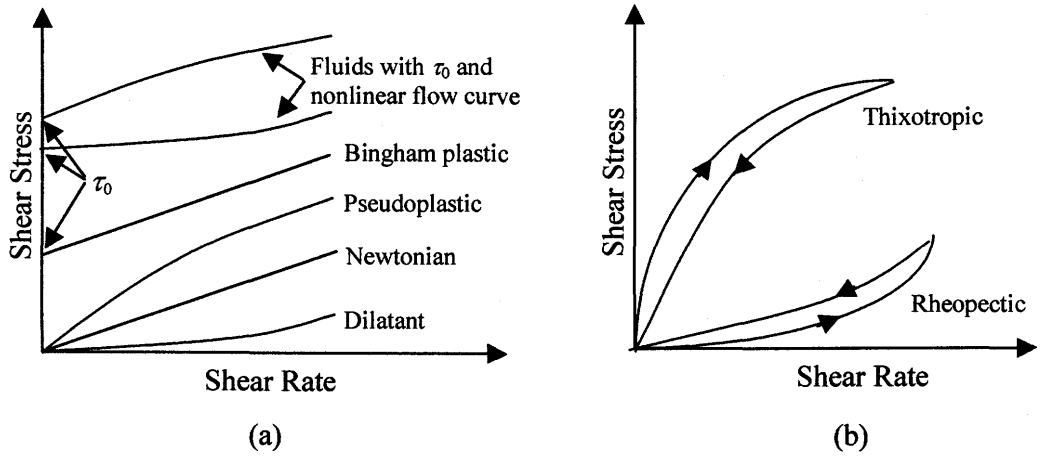

Figure 2.2 (a) Flow curves of time-independent fluids and (b) flow curves of time-dependent fluids.

Purely viscous time-dependent fluids (or time-dependent fluids for short) are those for which the shear rate is a function of both the magnitude and the duration of shear, and sometimes of the time lapse between consecutive applications of shear stress, all of which can be summarized that the time dependency is influenced by the work history of the fluid. Figure 2.2 (b) shows the flow curves of two common classes of such materials, thixotropic fluids and rheopectic fluids. Fluid is said to be thixotropic if its viscosity decreases with time; otherwise it is rheopectic. It is seen that such fluids have a hysteresis loop or memory whose shape depends upon the time-dependent rate at which the shear stress is applied.

Viscoelastic fluids are those that show partial elastic recovery upon the removal of a deforming shear stress. Such materials possess properties of both fluids and elastic solids.

Typically, the fluids employed for electronics packaging are purely viscous rheological ones; either time-independent or time-dependent.

2.2 Characterization of Time-Independent Rheological Behavior

Viscosity, defined as the ratio of shear stress to shear rate, is also called apparent viscosity for rheological fluids in the literature. As far as the time-independent rheological behaviour of fluids used in electronics packaging is concerned, the most important characteristic is the dependency of viscosity on shear rate and temperature. There are various empirical models available in the literature

[Holdsworth 1993, Benezech and Maingonnat 1994]. It is noted that most of them were developed for liquid food products, such as yoghurt, fruit juices, milk, etc. For the behaviour characterization of the fluids in electronics packaging, which are applied by means of dispensing, there should be another consideration. The model chosen and used must represent the fluid rheological behaviour as well as be easy and convenient to be integrated in the modelling of the fluid dispensing process.

One such model is the Power Law equation given by

$$\tau = K\dot{\gamma}^n \tag{2.1}$$

This equation was employed by Razban and Davies [1993 and 1995] for the behaviour characterization of Elastosol M23 (supplied by Evode Ltd.), which was dispensed for joint sealing or structural bonding. The other equation is the Generalized Power Law equation, i.e.,

$$\tau = \tau_0 + K\dot{\gamma}^n \tag{2.2}$$

Han and Wang [1997] used Equation 2.2 to represent the rheological behaviour of Hysol FP4510 (supplied by Dexter Corporation, USA), which is used for underfill encapsulation in electronics packaging.

In Equations 2.1 and 2.2, τ and τ_0 are the shear stress and the yield stress, respectively; $\dot{\gamma}$ is the shear rate; K and n are the consistency index with the unit of

Pa·s^n, and the flow behavior index (dimensionless), respectively. Physically, τ_0 is the critical value of shear stress at which fluid yields or starts to flow; K is a measure of viscousness - the higher K, the more viscous the fluid; and n is a measure of the degree of rheological behavior - the greater departure of n from unity, the more pronounced the rheological behaviour. The difference between the above two equations is that the Generalized Power Law equation includes the influence of the yield stress, while the Power Law equation does not. For a given fluid, the values of n, τ_0, and K are determined experimentally, while n is usually identified as a constant and τ_0 and K as functions of temperature.

2.3 Characterization of Time-Dependent Rheological Behavior

2.3.1 Time-dependent Generalized Power Law equation

As mentioned previously, time-dependent fluids are said to be either thixotropic if the viscosity decreases with time, or rheopectic if the viscosity increases with time. Based on our measurements, most of the fluids in electronics packaging exhibit thixotropic behaviour. One of the most promising models given in the literature to represent the thixotropic behaviour is the time-dependent Generalized Power Law equation. This model was proposed by Matinex-Paradilla and Hardy [1989] based on the Generalized Power Law equation, and it takes the form of

$$\tau = \tau_0 + K\dot{\gamma}^n t^{-m} \tag{2.3}$$

where t is time; m is the thixotropic index (dimensionless). Physically, m is a measure of the degree of time dependency - the greater departure of m from zero the more pronounced time dependency.

Equation 2.3 has been utilized with various degrees of success for the characterization of the rheological behavior of liquid food products. However, there are two drawbacks limiting the application of the equation. One is that the equation is not applicable to describe the equilibrium state of viscosity because, as time becomes very large, the second term on the right side of Equation 2.3 reduces to zero and the viscosity is only dependent upon the yield stress, which is obviously not true. The other drawback is that this equation is not valid for the situation where, upon the removal of the shear stress, the viscosity is gradually increasing with time. This situation occurs during the time lapse between consecutive applications of shear stress due to the interruption of a dispensing process. Therefore, a model that can overcome the above drawbacks is desired. One such model is based on structural theory.

2.3.2 Model Using Structural Theory

Cheng and Evans [1965] first proposed structural theory to describe the time-dependent rheological behaviour. Since then the theory has been greatly extended by other researchers [Petrellis and Flumerfelt 1993, Tiu and Boger 1974, De Kee and Turcotte, 1983, De Kee and Chan Man Fong 1993, Chan Man Fong *et al.* 1996]. The general idea of structural theory is to use a structural parameter, λ, to account for the time-dependent effects on flow behaviour. This parameter is associated with the

internal structure of fluid, which breaks down under shear and builds up at rest. Therefore, under the action of shear stress, the parameter continues to change until an equilibrium state is reached. The fluid viscosity is then assumed to associate with λ.

In structural theory, two constitutive equations are usually used: one is the state equation to describe the state of shear stress, and the other is the rate equation to describe the change rate of structural parameter. The state equation is expressed in the form

$$\tau = \eta(\dot{\gamma}\ \lambda) \cdot \dot{\gamma} \tag{2.4}$$

in which $\eta(\dot{\gamma}\ \lambda)$ is the viscosity, given by a function of the shear rate and the structural parameter. The rate equation is expressed by

$$\frac{d\lambda}{dt} = g(\dot{\gamma}\ \lambda) \tag{2.5}$$

in which the change rate of the structural parameter is described as the function $g(\dot{\gamma}\ \lambda)$, depending on the shear rate and the structural parameter.

In the literature, there are various forms of Equations 2.4 and 2.5 reported, motivated from the rheological behavior exhibited by the fluids considered. In this study, the following form of state equation is adopted for the fluids in electronics packaging, based on experimental measurements,

$$\tau = \lambda(\tau_0 + K\dot{\gamma}^n) \tag{2.6}$$

The rate equation takes the form of

$$\frac{d\lambda}{dt} = k_c(\lambda_i - \lambda) - k_d\lambda \tag{2.7}$$

where k_c and k_d are rate constants associated with the build-up or creation and break-down or destruction of the internal structure of fluid, respectively, and λ_i is the initial value of the structural parameter. It is noted that, as time becomes very large, the rate of build-up structure given in the first term on the right side of Equation 2.7 is approximately equal to that of break-down structure given in the second term, and the structural parameter reaches an equilibrium value. So the equilibrium value, λ_e, can be derived by equating the right hand side of Equation 2.7 to zero,

$$\lambda_e = \frac{k_c}{k_c + k_d}\lambda_i \tag{2.8}$$

The complete rheological characterization of the time-dependent fluids can then be described by Equations 2.6 and 2.7 with the parameters τ_0, K, n, k_c, k_d and λ_i or λ_e evaluated from experimental data.

2.3.3 Determination of Model Parameters

The parameters τ_0, K, and n can be determined at zero shear time (i.e., t=0) and assuming $\lambda = 1$. For this purpose, rewriting Equation 2.6 in logarithmic form

$$\log(\tau - \tau_0) = \log K + n \log \dot{\gamma} \tag{2.9}$$

n and K are then determined based on the linear regression of the measurement data of $\log(\tau - \tau_0)$ versus $\log(\dot{\gamma})$. τ_0 can be determined directly from the extrapolation of the data of τ versus $\dot{\gamma}$ at zero shear rate.

The determination of the parameters k_c, and k_d is complicated by the fact λ cannot be obtained explicitly from measurements. To overcome this difficulty, the determination of k_c and k_d is addressed for the two cases; (1) where the viscosity decreases with respect to time (called *viscosity decay*) when fluid is sheared at a constant shear rate; and (2) where the viscosity increases with respect to time (called *viscosity recovery*) upon the removal of a shear stress.

Case 1 – Viscosity Decay. Solving Equation 2.7 with the initial condition for structural parameter, i.e., λ=λ_i at t=0, and then combining the result with Equation 2.8 yields

$$\lambda = \lambda_e + (\lambda_i - \lambda_e)e^{-kt} \tag{2.10}$$

where $k = k_c + k_d$, is the sum of the rates of the build-up and break-down structures.

Recalling from Equation 2.6, λ can be related to the viscosity, η, which can be expressed as $\eta = \tau / \dot{\gamma}$,

$$\lambda = \frac{\eta}{\tau_0 \dot{\gamma}^{-1} + K\dot{\gamma}^{n-1}} \tag{2.11}$$

Note that Equation 2.11 is also valid at the initial and equilibrium states in which λ and η are simply replaced by λ_i and η_i (the viscosity at the zero shear time), or λ_e and η_e (the equilibrium viscosity), respectively. Hence, for a constant of $\dot{\gamma}$, one has

$$\frac{\lambda}{\lambda_e} = \frac{\eta}{\eta_e} \quad \text{and} \quad \frac{\lambda_i}{\lambda_e} = \frac{\eta_i}{\eta_e} \tag{2.12}$$

Dividing Equation 2.10 by λ_e and combining with the above equation yield

$$\frac{\eta}{\eta_e} - 1 = \left(\frac{\eta_i}{\eta_e} - 1 \right) e^{-kt} \tag{2.13}$$

Note that Equation 2.13 is expressed in terms of viscosity, in which η, η_i, η_e, and t can be directly obtained from the measurement data of viscosity versus time. Hence, the value of k can be determined using the regression method.

Case 2 – Viscosity Recovery. Upon the removal of shear stress, the rate of structure break-down becomes very small in comparison with that of structure build-up. Thus, by neglecting the term of structure break-down, Equation 2.7 reduces to

$$\frac{d\lambda}{dt} = k_c(\lambda_i - \lambda) \tag{2.14}$$

Similarly, solving the above equation with the structural parameter initial condition at the beginning of the viscosity recovery, i.e., $\lambda(t = t_1) = \lambda_1$, yields

$$\lambda = \lambda_i + (\lambda_1 - \lambda_i)e^{k_c \Delta t} \tag{2.15}$$

where $\Delta t = t - t_1$ is the time period since the shear stress is removed. Combining the above equation with Equation 2.12, one has

$$\frac{\eta}{\eta_i} - 1 = \left(\frac{\eta_1}{\eta_i} - 1\right)e^{-k_c \Delta t} \tag{2.16}$$

where η_1 is the viscosity at the beginning of the process of viscosity recovery. It is seen that the above equation is given in terms of viscosity, so k_c can also be determined from the measurements of viscosity versus time. Unfortunately, upon the removal of the shear stress, the viscosity in the fluid is not observed because of the zero shear stress, so it seems impossible to determine k_c from this point of view.

To solve this problem, a solution is proposed under the assumption that the change of viscosity is continuous. This assumption implies that the viscosities at the beginning and the end of the process of viscosity recovery can be determined from the data recorded just before the shear stress is removed and just after it is applied

again, respectively. Substituting the determinable viscosity at the end of the process, η_2, into Equation 2.16, one has

$$\frac{\eta_2}{\eta_i} - 1 = \left(\frac{\eta_1}{\eta_i} - 1 \right) e^{-k_c \Delta t_t} \tag{2.17}$$

where Δt_t is the total time period of the process of viscosity recovery. It is noted for the process of viscosity recovery that only one set of data of (Δt_t η_1 η_2) can be obtained, and so k_c is solely solved from the above equation. For the regressive determination of k_c, a number of data sets of (Δt_t η_1 η_2) are required, which can be obtained by repeating the process of viscosity recovery. For this purpose, Equation 2.17 is rewritten as

$$y_i = -k_c \Delta t_{ti} \qquad i = 1, 2, \cdots n \tag{2.18}$$

where n is the number of the data sets, and y is given by

$$y = \ln\left(\frac{\eta_2}{\eta_i} - 1 \right) - \ln\left(\frac{\eta_1}{\eta_i} - 1 \right) \tag{2.19}$$

2.4 Experimental Results

In the experiments presented here, the fluid FP4451 from Dexter Corporation is chosen, which is a kind of non-Newtonian fluid and used in die encapsulation in electronics packaging. Note that the experimental settings and the data analysis methods are also applicable to other fluids used in electronics packaging. For each measurement, a fresh degassed sample was used to eliminate the previous shear history as an additional variable. Degassing was accomplished by placing the sample in a syringe at room temperature until no trapped air was observed. It is noted that reproducible results could not be obtained unless the air present in each fresh sample was removed prior to testing on a rheometer.

2.4.1 The Rheometer for Measurements

Numerous instruments employing different rheometerical approaches are available commercially for the rheological measurements. The basic features of the rheometerical approaches, and of the main instrument types for their implementation are reviewed in many textbooks and research papers [Skelland 1967, Barnes *et al.* 1989, Irvine Capobianchi 1998, Chhabra and Richardson 1999, Nguren and Boger 1992, Holdsworth 1993].

In this study, the rheometer provided by Brookfield Engineering Laboratories, INC. is used. It employs a cone-and-plate geometry, as shown in Figure 2.3, which is fixation of a conical vertex perpendicular to and in point contact with a flat plate. The test sample of fluid is sheared under torsion flow within the gap between the

2.4.2 Time-Independent Rheological Behavior

Two kinds of experiments were conducted to investigate the time-independent rheological behavior. One is to measure the yield stress exhibited by the fluid. The other is to identify the dependency of viscosity on shear rate and temperature.

Based on the general definition of the yield stress as the stress limit between flow and non-flow conditions, in the literature numerous techniques were reported and developed for the yield stress measurement. A detailed review of them was given by Nguyen and Boger [1992]. Generally, these techniques can be divided into two categories; direct and indirect. Direct measurement relies on some independent assessment of the yield stress as the critical shear stress at which the fluid yields or starts to flow, while indirect measurement simply involves the extrapolation of the experimental data of shear stress versus shear rate to obtain the value of the yield stress at zero shear rate, which is commonly employed in engineering applications. In this study, the indirect measurement is adopted to determine the yield stress.

Using the rheometer described above, the fluid flow curves of shear stress versus shear rate were measured at various temperatures, which are shown in Figure 2.4. For each temperature, the shear stress was fitted to the shear rate using a second-order polynomial. Extrapolating it to zero shear rate, the yield stress was obtained. The determined yield stresses at various temperatures are shown in Figure 2.5, from which it is seen that the yield stress decreases with an increase in temperature. In turn, the yield stress was related to a function of temperature by

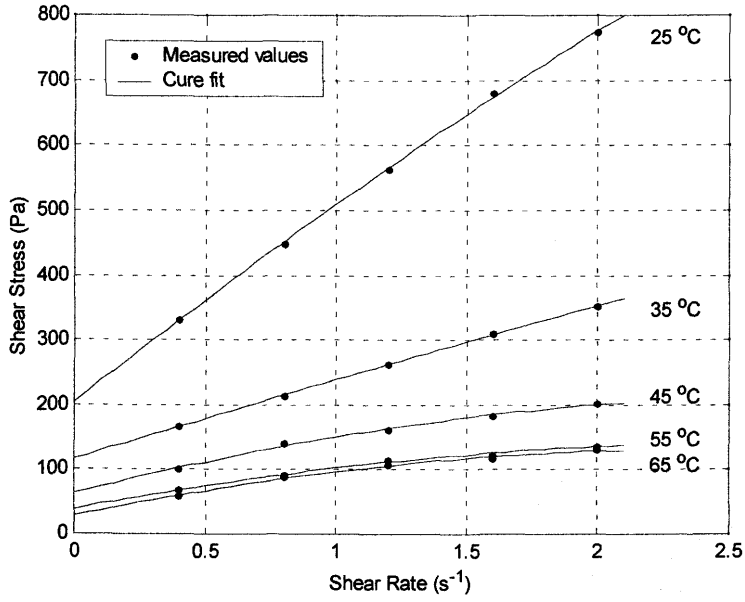

Figure 2.4 Shear stress versus shear rate at various temperatures.

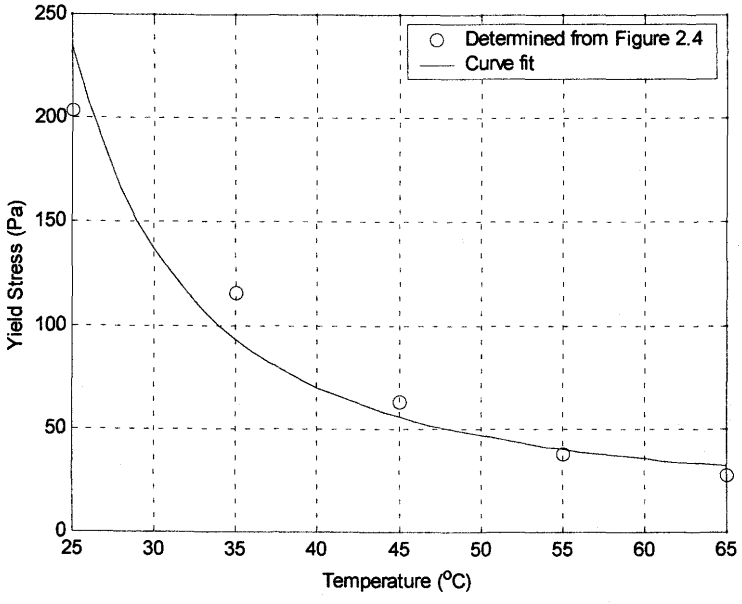

Figure 2.5 Dependency of yield stress on temperature.

$$\tau_0 = \tau_{00} e^{T_0/T} \tag{2.21}$$

where τ_{00} and T_0 are curve-fitting parameters. Based on the curve fitting process, the values for τ_{00} and T_0 are 9.225 Pa and 80.98 °C, respectively.

In the second experiment, the flow curves were also measured at different temperatures, but with higher shear rates. Note that, as the viscosity of FP 4451 exhibits time dependency that will be detailed later, each shear rate should be scanned or run as fast as possible in each measurement to reduce the effect of time. The viscosity was determined by $\eta = \tau / \dot{\gamma}$, and the results are shown in Figure 2.6. It is seen that the viscosity decreases as the shear rate increases. The viscosity curves were fit using the following equation, derived from Equation 2. 2,

$$\eta = \frac{\tau_0}{\dot{\gamma}} + K\dot{\gamma}^{n-1} \tag{2.22}$$

in which τ_0 is the value of the yield stress determined by Equation 2.21, n and K are curve-fitting parameters. By fitting, n is given the value of 0.5672, and K is a function of temperature as shown in Figure 2.7 and was correlated to temperature by

$$K = K_0 e^{T_k/T} \tag{2.23}$$

where K_0 and T_k are curve-fitting parameters. Based on the curve fitting process, the values for K_0 and T_k are 11.78 Pa.s and 107.8 °C, respectively.

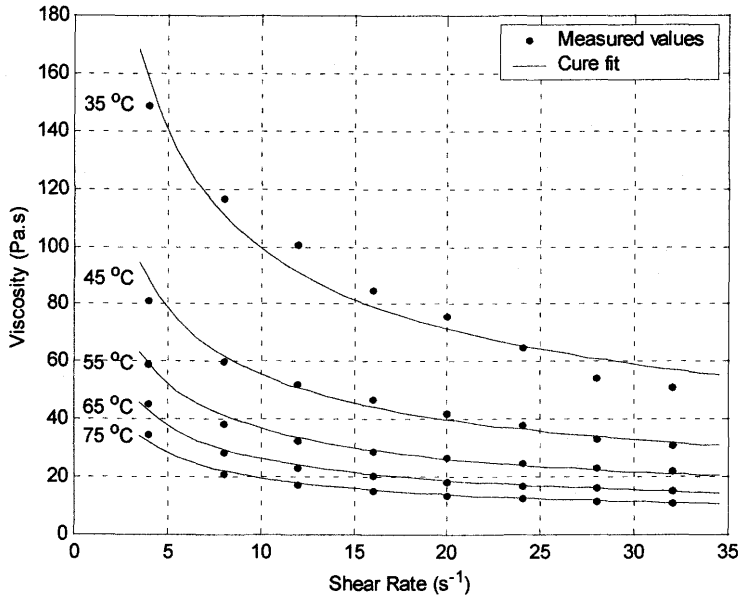

Figure 2.6 Viscosity versus shear rate at various temperatures.

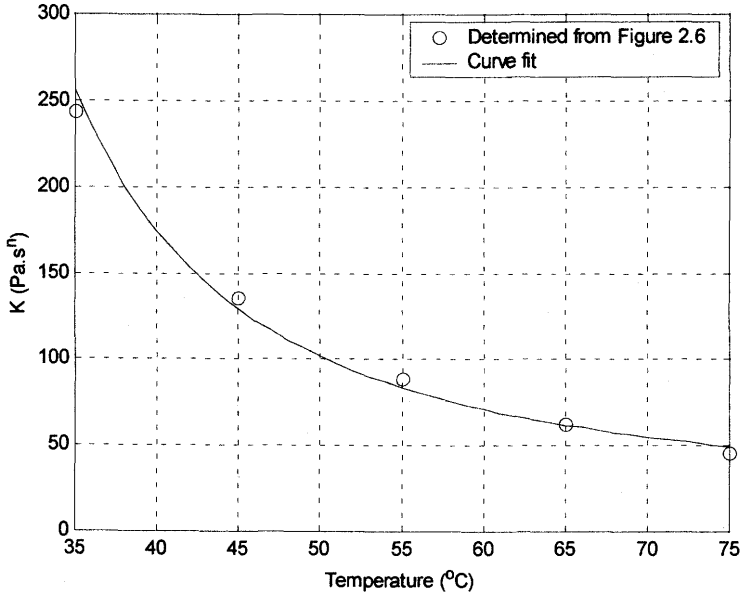

Figure 2.7 Dependency of K on temperature.

2.4.3 Time-Dependent Rheological Behavior

Two kinds of experiments were designed and conducted for the investigation of time-dependent rheological behavior. One is used to identify the time dependency in viscosity decay, and the other one is used to identify the time dependency in viscosity recovery.

In the first experiment, the sample of fluid was sheared continuously for a time period of 1hour at a given shear rate and temperature, and viscosity was measured as a function of time. Figure 2.8 shows the measured viscosity versus time at various shear rates with the temperature fixed at 40 °C. Figure 2.9 shows the measured viscosity versus time at various temperatures with the shear rate fixed as 3 s^{-1}. It can be seen that the viscosity change with time is dependent on both the shear rate and temperature. In particular, at higher shear rates or lower temperatures, the viscosity drops with time relatively faster, especially during the starting period of shearing; and with the shearing time increasing the change in viscosity becomes smoother until an equilibrium state is reached.

Equation 2.13 was used to correlate the data given in Figures 2.8 and 2.9, in which η, η_i, and η_e were obtained directly from these data, and the change rate, k, is the curve-fitting parameter. It was found that the value of k is not dependent on the shear rate and temperature, but approximately a constant value of 1.02, and that the ratio of the initial viscosity to the equilibrium viscosity, η_i/η_e, is associated with both the shear rate and temperature, as shown in Figures 2.10 and 2.11, respectively. In turn, η_i/η_e is related to the shear rate and temperature by

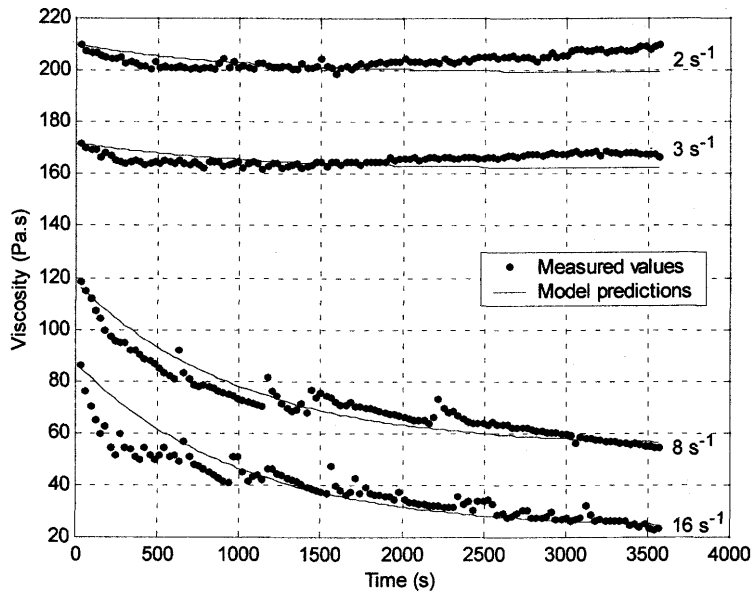

Figure 2.8 Viscosity versus time at various shear rates and the temperature of 40 °C.

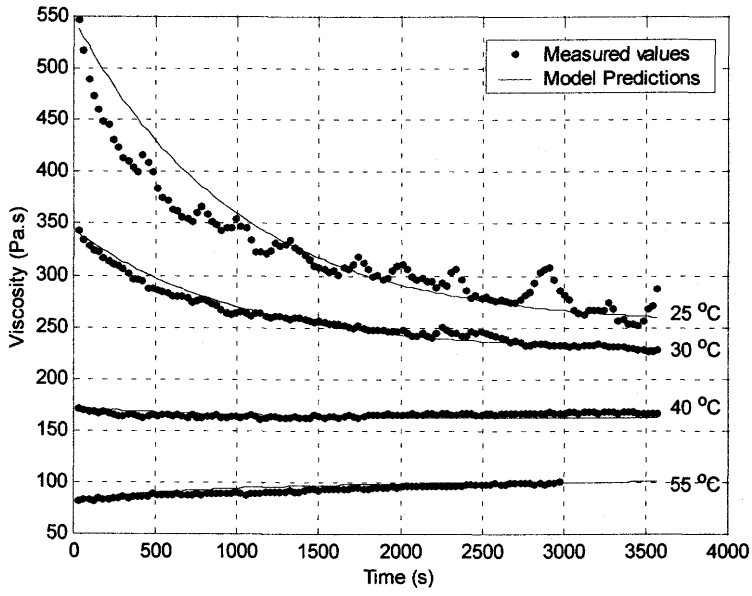

Figure 2.9 Viscosity versus time at various temperatures and the shear rate of 3 s^{-1}.

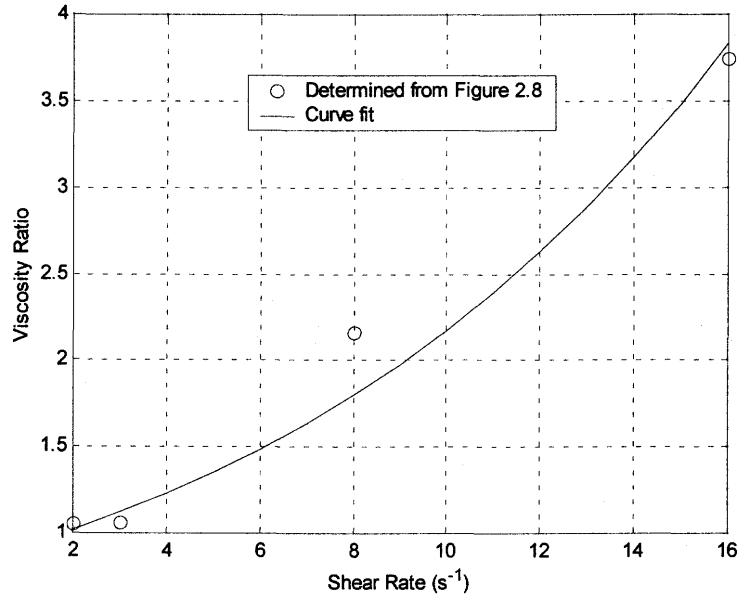

Figure 2.10 Dependency of η_i / η_e on the shear rate at a temperature of 40 °C.

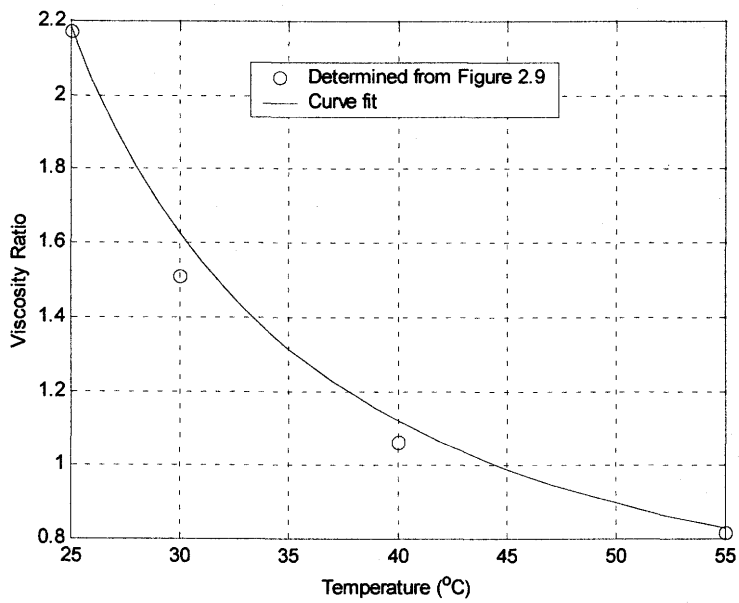

Figure 2.11 Dependency of η_i / η_e on temperature at a shear rate of 3 s^{-1}.

$$\frac{\eta_i}{\eta_e} = R_0 e^{(\frac{\dot{\gamma}}{\dot{\gamma}_R} + \frac{T_R}{T})} \tag{2.24}$$

where R_0, $\dot{\gamma}_R$, and T_R are the curve-fitting parameters. By fitting, they are given the values of 0.2777 (dimensionless), 10.58 s^{-1}, and 44.46 °C.

Using the values of these curve-fitting parameters, the predictions of the viscosity from Equations 2.13 and 2.24 are also shown as solid lines in Figure 2.8 and 2.9. A good agreement between the model predictions and measurements is evident.

To determine the effect on viscosity recovery of the removal of shear stress, the samples of fluid in this experiment were sheared discontinuously and viscosity was measured as a function of time. The discontinuous shearing condition is achieved by alternately switching between the condition of the sample being sheared at a constant shear rate and at rest condition. The time period of the rest state presents a situation where the shear stress is removed and the viscosity recovery occurs. Two time patterns of the discontinuous shearing condition, named *Pattern A* and *Pattern B*, were designed and used in this experiment. The time distributions in the patterns are listed in Table 2.1. Figures 2.12 and 2.13 show the measured viscosity versus time for the two time patterns, respectively, at the condition of $\dot{\gamma} = 3$ s^{-1} & $T = 30$ °C and $\dot{\gamma} = 8$ s^{-1} & $T = 40$ °C. It is important to note that there is no viscosity observed during the time period of the sample at rest condition.

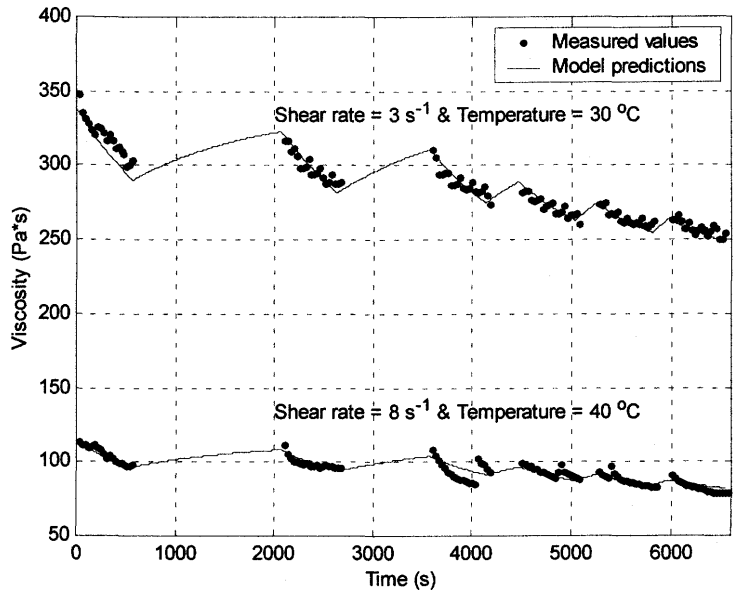

Figure 2.12 Viscosity versus time under the discontinuous shearing of *Pattern A*.

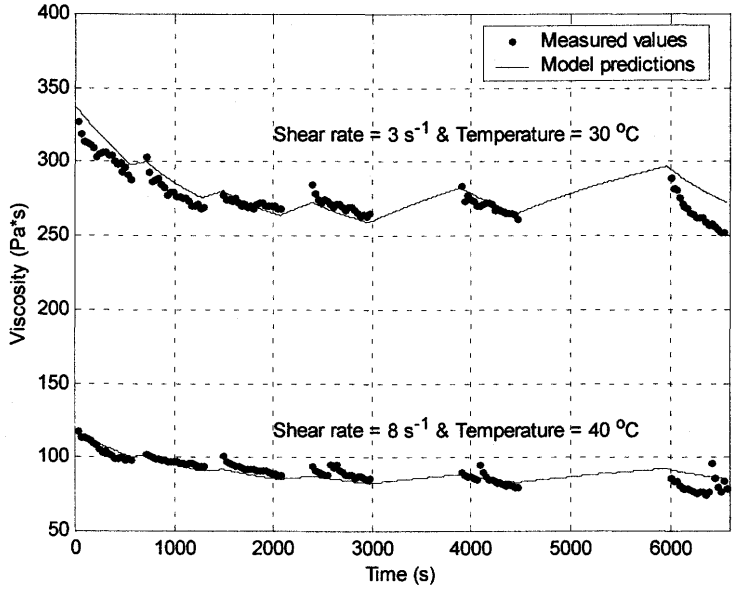

Figure 2.13 Viscosity versus time under the discontinuous shearing of *Pattern B*.

Table 2.1 Time distributions of the discontinuous shearing condition.

	1*	0*	1	0	1	0	1	0	1	0	1
Pattern A (minute)	10.0	25.0	10.0	15.0	10.0	5.0	10.0	3.0	10.0	2.0	10.0
Pattern B (minute)	10.0	2.0	10.0	3.0	10.0	5.0	10.0	15.0	10.0	25.0	10.0

* 1 - the sample is sheared at a constant shear rate; 0 - the sample is in rest

Equations 2.18 and 2.19 were used to determine the change rate, k_c, during the rest periods, in which η_1 and η_2 were obtained from the measured viscosity before the shear stress was removed and after it was applied again, respectively, and η_i was the initial viscosity measured previously. For the case where $\dot{\gamma} = 3$ s^{-1} & $T = 30$ °C, k_c is 5.71×10^{-4}, and for the case where $\dot{\gamma} = 8$ s^{-1} & $T = 40$ °C, k_c is 11.26×10^{-4}. Using these values, the viscosities during the rest periods were predicted from Equation 2.17. The predicted viscosities are shown as the solid lines in Figures 2.12 and 2.13, along with the viscosities predicted from Equation 2.13 for the shearing periods. It is seen that both the model predictions and the measurements are in close agreement.

The values of all the parameters related to the rheological behavior of FP4451, which were identified in this section, are summarized in Table 2.

Table 2.2 Values of the parameters related to the rheological behavior of FP4451.

Time-independent	τ_{00} (Pa)	T_0 (°C)	N	K_0(Pa.s)	T_k(°C)	
	9.225	80.98	0.5672	11.78	107.8	
Time-dependent	K	R_0	$\dot{\gamma}_R$ (s^{-1})	T_R(°C)	k_c	
	1.02	0.2777	10.58	44.46	5.71×10^{-4}*	11.26×10^{-4}*

* 5.71×10^{-4} is for the case where $\dot{\gamma} = 3$ s^{-1} and $T = 30$ °C, and 11.26×10^{-4} for the case where $\dot{\gamma} = 8$ s^{-1} and $T = 40$ °C.

2.5 Summary

This chapter presents a brief introduction to rheological fluids. One of the distinct characteristics of such a fluid is that the relationship between shear stress versus shear rate is non-linear at a given temperature and pressure, and is dependent on shear rate and even on the shearing time. The fluid behaviour is said to be time-dependent if it depends on the shearing time, otherwise the time-independent.

The characterization of rheological behaviour of fluids for electronics packaging is addressed from both time-independent and time-dependent perspectives. As far as the time-independent rheological behavior is concerned, the dependency of viscosity on the shear rate and temperature is very important. To represent the dependency, the Power Law equation and Generalized Power Law equation are reviewed and examined. Both of them give viscosity as a function of shear rate using the flow behaviour index, n. While the temperature dependency is included by means of the consistency index, K.

To characterize the time-dependent rheological behavior, the time-dependent Generalized Power Law is examined. This model is promising for the representation of the thixotropic behavior, but it is not applicable to describe the equilibrium viscosity as time becomes very large and the viscosity recovery upon the removal of shear stress. To overcome these shortcomings, a model using structural theory is introduced, in which a structural parameter is used to account for the time-dependent effects on the flow behavior. The model is applied to the two typical cases occurring in the fluid dispensing process, i.e. where viscosity decays when fluid is sheared at a

constant shear rate and where viscosity recovers when the shear stress is removed, and the method to determine the model parameters in these two cases is developed.

Experiments were conducted to investigate the rheological behavior of a typical fluid for electronics packaging, including the temperature dependency of yield stress, the shear rate and temperature dependencies of viscosity, the time dependency of viscosity while fluid is sheared continuously and discontinuously. The experimental results were compared to the predictions from the models presented in this chapter, indicating a good agreement between them.

3. STEADY-STATE MODELLING OF THE FLOW RATE OF FLUID DISPENSED

3.1 Introduction

The schematic diagram of a typical time-pressure dispensing process was shown previously in Figure 1.3 and is repeated here in Figure 3.1. In this process, the flow rate of fluid dispensed is the most important performance index. It directly affects the size of the profile of fluid formed on a board contributing significantly to the quality of an electronics package.

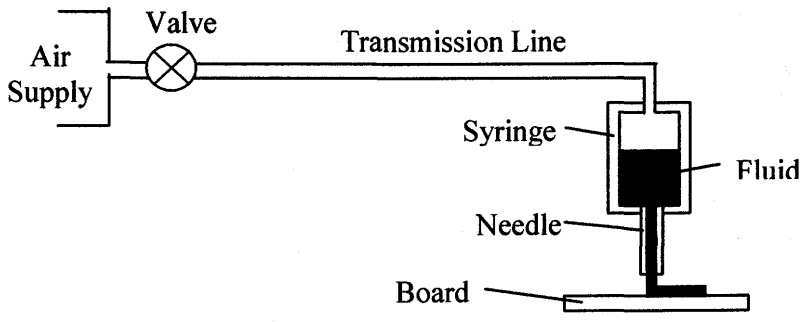

Figure 3.1 Schematic of a typical time-pressure dispensing process.

Due to the compressibility of the air in the transmission line and syringe, the pressure in the syringe will build up gradually until it reaches a steady-state value.

This dynamic process will be addressed in Chapter 6. In this chapter, it is assumed that the pressure in the syringe has reached a steady-state value and a model is developed to represent the steady-state flow rate of fluid dispensed.

3.2 Steady-State Modelling of the Flow Rate of Fluid Dispensed

It is assumed, for the dispensing process shown in Figure 3.1, that

(1) the fluid is incompressible and time-independent;

(2) the fluid is in steady laminar flow;

(3) there is no slip between the fluid and the syringe as well as needle walls; and

(4) the internal diameter of the syringe is much greater than that of the needle.

These conditions closely approximate the typical dispensing process. The geometry for this problem is shown in Figure 3.2, in which P_g and P_e denote the pressures at the air-fluid interface (being equal to the pressure in the syringe) and the exit of the needle (being equal to the atmospheric pressure), respectively. The other geometrical parameters shown in Figure 3.2 are self-explanatory. The pressure drop in the needle is first derived, followed by the flow rate of fluid dispensed.

3.2.1 Pressure Drop in the Needle

Applying the total energy conservation at the air-fluid interface and the exit of the needle [Skelland 1967], one has

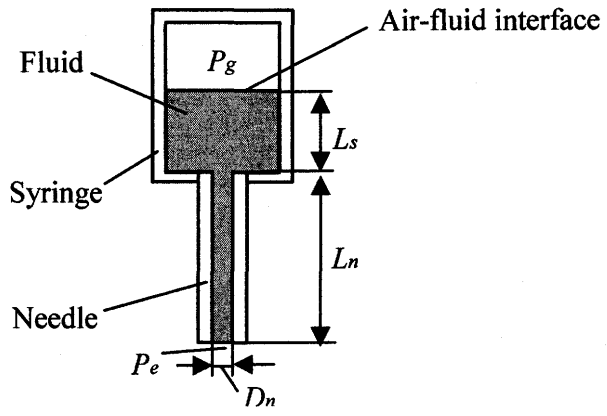

Figure 3.2 Geometry of the time-pressure dispensing process.

$$\frac{P_g}{\rho}+(L_s+L_n)g+\frac{u_1^2}{2\alpha_1}=\frac{P_e}{\rho}+\frac{u_2^2}{2\alpha_2}+\sum F \tag{3.1}$$

where ρ is the fluid density, g is the gravitational acceleration, u_1 (u_2) and $\alpha_1(\alpha_2)$ are the average velocity and the kinetic energy correction factor at the air-fluid interface and the exit of the needle, respectively, and $\sum F$ is the sum of all friction losses between the air-fluid interface and the exit of the needle.

From assumption (4), given in the beginning of this section, the term $u_1^2/(2\alpha_1)$ on the left side of Equation 3.1 can be eliminated as u_1 is approximately equal to zero, and the friction losses $\sum F$ are predominantly those associated with flow in the needle. Thus

$$\sum F = \frac{\Delta P}{\rho} + K_c \frac{u_2^2}{2} \tag{3.2}$$

where ΔP is the frictional pressure drop in the needle, K_c is the entrance loss correction factor. The first term is the energy used to overcome friction in the fully-developed flow through the needle and the second term accounts for the minor losses due to the entrance effect, flow-through fitting, etc.

Substituting Equation 3.2 into Equation 3.1 and solving for the frictional drop in the needle, one has

$$\Delta P = P_g - P_e + (L_s + L_n)\rho g - \rho u_2^2 (\frac{1}{2\alpha_2} + \frac{K_c}{2}) \tag{3.3}$$

It should be noted that, for non-Newtonian fluids, the evaluation of the kinetic energy correction factor α and the entrance loss correction factor K_c is very difficult, and not well defined in the literature. Very limited measurements [Bogue 1959, Weltmann and Keller 1957] on non-Newtonian fluids have indicated that the combined correction for kinetic energy effects and entrance effects is the same as that for Newtonian fluids. The method of evaluation of α and K_c for Newtonian fluids are adopted here to calculate the frictional pressure drop across the needle. In the case of Newtonian fluids, α has the value of 0.5, and K_c is suggested to be 0.23 for a slightly rounded entrance by Foust *et al.* [1960]. Thus, the expression for calculating the frictional pressure drop in the needle can be rewritten as,

$$\Delta P = P_g - P_e + (L_s + L_n)\rho g - 1.12\rho u_2^2 \tag{3.4}$$

3.2.2 Flow Rate of Fluid Dispensed

Consider a cylindrical tube of radius, r, of fluid in the needle, as shown in Figure 3.3, the equilibrium of forces acting on the fluid gives

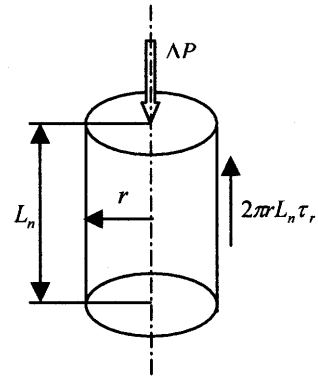

Figure 3.3 A cylindrical element of fluid in the needle.

$$2\pi r L_n \tau_r = \pi r^2 \Delta P \tag{3.5}$$

where τ_r is the shear stress on the outside surface of the element and L_n the length of element (same as the needle length here). The term in the left side is the force acting on the outside surface of the element, resulting from the shear stress, and the term in the right side is the force due to the pressure drop ΔP. Equation 3.5 can be rewritten as

$$\tau = \frac{r\Delta P}{2L_n} \tag{3.6}$$

Based on the characterization of the fluid behaviour discussed in the preceding chapter, one can obtain the relationship between shear stress and shear rate in fluid. Assume that the relationship is generally expressed as

$$\dot{\gamma} = f(\tau) \tag{3.7}$$

Also, it is known that the shear rate presents the rate of the velocity change along the radial direction, i.e.,

$$\dot{\gamma} = -\frac{\mathrm{d}u}{\mathrm{d}r} \tag{3.8}$$

Integrating the above equation and combining with Equation 3.7, the velocity at r, $u(r)$, can be expressed by

$$u(r) = \int_R^r [-\dot{\gamma}]dr = \int_r^R f(\tau)dr \tag{3.9}$$

where R is the radius of the needle. Thus, the volumetric flow rate of fluid dispensed, Q, can be established by integrating the velocity over the cross section of the needle as

$$Q = \int_0^R u(r)2\pi r\mathrm{d}r = \frac{\pi R^3}{\tau_w^3}\int_0^{\tau_w} \tau^2 f(\tau)\mathrm{d}\tau \tag{3.10}$$

where τ_w is the shear stress at the needle wall. It can be obtained from Equation 3.6 with the substitution of $r = R$.

If the time-independent fluid behaviour is described by Generalized Power Law equation described in the preceding chapter, the flow rate of fluid dispensed can be derived from Equation 3.10, which is given as follows:

From Equation 2.2, the Generalized Power Law equation is re-written as

$$\dot{\gamma} = \left(\frac{\tau - \tau_0}{K}\right)^{1/n} = \frac{1}{K^{1/n}}\left(\frac{r\Delta P}{2L} - \tau_0\right)^{1/n} \tag{3.11}$$

It is noted that the profile of shear rate in fluid is not continuous because of yield stress. From $r = r_0 = 2L\tau_0 / \Delta P$ to the wall, the shear stress in fluid is greater than the yield stress, and the shear rate is exactly described by Equation 3.11. However, from $r = 0$ to $r = r_0$, the shear stress is not large enough to overcome the yield stress, so the shear rate is zero and the fluid flows as a plug. The velocity profile of the fluid flowing in the needle can be obtained by using Equation 3.9 and given by

$$v_1 = \frac{2Ln}{K^{1/n}\Delta P(n+1)}\left(\left(\frac{R\Delta P}{2L} - \tau_0\right)^{(n+1)/n} - \left(\frac{r\Delta P}{2L} - \tau_0\right)^{(n+1)/n}\right) \qquad \text{for} \qquad r_0 \le r \le R \tag{3.12}$$

$$v_2 = \frac{2Ln}{K^{1/n}\Delta P(n+1)}\left(\frac{R\Delta P}{2L} - \tau_0\right)^{(n+1)/n} \qquad \text{for} \qquad r \le r_0 \tag{3.13}$$

Thus, the volumetric flow rate is obtained by summing the two flows as

$$Q = \int_0^R 2\pi r v_1 \mathrm{d}r + \int_0^{r_0} 2\pi r v_2 \mathrm{d}r$$
$$= \frac{\pi R^3}{K^{1/n}\tau_w^3}\left(\tau_w - \tau_0\right)^{(n+1)/n}\left[\frac{n}{3n+1}\tau_w^2 + \frac{2n^2}{(2n+1)(3n+1)}\tau_w\tau_0 + \frac{2n^3}{(n+1)(2n+1)(3n+1)}\tau_0^2\right] \tag{3.14}$$

If the yield stress is very small, i.e. the fluid behaviour can be described by Power Law equation given in Equation 2.1, the flow rate can be derived by letting $\tau_0 = 0$ in Equation 3.14. Then one has

$$Q = \frac{n\pi R^3}{3n+1}\left(\frac{\tau_w}{K}\right)^{1/n} \tag{3.15}$$

3.3 Experimental Verification

3.3.1 Experimental Settings

For model verification, experiments were conducted using a typical dispensing system, the DS 500 precision dispensing system provided by Assembly Automation Limited, Hong Kong. An overview of this system is shown in Figure 3.4 (a), and a close-up view of the dispensing head and chuck is provided in Figure 3.4 (b). The dispensing head is used to hold the dispensers and provide motion in three directions. The chuck holds workpieces or PCBs on it using a vacuum method. In

this system, the temperatures of dispenser needle and the chuck can be controlled separately with the resolution of ± 1 °C.

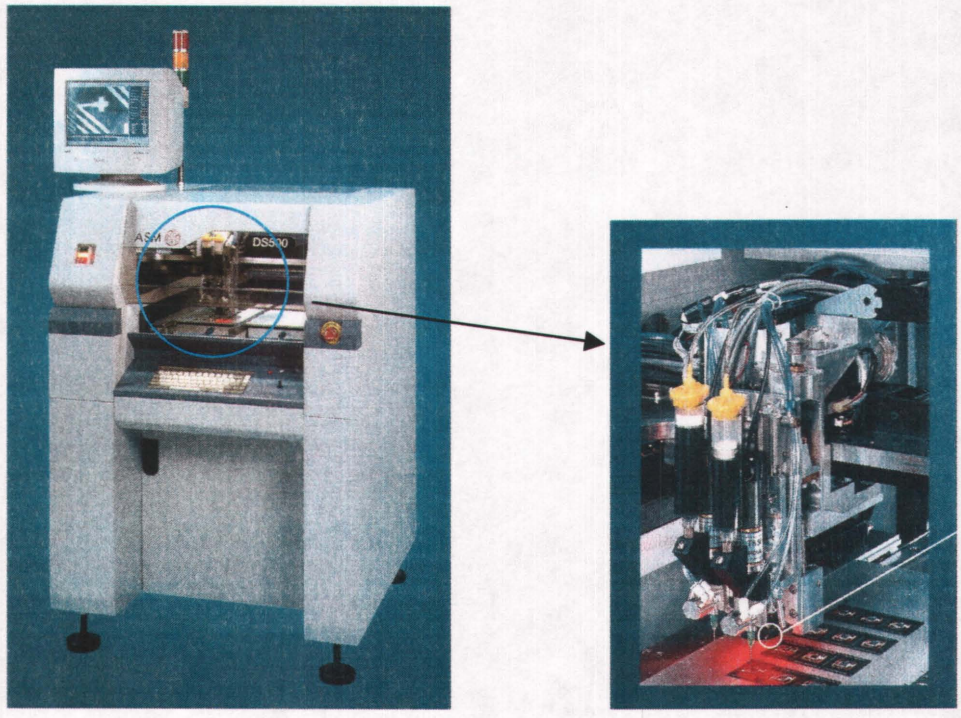

(a) (b)

Fig. 3.4 DS 500 precision dispensing system provided by Assembly Automation Limited, Hong Kong [ASM, 2000]; (a) overview and (b) dispensing head and chuck.

In this dispensing system, the air supply of Σ-MX 9000 SMII provided by Musashi Engineering, Inc. is used. This air supply can provide pressurized air with a pressure range of 20 ~ 700 kPa and a resolution of 1 kPa [Musashi].

3.3.2 Experimental and Simulation Results

The objective of the experiment is to investigate the relationship between the flow rate of fluid dispensed and the air pressure and the needle temperature for the validation of the model developed in this chapter. Note that, as the instantaneous flow rate of fluid dispensed is difficult to measure directly, an average flow rate is used in the experiment.

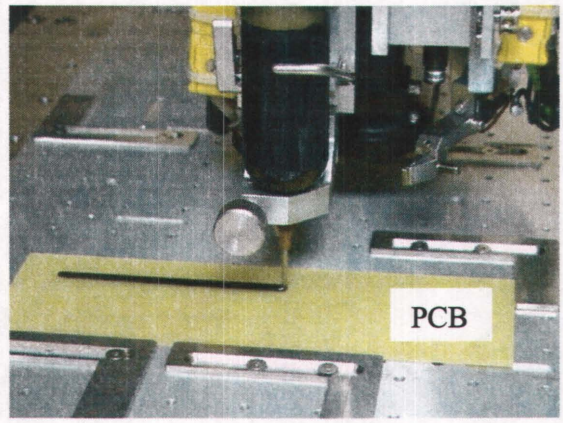

Figure 3.5 Dispensing a line on a PCB using DS 500 precision dispensing system.

In the experiment, the fluid FP® 4451 (provided by Dexter Corporation, USA) was chosen for dispensing, and the dispensing system described above was controlled to dispense lines on PCBs, as shown in Figure 3.5. The dispensing conditions for this experiment are given in Table 3.1. Under these conditions, the dispensing process was controlled to last for a time period of 100 seconds, and the average flow rate was determined by weighing the amount of fluid dispensed during this period using an electronic balance with a resolution of 0.01 mg. Changing the

air pressure and needle temperature while maintaining other dispensing conditions fixed, the dispensing process was repeated so that various flow rates could be obtained. It is noted in this experiment that, in order to reduce the involvement of the time-dependent behavior of FP® 4451 shown in the preceding chapter, the break period between two dispensing processes had to be maintained for a long enough time period to enable the recovery of the fluid viscosity. In this experiment, the break period was set as 10 minutes. The measured flow rates versus the air pressure and the needle temperature are shown in Figures 3.6 and 3.7, respectively.

Table 3.1 Conditions for dispensing lines.

Parameters	**Values**
Air pressure	2.45×10^5 Pa
Needle temperature	45 °C
PCB temperature	100 °C
Dispenser movement velocity	3 mm/sec.
Distance between needle and PCB	1.5 mm
Length of needle	16 mm
Internal diameter of needle	0.92 mm

Simulation has been carried out using the models developed in this chapter. For calculating the flow rate of fluid dispensed, the time-independent behaviour of FP® 4451, which was identified and given in previous chapter, was used and substituted into the flow rate model given in Equation 3-12. Then the amount of fluid dispensed per second was determined by multiplying the calculated flow rate with the fluid density (1780 Kg/m^3). The simulation was performed using Matlab, and the predicted results are shown in Figures 3.6 and 3.7, along with the measured results.

cone and the plate. The cone is usually made very obtuse (θ less that 4°), and this small cone angle ensures that shear rate is constant throughout the shearing gap. This is of particular advantage when investigating time-dependent flow behaviour because all fluid in the sample experiences the same shear history. The basic measurement of the rheometer is the summation of torque over the conical surface as a function of cone angular velocity, from which the fundamental flow curve of shear stress vs. shear rate can be established. Shear stress and shear rate are related to the torque, T, and the cone angular velocity, ω, respectively, which are given by

$$\tau = \frac{3T}{2\pi r^2} \quad \text{and} \quad \dot{\gamma} = \frac{\omega}{\sin\theta} \tag{2.20}$$

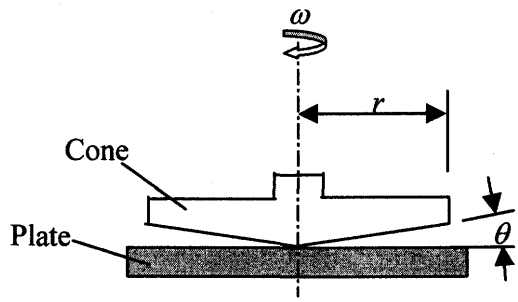

Figure 2.3 Cone-and-plate geometry.

In the experiments, a spindle with the cone geometry having a radius of 12.0 mm and an angle of 3.0 degree was chosen, and a fluid sample of 0.5 ml was required to fill the shearing gap between the cone and the plate. In addition, for the rheometer, the temperature of the cone-and-plate could be controlled within ± 0.1 °C through using an embedded temperature probe and a constant temperature bath [Brookfield].

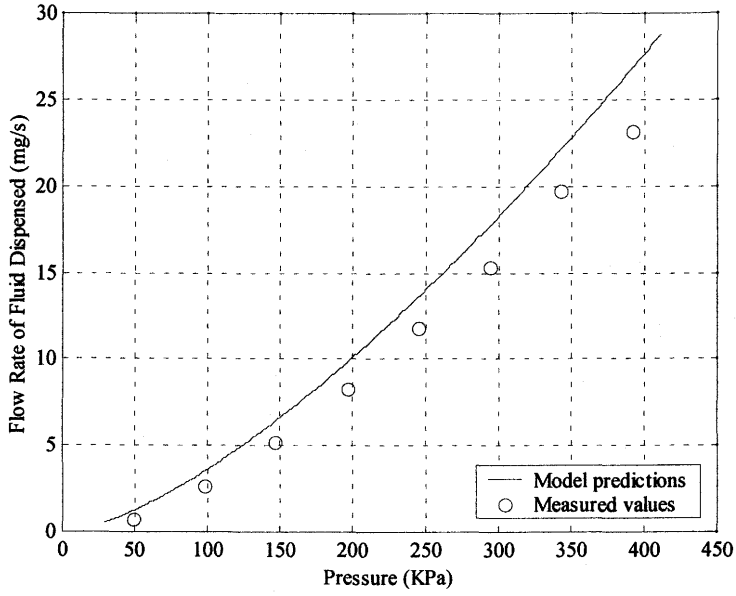

Figure 3.6 Measured and predicted effect of the driving air pressure on the fluid flow rate through the needle.

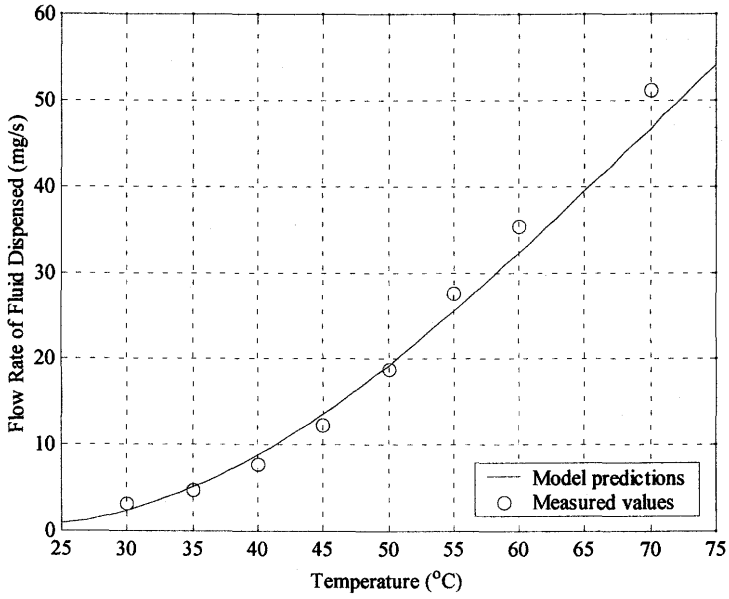

Figure 3.7 Measured and predicted effect of temperature on the fluid flow rate through the needle.

It can be seen that the simulation results are in close agreement with the experimental results, indicating that the model developed in this chapter is very promising for representing the flow rate. The discrepancy between them mainly results from the erroneous characterization of the fluid behaviour. There are two factors responsible for this inaccuracy. One is that the temperatures of a rheometer for identifying the fluid behaviour and the needle in the dispensing system are manipulated by different control systems. So very little difference between them can cause a big difference in the fluid behaviour because of the sensitivity of fluid behaviour to temperature. The other factor is the discrepancy of flow behaviour between different batches of fluid. The discrepancy of the flow rates due to the erroneous characterization of the fluid behaviour will be dealt with in Chapter 5.

3.4 Summary

This chapter presents the development of a steady-state model to represent the flow rate of fluid dispensed in the time-pressure dispensing process, under the assumption that the pressure in the syringe has reached a steady-state value. This assumption is valid when the dispensing process is proceeding continuously with given dispensing conditions, for example, dispensing lines on boards.

By applying the energy conservation at the air-fluid interface and the exit of the needle, the pressure drop in the needle is derived, taking into account the energy needed to overcome friction in the fully-developed flow and the minor losses due to the entrance effect, flow-through fitting, etc. Combining the representation of the

pressure drop with the characterization of the fluid behavior, a model is developed to represent the steady-state flow rate of fluid dispensed. From the model development, it can be seen that the flow rate of fluid dispensed is affected by factors such as the air supply pressure, the fluid temperature, etc.

To investigate experimentally the flow rate of fluid dispensed and validate the model developed, experiments were conducted on the DS500 precision dispensing system. They indicated that the flow rate could be significantly affected by the air supply pressure and the fluid temperature, and that the experimental results are in close agreement with the simulation results using the model developed.

4. MODELLING OF THE SHAPE OF FLUID FORMED ON A BOARD

In the preceding chapter, the flow rate of fluid dispensed was addressed in the fluid dispensing process. Once the fluid is dispensed or extruded from the needle, it drops onto a board, and then flows or spreads on the board until an equilibrium profile is formed. The cross-sectional shape of the profile is another very important index to measure the process performance. This chapter is to deal with the spreading of fluid on a board and to present the development of a model to represent the equilibrium shape of fluid formed on a board.

4.1 Problem Description and Related Research

4.1.1 Problem Description

Consider that fluid is spreading on a smooth, horizontal rigid board located at position z=0 and kept at a constant temperature, T=T_w, regulated by a temperature controller in the dispensing process, as shown in Figure 4.1. The fluid is surrounded by ambient air of temperature T_∞, and of relatively small viscosity and thermal conductivity compared to those of the fluid. In the fluid dispensing process, the

profiles of a line or dot can be formed on a board, depending on whether the needle moves horizontally or not. So the spreading of fluid can be considered in either two-dimensional Cartesian coordinates (x, z) for a line or axisymmetric cylindrical coordinates (r, z) for a dot.

In Figure 4.1, a represents the contact line between the fluid and the board, which will move with the spreading of fluid on the board until an equilibrium state is reached. h denotes the interface between the fluid and the ambient air. The problem considered in this chapter is to represent the interface mathematically so that the shape of the fluid formed on the board can be determined.

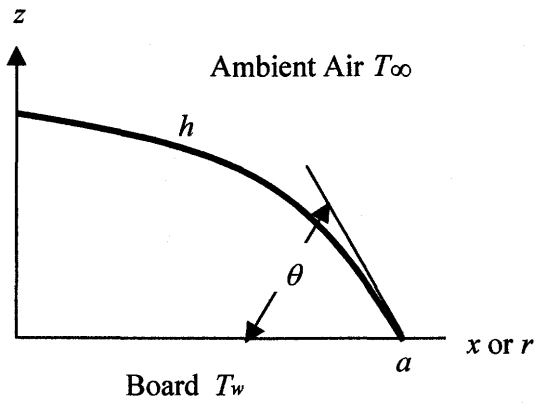

Figure 4.1 Half schematic of the spreading of fluid on a board.

4.1.2 An Overview of Related Research

The spreading of fluid on a smooth board is considered a fundamental problem in fluid mechanics and has attracted much attention [Schonhorn *et al.* 1966, Newman 1968, Greenspan 1978, Dussan V 1979, Hocking and Rivers 1982,

Ehrhard and Davis 1991, Haley and Miksis 1991, Chen *et al.* 2000]. The spreading process involves bulk, surface and line forces intrinsically coupled through a moving-boundary problem. In general, the velocity and thermal fields in the fluid are governed by the Navier-Stokes, continuity, and energy equations [Ehrhard and Davis 1991, Haley and Miksis 1991]:

$$\begin{aligned} &\rho\left\{\frac{\partial \boldsymbol{v}}{\partial t}+\boldsymbol{v}\cdot\nabla\boldsymbol{v}\right\}=-\nabla p+\mu\nabla^2\boldsymbol{v}-\rho g\boldsymbol{k}, \\ &\nabla\cdot\boldsymbol{v}=0, \\ &\rho c_p\left\{\frac{\partial T}{\partial t}+\boldsymbol{v}\cdot\nabla T\right\}=\lambda\nabla^2 T. \end{aligned} \tag{4.1}$$

where $\boldsymbol{k}=[0\ \ 1]^{\mathrm{T}}$, $\boldsymbol{v}=[u\ \ w]^{\mathrm{T}}$ is the velocity vector, p is the pressure, T is the temperature of the fluid, and μ, c_p and λ are the viscosity, specific heat and the thermal conductivity of the fluid, respectively.

Given the boundary and initial conditions, one could solve the above equations as function of time. In general, however, this is very difficult as what is involved is a moving-boundary problem for the Navier-Stokes equations. The problem can be simplified by using the lubrication approximation which assumes that the ratio of the height to the width of a line or the radius of a dot is very small [Greenspan 1978, Ehrhard and Davis 1991, Haley and Miksis 1991]. However, this assumption is not applicable to the case of fluid dispensing because the height of fluid formed is the same order of magnitude as the width or the radius. Fortunately, for the fluid dispensing process, what is concerned with is not the spreading process, but the outcome of this process, i.e. the final equilibrium shape of fluid formed on the

board. Therefore, one can establish the final equilibrium conditions and apply them to Equation 4.1 to simplify the problem, which will be detailed later in Section 4.3.

4.2 Introduction to Surface Tension and Contact Angle

In this section, two concepts of surface tension and contact angle, which are very important for the spreading of fluid on a board, are introduced and discussed.

4.2.1 Surface Tension

Surface tension refers to the basic thermodynamic parameter of the fluid and solid interface. It is governed by intermolecular interactions, and arises from the surface molecule interactions not only with neighboring molecules of the same phase, but also with the nearby molecules of the adjacent phase [Summ 1997, Adamson and Gast 1997]. Surface tension can be specified as a force exerted on a unit length contour bounding the fluid surface. This force is directed at a tangent to the surface and along the inner perpendicular to the contour, so that the dimension of surface tension is N/m. The surface tension is usually determined experimentally and then fit as a function of temperature for a given fluid [Tummala and Rymaszewski, 1989, Ehrhard and Davis 1991, Summ 1997, Han and Wang 1997].

The surface tension is of principal importance for the spreading of fluid on a board. The Laplace equation [Laplace 1806] manifests the relationship between the

surface tension, σ, and the pressure difference, Δp, across the curved fluid interface, as

$$\Delta p = \sigma(\frac{1}{r_1} + \frac{1}{r_2}) \tag{4.2}$$

where r_1 and r_2 are the principal curvature radii. For the case of a line formed on a board in the fluid dispensing process, the principal curvature radii shown in Figure 4.2 (a) are given by

$$r_1 = \frac{h''}{(1+h'^2)^{3/2}}, \qquad r_2 = \infty \tag{4.3}$$

For the case of a dot, the principal curvature radii shown in Figure 4.2 (b) are

$$r_1 = \frac{h''}{(1+h'^2)^{3/2}}, \qquad r_2 = r\frac{h'}{(1+h'^2)^{1/2}} \tag{4.4}$$

in Equations 4.3 and 4.4, h' and h'' denote the first and second derivatives with respect to x or r.

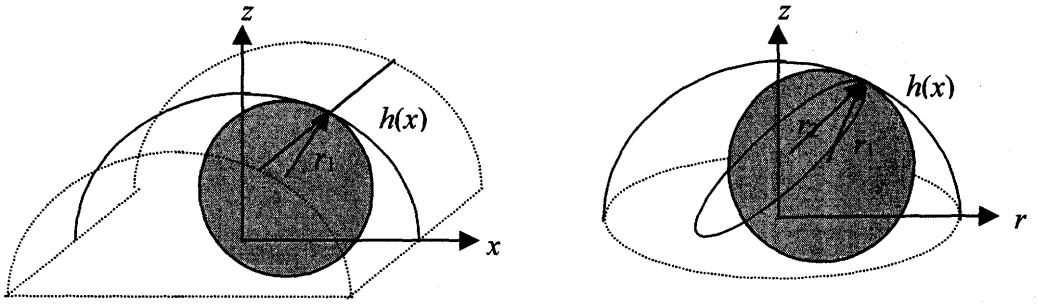

(a) (b)

Figure 4.2 Principal curvature radii; (a) a line and (b) a dot.

Substituting Equations 4.3 and 4.4 into Equation 4.2, respectively, yield

$$\Delta p = \sigma \frac{\mathrm{d}}{\mathrm{d}x}\left\{\frac{\mathrm{d}h(x)}{\mathrm{d}x}\left[1+\left(\frac{\mathrm{d}h(x)}{\mathrm{d}x}\right)^2\right]^{-1/2}\right\} \tag{4.5l}$$

$$\Delta p = \sigma \frac{1}{r}\frac{\mathrm{d}}{\mathrm{d}r}\left\{r\frac{\mathrm{d}h(r)}{\mathrm{d}r}\left[1+\left(\frac{\mathrm{d}h(r)}{\mathrm{d}r}\right)^2\right]^{-1/2}\right\} \tag{4.5d}$$

In the above equation numbers, *l* denotes for a line and *d* for a dot, which will also be used in the rest of this chapter.

4.2.2 Contact Angle

It is observed that in most instances a fluid placed on a solid board will not wet the board but remains as a drop having a definite angle of contact between the fluid

and board. This angle is called the contact angle shown as θ in Figure 4.1. Hundreds years ago, Young [1805] first derived an expression for the contact angle based on the surface tensions of the three material boundaries (air/fluid, fluid/board, and board/air). Over the past 50 years, extensive studies have been involved in the characterization of the contact angle and its influence on the spreading of fluid on solid surfaces. A comprehensive review of these studies was provided by Adamson and Gast [1997]. In these studies, the experimental determination of contact angle is important, and, for this purpose, various techniques have been developed and reported. One popular method is to measure the contact angle directly by drawing on an enlarged photograph of a line tangent to the fluid/air interface at the contact line. For this method, the limiting factor usually lies in the reproducibility of the measurements. In addition, similar to the surface tension, the contact angle is also temperature dependent [Han and Wang 1997 Adamson and Gast 1997].

As shown in Figure 4.1, due to the contact angle, there is a contact-angle condition at the contact line, i.e., the interface slope h' at the contact line at x or $r = a$ must satisfy the compatibility boundary condition given by

$$\left.\frac{dh}{dx}\right|_{x=a} = -\tan(\theta) \tag{4.6l}$$

$$\left.\frac{dh}{dr}\right|_{r=a} = -\tan(\theta) \tag{4.6d}$$

4.3 Modelling of the Shape of Fluid Formed on a Board

4.3.1 Equilibrium Conditions of the Spreading of Fluid on a Board

Once the spreading of fluid on a board reaches an equilibrium state, the following conditions must be satisfied.

(1) There is no movement in fluid.

$$\begin{aligned} u = 0; \quad \dot{u} = 0; \quad \ddot{u} = 0 \\ \omega = 0; \quad \dot{\omega} = 0; \quad \ddot{\omega} = 0 \end{aligned} \tag{4.7}$$

(2) Fluid reaches the same temperature as the board.

$$T = T_w \tag{4.8}$$

(3) The interface between the fluid and the air is symmetric and smooth.

$$\left.\frac{\mathrm{d}h(x)}{\mathrm{d}x}\right|_{x=0} = 0 \tag{4.9l}$$

$$\left.\frac{\mathrm{d}h(r)}{\mathrm{d}r}\right|_{r=0} = 0 \tag{4.9d}$$

(4) The volume of fluid is conserved throughout the spreading process under the assumption that fluid is assumed incompressible. Therefore, the following equations are established.

$$Q = 2v\int_0^a h(x)\mathrm{d}x \tag{4.10l}$$

$$V = Qt = \pi\int_0^{h(0)} r(h)^2\,\mathrm{d}h \tag{4.10d}$$

where Q is the volumetric flow rate of the fluid dispensed, v the velocity of the needle movement, a the position of the equilibrium contact line, V is the dot volume, t the dispensing time, $h(0)$ the height at $r = 0$, and $r(h)$ the inverse function of $h(r)$.

In addition, the interface retains an equilibrium shape under the actions of the surface tension and the pressure difference across the interface, and so Equation 4.5 must be satisfied. Also, a boundary condition is needed at the contact line, and it is given by Equation 4.6.

4.3.2 Equilibrium Shape of Fluid Formed on a Board

To represent the equilibrium shape formed on a board, substituting the equilibrium conditions described in Equations 4.7 and 4.8 into Equation 4.1 yields

$$\frac{\mathrm{d}p}{\mathrm{d}z} = -\rho g \tag{4.11}$$

Solving the above equation, the pressure in the fluid at height h is

$$p = p_0 - \rho g h \tag{4.12}$$

where p_0 is the pressure at h=0. Thus, the pressure difference Δp across the interface at height h can be obtained by

$$\Delta p = p - p_a = p_0 - p_a - \rho g h \tag{4.13}$$

where p_a is the pressure in the air around the fluid. Substituting the above equation into Equation 4.5 yields

$$p_0 - p_a - \rho g h(x) = \sigma \frac{\mathrm{d}}{\mathrm{d}x}\left\{ \frac{\mathrm{d}h(x)}{\mathrm{d}x}\left[1 + \left(\frac{\mathrm{d}h(x)}{\mathrm{d}x} \right)^2 \right]^{-1/2} \right\} \tag{4.14l}$$

$$p_0 - p_a - \rho g h(r) = \sigma \frac{1}{r}\frac{\mathrm{d}}{\mathrm{d}r}\left\{ r\frac{\mathrm{d}h(r)}{\mathrm{d}r}\left[1 + \left(\frac{\mathrm{d}h(r)}{\mathrm{d}r} \right)^2 \right]^{-1/2} \right\} \tag{4.14d}$$

Using the above equations and the equilibrium conditions given by Equations 4.6, 4.9, and 4.10, a numerical solution can be obtained for the final equilibrium shape $h(x)$ for a line or $h(r)$ for a dot.

4.4 Experimental Verification

The objective of the experiments is to determine the influence of the board temperature on surface tension and contact angle and to validate the model developed in this chapter. All experiments were performed using the dispensing system described in Chapter 3, and the fluid FP® 4451 was chosen for dispensing.

4.4.1 Influence of the Board Temperature on Surface Tension and Contact Angle

To identify the influence of the board temperature on surface tension and contact angle, a number of lines of fluid were dispensed on boards with various temperatures. Once the lines reached equilibrium shape, the width and height of the cross section of each line (as an example, Figure 4.3 shows the cross section), were measured using the HISOMET-II, which is a non-contact depth measuring microscope using an optical focal point detection system. The measured widths and heights are given in Table 4.1, along with the board temperatures and the cross-section areas of the lines. The area of each line, A, was determined by

$$A = \frac{W}{\rho L} \tag{4.15}$$

where W and L are the measured weight and length of the line. It is noted that the corss-section area is conserved during the spreading process.

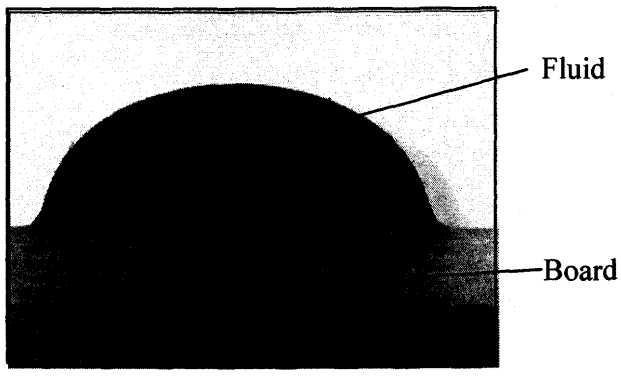

Figure 4.3 Cross section of a line of fluid dispensed on a board.

Table 4.1 Measured widths, heights, and cross-section areas of lines of fluid dispensed on boards with various temperatures.

	Line 1	Line 2	Line 3	Line 4	Line 5
Board Temperature (°C)	45	65	85	105	125
Width (mm)	1.372	1.357	1.300	1.271	1.296
Height (mm)	3.130	3.583	4.287	4.905	5.566
Area (mm^2)	3.3173	3.3886	3.8761	4.4112	5.0889

At each board temperature, based on the measured width, height and cross-section area of the line, the surface tension and contact angle were solved numerically using Matlab based on the model developed in this chapter. The surface tensions and contact angles at various temperatures are shown in Figures 4.4 and 4.5, respectively. Both the surface tension and contact angle decrease with an increase in temperature. In turn, they can be fitted to the temperature using a second-order polynomial, respectively,

$$\begin{aligned} \sigma &= C_{2\sigma}T^2 + C_{1\sigma}T + C_{0\sigma} \\ \theta &= C_{2\theta}T^2 + C_{1\theta}T + C_{0\theta} \end{aligned} \tag{4.16}$$

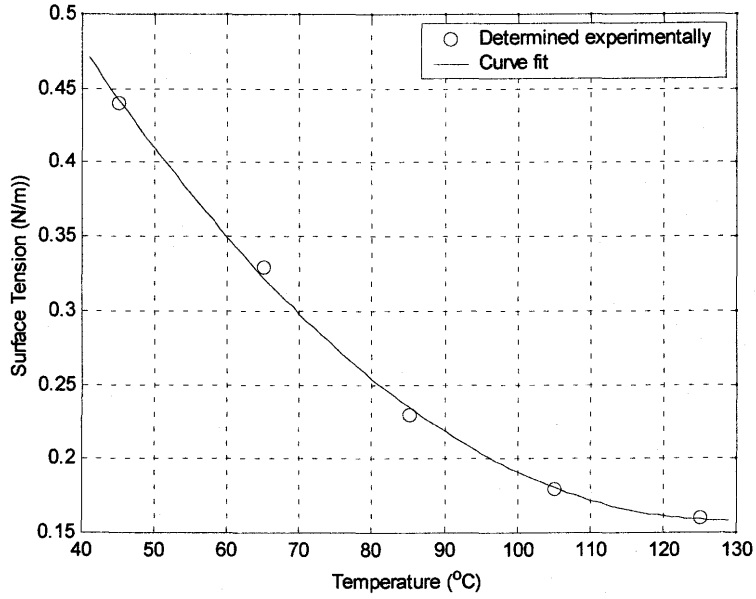

Figure 4.4 The influence of board temperature on the surface tension of the dispensed fluid.

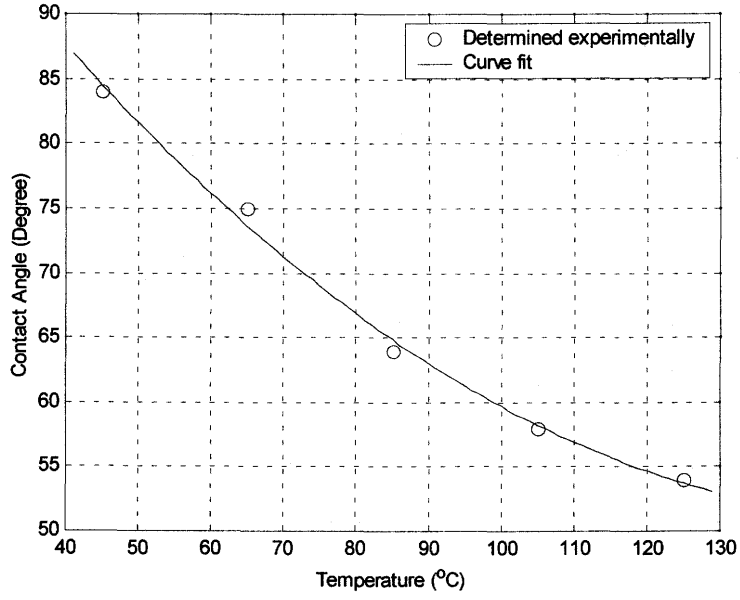

Figure 4.5 The influence of board temperature on the contact angle between the dispensed fluid and the board.

where Cs are curve-fitting parameters and their values are listed in Table 4.2. The fitted results are shown as solid lines in Figures 4.4 and 4.5.

Table 4.2 Values of curve-fitting parameters.

	$C_{2\sigma}$	$C_{1\sigma}$	$C_{0\sigma}$	$C_{2\theta}$	$C_{1\theta}$	$C_{0\theta}$
Values	4.11×10^{-5}	-0.0105	0.8336	0.0027	-0.8408	116.93

4.4.2 Validation of the Shape Model

In this experiment, two sets of lines of fluid were dispensed; one set was dispensed on the boards with the temperatures of 45°C, 65°C, 85°C, 105°C, and 125°C, respectively, and the other set was dispensed on the boards with the same temperature of 100 °C. As in the previous experiments, the widths, heights, and cross-sectional areas of all lines were measured. For the set of lines dispensed on boards with different temperatures, the measured results are given in Table 4.3. For the other set of lines, the measured widths and heights versus the cross-section areas are shown in Figures 4.6 and 4.7.

Simulations using Matlab to determine the width and height of a line were performed based on the model developed in this chapter. First, Equation 4.16 with parameters identified in the preceding experiment is used to calculate the surface tension and contact angle at various temperatures. They are then substituted into the model developed in this chapter to numerically determine the width and height of a line for a given cross-sectional area. The simulation results for the set of lines

dispensed on boards with different temperatures are also shown in Table 4.3 for comparison; and the simulation results for the set of lines dispensed on boards with the same temperature are shown as solid lines in Figures 4.6 and 4.7. It is seen that the simulation results are in close agreement with the experimental ones, which indicate that the model developed in this chapter is very effective in representing the shape of fluid formed on a board.

Table 4.3 Measured and predicted widths, heights of lines with various board temperatures and cross-section areas.

	Line 1	Line 2	Line 3	Line 4	Line 5
Area (mm^2)	6.9140	7.1458	8.6380	9.7616	11.2062
Board Temperature (°C)	45	65	85	105	125
Measured width (mm)	4.523	5.153	6.396	7.388	8.500
Predicted width (mm)	*4.555*	*5.229*	*6.418*	*7.529*	*8.629*
Measured height (mm)	2.006	1.828	1.826	1.778	1.787
Predicted height (mm)	*1.976*	*1.838*	*1.839*	*1.794*	*1.778*

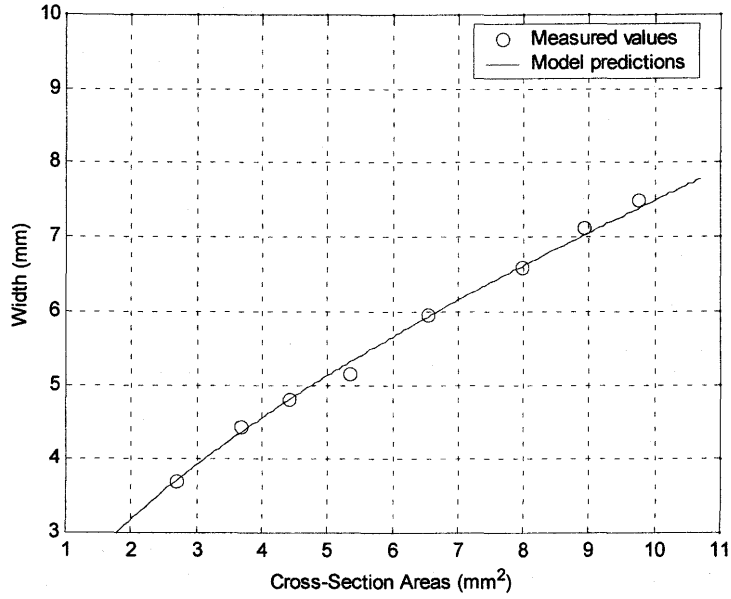

Figure 4.6 Measured and predicted widths of lines dispensed on the board at a board temperature of 100 °C.

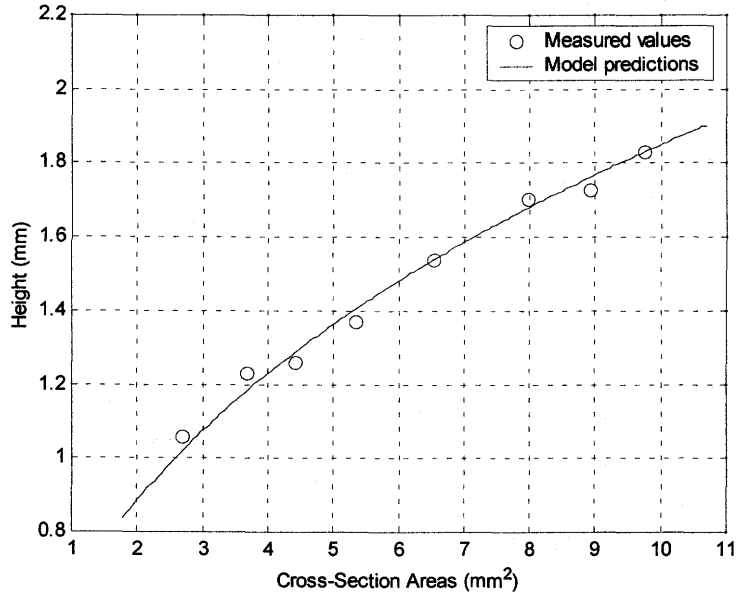

Figure 4.7 Measured and predicted heights of lines dispensed on the board at a board temperature of 100 °C.

4.5 Summary

Modelling the shape of fluid formed on a board in the dispensing process is a fundamental problem in fluid mechanics, i.e., the spreading of fluid on a smooth solid, which is a moving-boundary problem coupled with bulk, surface and line forces. This chapter has presented a brief review of the problem, indicating that it is extremely complicated to solve this problem unless some assumptions are made. Also, this chapter has introduced two concepts; surface tension and contact angle, which are important for the spreading of fluid on a board. To represent the equilibrium shape of fluid formed on a board, this chapter has established the equilibrium conditions and applied them to simplify the general equation that governs the spreading of fluid on a board. As a result, a model representative of the equilibrium shape of fluid was developed.

To investigate the influence of the board temperature on the surface tension and contact angle, experiments of dispensing lines on boards at various board temperatures were conducted. Surface tensions and contact angles at different temperatures were determined by using the model developed. Both surface tension and contact angle are temperature dependent and are fitted as second order polynomial functions of temperature. To validate the effectiveness of the model, the experiment of dispensing lines on boards with different temperatures and on boards with the same temperature was conducted. The measured widths and heights of the lines were compared with those obtained from the model, showing that the model is very effective in representing the shape of fluid on a board in the fluid dispensing process.

5. REPRESENTATION OF THE INFLUENCE OF TIME-DEPENDENT FLUID BEHAVIOR USING MODEL UPDATING

In the previous two chapters, models representative of the flow rate of fluid dispensed and the shape of fluid formed on boards were developed. It is noted in these model developments that fluid behavior is assumed time-independent. This assumption, however, is not always valid. As indicated in Chapter 2, most fluids employed in electronics packaging exhibit time-dependent flow behavior. The behaviour has a significant influence on the time-pressure dispensing process, and the representation of this influence is an extremely challenging task. The current state of the art in fluid mechanics does not provide a satisfactory solution to this problem. Developing a model from the first principles of fluid mechanics may not be an effective method in this situation because the shear history of fluid has to be known accurately. This chapter takes a different approach, model updating, to seek a solution to this problem.

5.1 Introduction to Model Updating

Using data acquired from a physical test or experiment, model updating is a method to improve a model by updating some parameters in the model that are considered to be less accurately modelled, so that the model can replicate or reproduce the experimental data. This method has been widely used in the improvement of models for structural dynamics [Foster and Mottershead 1990, Friswell and Penny 1992, Brughmans *et al.* 1993, Mottershead and Friswell 1993, Friswell and Mottershead 1995, Ben-Hai and Natke 1992, Fritzen and Zhu 1991].

The method of model updating can be briefly explained as follows. In Figure 5.1, two spaces are denoted; one is the space of parameters, $\boldsymbol{X}$, in which X_0 represents the vector of the initial parameter-values that are less accurately modeled in the primary stage of the model development and therefore in greater need of updating, and the other space is the performance of the system or process considered, $\boldsymbol{Y}$. Model prediction can be regarded as a mapping from $\boldsymbol{X}$ to $\boldsymbol{Y}$, for example, Y_0 is mapped from X_0. Due to the inaccuracy of modeling X_0, Y_0 disagrees with the measured performance, denoted by Y_m in the performance space. Model updating is considered as the inverse of model prediction with the objective of estimating the parameter change, ΔX, in the parameter space based on the performance difference, ΔY, so that the model using the updated parameters can accurately reproduce Y_m.

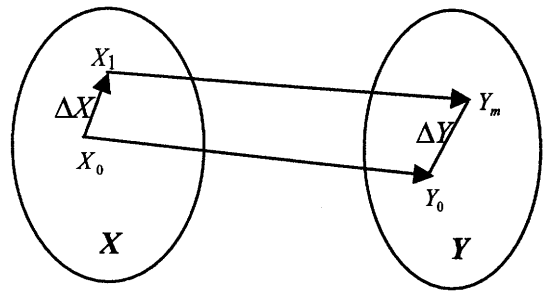

Figure 5.1 General model updating layout.

The complete process of model updating includes three parts; model preparation, performance measurement, and parameter estimation [Friswell and Mottershead 1995]. A model that will be updated requires, in its preparation, the consideration of factors not normally taken into account in regular model development. Of these, the parameterization of the inaccurate parts of the model is the most important. The model predictions should be sensitive to small changes in the parameters, otherwise updating will result in a change to the parameter of uncertain value because the difference between predictions and measurement data has been reconciled by change to other (more sensitive) parameters that might be less in need of updating. Measurement of the system performance is another important part in model updating, and the extent to which the model can be improved by this updating method depends upon the accuracy of measurements. In general, measurements are imprecise due to instrumentation noise, so it is always suggested that high quality hardware and advanced filtering technology be used. The estimation methods used in model updating are closely related to those of system identification. System identification addresses the problem of determining the order and structure of a

model from measurement data. Once the form of the structure has been decided upon, the coefficients are established by means of parameter estimation, which is performed on-line. In contrast, model updating is usually performed off-line using batch processing techniques. The aim is to generate improved models that may be applied to obtain predictions for alternative loading arrangements and modified structural configurations [Friswell and Mottershead 1995].

5.2 Model Preparation and Problem Description

In this section, the model for the time-pressure fluid dispensing process is summarized from the previous chapters. Then, the problem of representing the influence of time-dependent fluid behaviour on the dispensing process by model updating is described and presented.

Consider that fluid behaviour is characterized by the Generalized Power Law equation, the flow rate of fluid dispensed, Q, is repeated here from Chapter 3 (Equation 3.14).

$$Q = \frac{\pi D_n^3}{8K^{1/n}\tau_w^3}(\tau_w - \tau_0)^{(n+1)/n}\left[\frac{n}{3n+1}\tau_w^2 + \frac{2n^2}{(2n+1)(3n+1)}\tau_w\tau_0 + \frac{2n^3}{(n+1)(2n+1)(3n+1)}\tau_0^2\right] \tag{5.1}$$

The equilibrium shape of fluid formed on boards, $h(x)$, is obtained by numerically solving the following equation (repeated from Equation 4.14) with equilibrium conditions given by Equations 4.6, 4.9, and 4.10 of Chapter 4,

$$p_0 - p_a - \rho g h(x) = \sigma \frac{\mathrm{d}}{\mathrm{d}x}\left\{\frac{\mathrm{d}h(x)}{\mathrm{d}x}\left[1+\left(\frac{\mathrm{d}h(x)}{\mathrm{d}x}\right)^2\right]^{-1/2}\right\} \tag{5.2}$$

The height, H, of the determined shape is an important measurement in the control of fluid dispensing for electronic packaging. Together with the flow rate obtained from Equation 5.1, they span and constitute the performance space in model updating, which is denoted by,

$$Y = [Q, H]^{\mathrm{T}} \tag{5.3}$$

In the above model, there are five parameters involved, which are; τ_0 - yield stress, K - the consistency index, n - the flow behavior index, σ - the surface tension, and θ - the contact angle. These parameters sensitively affect the model prediction. As mentioned previously, the parameter values cannot be derived theoretically and have to be identified experimentally. Due to the discrepancy between the experiments for parameter identification and the real dispensing process, errors between the identified values and the actual values of these parameters are inevitable. Therefore, these parameters are considered as the least accurate component of the model and need to be updated. They span and constitute the parameter space in model updating, denoted by,

$$X = [\tau_0, K, n, \sigma, \theta]^{\mathrm{T}} \tag{5.4}$$

In this chapter, the values of these parameters are considered as time-variable due to the time-dependent fluid behavior, i.e. $X = X(t)$. For the same reason, the measured process performance is also a function of time, i.e. $Y_m = Y_m(t)$. The time-variable parameters and performance make this situation different from the circumstances where model updating is normally applied. As an extension of its application, model updating in this chapter is used to update and track the time-variable parameters, $X(t)$, so that the updated model can reproduce the measured performance, $Y_m(t)$, thereby representing the influence of time-dependent fluid behaviour on the dispensing process.

In the rest of the chapter, $X(t)$ and $Y_m(t)$ are still denoted by X and Y_m, respectively, for convenience.

5.3 Model Updating Approach

5.3.1 Linearization of Model and Sensitivity Matrix

From the model given in the last section, it is seen that the mapping from the parameter space $X = [\tau_0, K, n, \sigma, \theta]^{\mathrm{T}}$ to the performance space $Y = [Q, H]^{\mathrm{T}}$ is non-linear. For model updating, linearization of the mapping is necessary and can be

achieved using a Taylor series expansion for the mapping. As a result, the following linear approximation can be obtained.

$$\Delta Y = S \cdot \Delta X \tag{5.5}$$

where $S \in R^{2\times5}$ is called *sensitivity matrix*, ΔX is the parameter perturbation in the parameter space, and ΔY is the linear part of the change in the process performance caused by ΔX.

The sensitivity matrix, S, is developed from the first partial derivative of the process performance with respect to the parameters, and given by

$$S = \begin{bmatrix} \frac{\partial Q}{\partial \tau_0} & \frac{\partial Q}{\partial K} & \frac{\partial Q}{\partial n} & 0 & 0 \\ \frac{\partial H}{\partial \tau_0} & \frac{\partial H}{\partial K} & \frac{\partial H}{\partial n} & \frac{\partial H}{\partial \sigma} & \frac{\partial H}{\partial \theta} \end{bmatrix} \tag{5.6}$$

in which the zero elements represent the flow rate, Q, being independent upon σ and θ. The non-zero elements in the first row can be directly evaluated from Equation 5.1. The elements in the second row cannot be directly evaluated because no closed-form function is available. In such a situation, numerical finite difference approximations are used by perturbing the parameters individually.

5.3.2 Model Updating Using Singular Value Decomposition

Based on ΔY, which is the difference between the measured performance and model prediction, model updating is aimed to estimate the parameter change, ΔX, from Equation 5.5, thereby obtaining the updated parameters. It is important to note that $S^{\mathrm{T}}S$ is rank deficient in the problem considered here because the number of scalar equations included in Equation 5.5 is less than the number of the parameters needed to update. This problem is said to be under-determined and there are an infinite number of sets of parameter changes that satisfy Equation 5.5. The issue is which set of parameter change is the best choice. Considering that the values of the updated parameters are initially identified by experiments within an acceptable confidence level, choosing the smallest parameter change is a natural and reasonable approach. This allows the use of the singular value decomposition (SVD) method for the updating.

The singular value decomposition (SVD) of the sensitivity matrix is given by [Golub and Kahan 1965]

$$S = U \begin{bmatrix} \Sigma & 0 \\ 0 & 0 \end{bmatrix} V^{\mathrm{T}} \tag{5.7}$$

where $\Sigma \in R^{2\times 2}$ is a diagonal matrix containing the singular values of matrix S in descending order ($\sigma_1 \geq \sigma_2$), i.e., $\Sigma = \mathrm{diag}(\sigma_1 \ \sigma_2)$, and $U \in R^{2\times 2}$ and $V \in R^{5\times 5}$ are orthonormal matrices. The pseudo-inverse of S is given by

$$D = \begin{Bmatrix} d_1 \\ d_2 \end{Bmatrix} \tag{5.13}$$

then Equation 5.9 can be rewritten in the form,

$$\left\| \Delta Y - S\Delta \widehat{X} \right\|_2 = \left\| \begin{Bmatrix} c_1 \\ c_2 \end{Bmatrix} - \begin{bmatrix} \Sigma & 0 \\ 0 & 0 \end{bmatrix} \begin{Bmatrix} d_1 \\ d_2 \end{Bmatrix} \right\|_2 = \left\| \begin{Bmatrix} c_1 - \Sigma d_1 \\ c_2 \end{Bmatrix} \right\|_2 \tag{5.14}$$

The above equation will be a minimum if $d_1 = \Sigma^{-1} c_1$ and the value of d_2 is arbitrary. The solution, $\Delta \widehat{X}$, obtained if $d_1 = \Sigma^{-1} c_1$ and $d_2 = 0$, is given from Equation 5.11 such that

$$\Delta X = V \begin{Bmatrix} \Sigma^{-1} c_1 \\ 0 \end{Bmatrix} = V \begin{bmatrix} \Sigma^{-1} & 0 \\ 0 & 0 \end{bmatrix} \begin{Bmatrix} c_1 \\ c_2 \end{Bmatrix} \tag{5.15}$$

By combining the above equation with Equation 5.10 an estimate of ΔX can be obtained in terms of the pseudo-inverse of S given in Equation 5.8, i.e.

$$\Delta X = S^{+} \Delta Y \tag{5.16}$$

It can be seen from Equation 5. 15 that for any solution when $d_2 \neq 0$, one has

$$\left\| \Delta X_{d_2 \neq 0} \right\| > \left\| \begin{Bmatrix} \Sigma^{-1} c_1 \\ 0 \end{Bmatrix} \right\| \tag{5.17}$$

Hence, the SVD solution given in Equation 5.16 is the unique minimum norm solution.

It can be seen from Equation 5.16 that the errors in measurements are propagated through ΔY to the estimate of parameter change, ΔX. This propagation is proportionally dependent on the condition number of S_j [Friswell and Mottershead 1995], and is given by,

$$C = \frac{\sigma_1}{\sigma_2} \tag{5.18}$$

To reduce this error propagation, the condition number should be small. Rewriting Equation 5.5 yields

$$\Delta Y = (SN)N^{-1}\Delta X = S_m N^{-1}\Delta X \tag{5.19}$$

where $N \in R^{5\times5}$ is a diagonal matrix containing the initial parameter values, i.e. $N = \text{diag}(X_0)$, and S_m is the modified sensitivity matrix obtained by multiplying N. In this problem, it was found that the condition number of S_m could be much smaller than that of S for typical fluid dispensing process settings. Hence, instead of S, S_m is used in model updating. Similarly, the singular value decomposition is applied to S_m to obtain its pseudo-inverse, S_m^+. An estimate, ΔX, can be obtained from Equation 5.19

$$\Delta X = NS_m^+ \Delta Y \tag{5.20}$$

Thus, the updated parameters are established in full with the substitution $\Delta Y = Y_m - Y_0$

$$X_1 = X_0 + diag(X_0) S_m^+ (Y_m - Y_0) \tag{5.21}$$

5.3.3 Recursive Scheme of Model Updating

The singular value decomposition allows us to find ΔX, and the updated parameters, X_1. It is noted that the process is performed based on a linear mapping from the parameter space to the performance space. In practice, the influence of the non-linearity has to be considered.

Suppose e is the acceptable maximum value of the difference between the measured performance and the model prediction, i.e.

$$\|Y_m - Y_1\| \le e \tag{5.22}$$

where Y_1 is the model prediction based on the updated parameter X_1. Due to the influence of the non-linearity, the above equation may not be satisfied. In such a case, the process presented in the above has to be repeated. The second process can be established using the following substitutions

$$S_m = S_m(X_0 + \Delta X)$$
$$\Delta Y = Y_m - Y_1 \tag{5.23}$$

As a result, a new updated parameter, X_1, can be obtained. If the Condition 5.22 is satisfied, the latest X_1 is then accepted. Otherwise, the above process has to be repeated until the condition is satisfied. Therefore, a recursive scheme can be developed to update the parameters iteratively. The flowchart of the recursive scheme is shown in Figure 5.2.

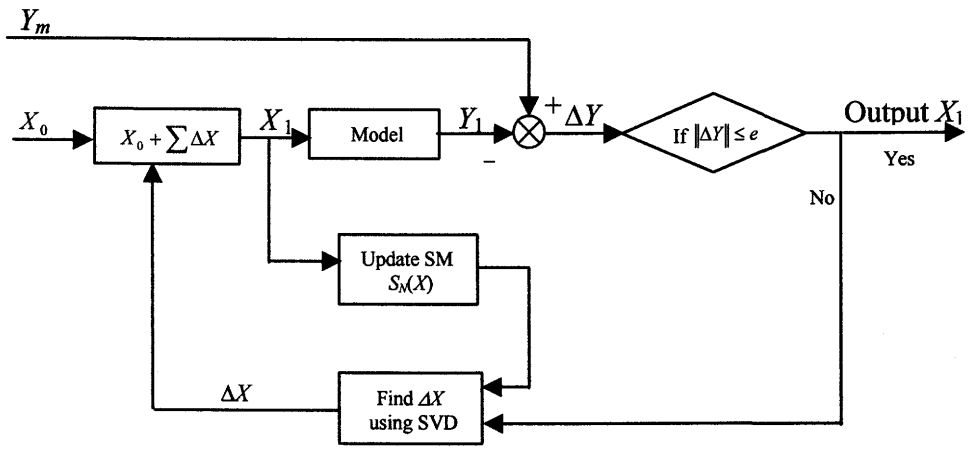

Figure 5.2 Flowchart of the recursive scheme of model updating.

From the above analysis, it is seen that, once a measurement of the process performance is available, the recursive scheme can be used to update the parameters so that the model can replicate the measured performance. Therefore, if the process performance can be measured with a proper sampling period, model updating can be used to track the time-variable parameters in the model, while representing the influence of time-dependent fluid behaviour on the dispensing process.

5.4 Experiments and Model Updating Results

To validate the effectiveness of the above model updating method in fluid dispensing processes, experiments were conducted on the dispensing system described in Chapter 3. In the experiment, fluid FP® 4451 was chosen for dispensing. The system was controlled to dispense lines on PCBs using the settings listed in Table 5.1.

Table 5.1 Settings of the fluid dispensing process.

Description	Values
Pressure of the pressurized air (Pa)	343,000
Needle temperature (°C)	45
Board temperature (°C)	100
Ambient temperature (°C)	25
Velocity of the Needle Movement along Y Axis (mm/s)	3
Internal Diameter of Needle (mm)	0.92
Length of Needle (mm)	16.0

Under these settings, the model given in Section 5.2 with the model parameter values listed in Table 5.2 is used to determine the process performance, i.e., the flow rate of fluid dispensed and the height of the shape of fluid formed on PCBs. The results are also shown in Table 5.2.

Table 5.2 Model parameter values and model predictions.

	Parameters					Model Predictions	
	τ_0, Pa	K, Pa·s^n	n, Dimensionless	σ, N/m	θ, Degree	Q, mm^3/s	H, mm
Values	55.784	198.232	0.602	0.209	75.028	7.609	1.124

To illustrate the influence of the time-dependent fluid behaviour on the process performance, the flow rate and the height were sampled randomly over a working day (8 hours), and the measured results are given in Table 5.3. It is seen that the measured performance can deviate from the model prediction significantly in a working day due to the time-dependent fluid behaviour.

Table 5.3 Process performance sampled randomly over a working day (8 hours).

Sample No.	1	2	3	4	5	6	7	8	9	10
Q_m, mm^3/s	6.793	7.228	6.132	6.327	5.888	6.320	6.834	6.448	6.615	6.152
H_m, mm	1.071	1.076	1.002	1.018	0.973	1.037	1.047	1.026	1.023	0.996

Based on the above measured performance, the model updating method was applied with the objective of updating the model parameter so that the model can still reproduce the measured performance. In model updating, the difference between the measured and predicted performance is determined according to the following definition such that the flow rate and the height have the same order of magnitude, i.e.,

$$\|Y_m - Y\| = \sqrt{\frac{|Q_m - Q|}{\pi v} + (H_m - H)^2} \tag{5.24}$$

where v is the velocity of the needle movement. In this study, the maximum difference (or acceptable error) calculated from the above equation is set as 0.02. For each set of the measurement data, i.e., $Y_m = [Q_m, H_m]^T$, the recursive scheme shown in Figure 5.2 was applied to update the parameters. As an example, Table 5.4

shows the updated parameters and model prediction at each iteration for the first set of data, i.e. $Y_m = [6.793, 1.071]^T$. On convergence, it is seen that the model with updated parameters can accurately reproduce the measured performance. Using all sets of measurement data, Figure 5.3 shows the results of the updated parameters, in which the parameters are given in terms of values normalized with respect to their initial values, and Table 5.5 shows the difference between the measured performance and the predicted performance after model updating, calculated using Equation 5.24. It is seen that, by updating the model parameters, the model is still capable of accurately replicating the process performance at all sampling points, which indicates the effectiveness of model updating to represent the influence of time-dependent fluid behaviour on the process performance.

Table 5.4 Results of model updating using the data $Y_m = [6.793, 1.071]^T$.

	Parameters					Model predictions	
	τ_0, Pa	K, Pa·s^n	n, Dimensionless	σ, N/m	θ, Degree	Q, mm^3/s	H, mm
Initial	55.784	198.232	0.602	0.209	75.028	7.609	1.124
1th iteration	55.788	199.827	0.616	0.212	83.004	6.852	1.133
2th iteration	55.788	199.959	0.616	0.214	75.844	6.794	1.072

Table 5.5 Difference between the measured performance and the predicted performance after model updating.

Sample No.	1	2	3	4	5	6	7	8	9	10
Difference	0.007	0.011	0.002	0.002	0.003	0.004	0.004	0.003	0.003	0.004

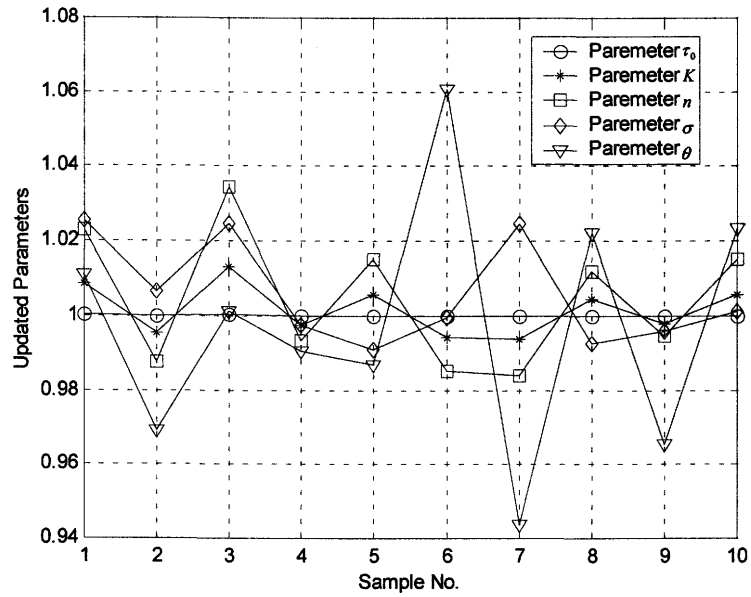

Figure 5.3 Normalized values of updated parameters over a typical working day.

5.5 Summary and Discussions

The representation of the influence of time-dependent fluid behaviour on the time-pressure fluid dispensing process is a challenging task. The current state of the art in fluid mechanics does not provide a satisfactory solution to this problem. The motivation of this chapter is to look into solutions to this problem from a different perspective, i.e., model updating. Using experimental data, model updating is a method to improve a model by updating the parameters that are considered less accurately modelled.

Mathematically, the application of model updating to the fluid dispensing process results in an under-determined problem. Singular value decomposition

(SVD) is applied on the sensitivity matrix to find a unique minimum norm solution. To alleviate the error propagation, a modified sensitivity matrix having a smaller condition number is actually employed, which is obtained from multiplying the sensitivity matrix by a diagonal matrix containing the initial parameter values. Considering the influence of the non-linearity of the model, a recursive scheme is developed to update parameters iteratively until the model can reproduce the measurement data within an acceptable error. Note that the above strategy is utilized for model updating by using one set of measurement data.

It was observed in previous experiments that the change of the influence of time-dependent fluid behaviour on the performance of the time-pressure dispensing process is slow with respect to time. As a result, it is possible to measure the process performance with a proper sampling period to represent the process-performance change with time. Thereby, the above strategy can be used to update the parameters, which are considered time-variable, so that the updated model can track and represent the influence of time-dependent fluid behaviour. The strategy of model updating is actually a preparation for controlling fluid dispensing, in which, based on the updated model, a control action can be generated to compensate for the influence of the fluid time-dependent behaviour in order to achieving the performance consistency. This work will be presented in Chapter 7.

To validate the effectiveness of the novel application of model updating, experiments were conducted to dispense lines on PCBs, and the process performance (i.e. the flow rate of fluid dispensed and the shape of fluid formed on PCBs) sampled randomly over a working day were used to update the model. The

results show that model updating is an effective method to represent the influence of time-dependent fluid behaviour in time-pressure dispensing.

6. DYNAMIC MODELING OF THE FLOW RATE OF FLUID DISPENSED

6.1 Introduction

In Chapter 3, a steady-state model for the flow rate of fluid dispensed in the time-pressure dispensing process was presented. The development of this model assumed that the pressure in the syringe had reached a steady-state value, so the influence of air compressibility can be neglected. However, in many applications of fluid dispensing, such as SMT, small amounts of fluid need to be dispensed by applying short-duration pressure pulses (typically 50 ms to 250 ms), in which air compressibility can have a significant influence on the amount of fluid dispensed under each pressure pulse. To represent the amount, a physical model to represent the flow rate dynamics, taking into account air compressibility, is obviously desirable and necessary.

This chapter presents the development of such a model. It includes two major steps; the representation of the transient response of pressure built up in the syringes by taking into account the compressibility of the air in the transmission line and syringe, and the representation of the flow rate by combining the pressure transient response and the influence of fluid inertia.

6.2 Dynamic Modelling of the Pressure in the Syringe

The schematic of time-pressure dispensing given previously in Figure 1.3 is repeated here in Figure 6.1. As far as the transient response of pressure in the syringes is concerned, the dynamics of the valve, the air transmission line, and the air in the syringe need to be considered.

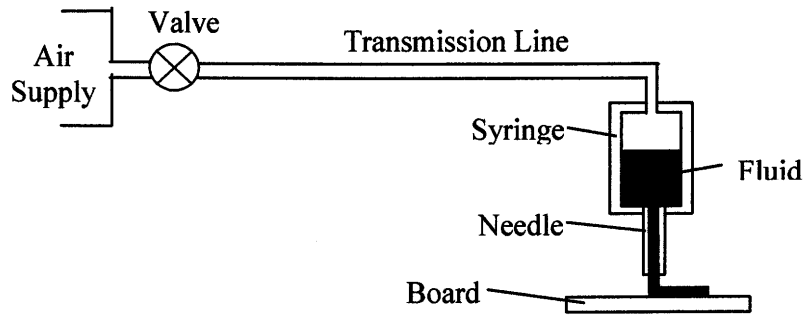

Figure 6.1 Schematic of a typical time-pressure dispensing process.

6.2.1 The Pneumatic Solenoid Valve

In time-pressure dispensing, a solenoid valve is usually used for the purpose of regulating the pressure-pulse width. A typical structure of this type of valve is schematically shown in Figure 6.2. It mainly consists of a poppet, a core, a coil, and a spring. As a current passes through the coil, a magnetic force is generated and acts on the core and then on the poppet, tending to move the poppet and open the valve, which is normally closed under the spring force.

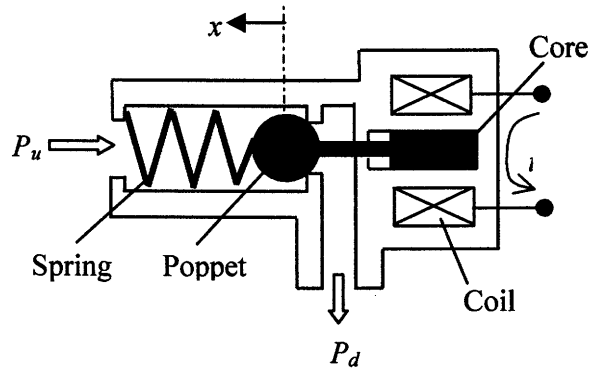

Figure 6.2 Schematic of a pneumatic solenoid valve.

By applying the equilibrium equation of the forces acting on the poppet, the motion of the poppet, x, is governed by [Ye *et al.* 1992],

$$m\ddot{x} + b\dot{x} + kx = F_m - F_a - kl_0 \tag{6.1}$$

where m is the total mass of both the poppet and the core, b is the viscous friction coefficient, k is the spring stiffness, l_0 is the initial compressed length of the spring, F_m is the magnetic force dependent on the current passing through the coil [Pawlak and Nehl 1988], and F_a is the flow force, which depends on the upstream and downstream pressures and the geometry of the poppet and the restricted passage as well [Andersen 1967, McCloy and Martin 1980].

The area of the air flow passage of the valve, A, is a function of the position of poppet and depends on the geometry of the poppet, i.e.,

$$A = f_a(x) \tag{6.2}$$

By assuming an isentropic process, the mass flow rate of air through the valve can be written as [Andersen 1967, McCloy and Martin 1980]

$$\dot{m} = \frac{C_m C_d A P_u}{\sqrt{T_u}} \tag{6.3}$$

where P_u is the upstream pressure, T_u is the upstream air temperature, C_m and C_d are the mass flow parameter and discharge coefficient, respectively. Coefficients C_m and C_d are given by

$$C_m = \begin{cases} \sqrt{\dfrac{\gamma}{R}\left(\dfrac{2}{\gamma+1}\right)^{\frac{\gamma+1}{\gamma-1}}} = 0.0405 & \dfrac{P_d}{P_u} < 0.528 \text{ for air} \\ \sqrt{\dfrac{2\gamma}{R(\gamma-1)}\left[\left(\dfrac{P_d}{P_u}\right)^{\frac{2}{\gamma}} - \left(\dfrac{P_d}{P_u}\right)^{\frac{\gamma+1}{\gamma}}\right]^{\frac{\gamma+1}{\gamma}}} & \dfrac{P_d}{P_u} \geq 0.528 \text{ for air} \end{cases} \tag{6.4}$$

and

$$C_d = \frac{\dot{m}_{\text{measured}}}{\dot{m}_{\text{calculated with } C_d=1}} \tag{6.5}$$

in which γ is the ratio of the specific heats (1.4 for air), R a constant (287 J/kg/K for air), and P_d the downstream pressure.

It is noted that the product of the terms, C_dA, in Equation 6.3 is usually combined into one term for engineering use, and is called the effective area. It can be seen that the effective area is ultimately dependent not only on the current passing through the coil, but also on the internal structure of the solenoid valve that is in general not known by the user and not easily measured. So it is rather difficult and not a very effective way to develop an analytical model to represent the effective area. In this study, an experimental method is employed to identify the effective area, which will be described in Section 6.4.2 later on.

6.2.2 The Air Transmission Line

Figure 6.3 shows the pneumatic transmission line in time-pressure dispensings, with one end connected to a valve and the other end to an orifice. The mass flow rates at the two ends are denoted by $\dot{m}_1$ and $\dot{m}_2$, respectively.

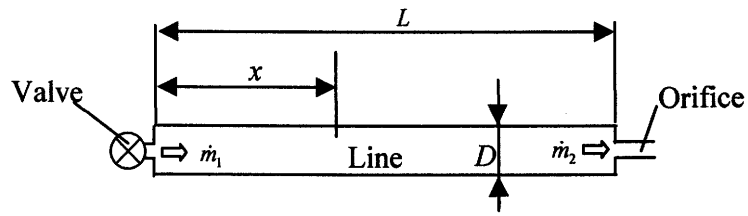

Figure 6.3 Schematic of a pneumatic transmission line.

The pressure in the line is a function of the position along the line and time. Assuming the flow in the line is laminar, one-dimensional, and adiabatic, the pressure is generally governed by the following partial differential equations [Schuder and Binder 1959, Brown 1962, Andersen 1967]

$$\frac{\partial p}{\partial x} = -\frac{32\mu}{D^2}u - \frac{p}{RT_l}\frac{\partial u}{\partial t}$$
$$\frac{\partial p}{\partial t} = -\gamma p\frac{\partial u}{\partial y} \tag{6.6}$$

where x is the distance from the sending end, p and u are the pressure and the air flowing velocity at x, and D, T_l, and μ are the line internal diameter, the line average temperature, and the dynamic viscosity of air, respectively.

Combining the boundary and initial conditions, one could solve the above equations. In general, however, this is an extremely demanding task and in most cases not practical unless some further assumptions are introduced. Some work in the general field has been reported in the literature. Bradner [1949], Iberall [1951], Rohmann and Grogan [1957], Franke *et al.* [1972] addressed the frequency response of the pressure in the transmission line as a harmonic pressure excitation occurs at one end of the transmission line. Bchuder and Binder [1959] exclusively investigated the response of transmission lines to a step excitation. Extension to the above studies was given by Hougen et. al. [1963] and Andersen [1967], in which the first- and second-order models were used to represent the response of transmission lines. Brown [1962] introduced the characteristic impedances of a transmission line, i.e., series impedance and shunt admittance, to represent the transient response. It is important to note that one of the most common assumptions used in the above studies is that the pressure change in the line is small in comparison with the mean pressure such that the air density can be treated as constant and evaluated at the mean pressure. This assumption makes it possible to simplify the above equation.

Unfortunately, this assumption is not valid for the dispensing process where the pressure changes significantly, moving from a pressure of one bar to several bars. In order to simplify this problem without loss of generality, a lumped parameter analysis is used for the transmission line, in which the line is modeled as a fixed volume chamber between the valve and the orifice. This assumption is reasonable for the dispensing process, considering that the line length (typically 2-4 m) is short and the resistance of the transmission line to the air flow is negligible in comparison with the resistance of the orifice. Under this assumption, the line pressure, P_l, is considered as uniform and governed by

$$\frac{dP_l}{dt} = \frac{\gamma R T_l}{A_l L}(\dot{m}_1 - \dot{m}_2) \tag{6.7}$$

where A_l, L, and T_l are the line cross-section area, length, and temperature, and $\dot{m}_1$ and $\dot{m}_2$ are the mass flow rates through the valve and orifice, correspondingly, which can be determined by Equation 6.3.

6.2.3 The Air in the Syringe

In time-pressure dispensing, the syringe contains air and fluid simultaneously, with the top connected to an orifice and the bottom to a needle, as shown in Figure 6.4. One of the distinct characteristics is that, as the dispensing proceeds, the fluid amount left in the syringe decreases while the air volume increases. The air in the syringe must be modelled as a time varying volume.

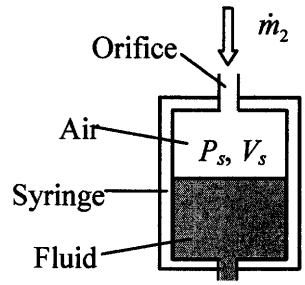

Figure 6.4 Schematic of a syringe containing air and fluid.

Provided that the air pressure in the syringe is treated as uniform, it can be given by [Andersen 1967]

$$\frac{dP_s}{dt} = -\frac{rP_s}{V_s}\frac{dV_s}{dt} + \frac{rRT_s}{V_s}\dot{m}_2 \tag{6.8}$$

where P_s, V_s, and T_s are the pressure, air volume, and temperature of the syringe, respectively, and $\dot{m}_2$ is the mass flow rate of the air into the syringe through the orifice.

If the internal diameter of syringe is much greater than that of the needle, the first term of the right side of Equation 6.8 can be neglected because of very small dV_s / dt. In such a case, Equation 6.8 can be reduced to

$$\frac{dP_s}{dt} = \frac{rRT_s}{V_s}\dot{m}_2 \tag{6.9}$$

$$S^{+} = V\begin{bmatrix} \Sigma^{-1} & 0 \\ 0 & 0 \end{bmatrix} U^{\mathrm{T}} \tag{5.8}$$

An important property of the SVD in model updating is that its application to the under-determined problem results in a unique minimum norm solution [Friswell and Mottershead 1995]. Consider,

$$\left\| \Delta Y - S\Delta\hat{X} \right\|_2 = \left\| U^{\mathrm{T}} \left(\Delta Y - SVV^{\mathrm{T}} \Delta\hat{X} \right) \right\|_2 \tag{5.9}$$

where $\Delta\hat{X}$ is the estimate of ΔX, and $\| \cdot \|_2$ represent the 2-norm of a vector.

Let

$$C = U^{\mathrm{T}} \Delta Y \tag{5.10}$$

$$D = V^{\mathrm{T}} \Delta X \tag{5.11}$$

If C and D are partitioned such that

$$C = \begin{Bmatrix} c_1 \\ c_2 \end{Bmatrix} \tag{5.12}$$

6.2.4 The Pressure in the Syringe

The transient response of the pressure in the syringe can be determined by integrating the dynamics of the components connected between the air supply and the syringe. The flow chart of this integration is shown in Figure 6.5, in which P_{as} denotes the pressure of the air supply.

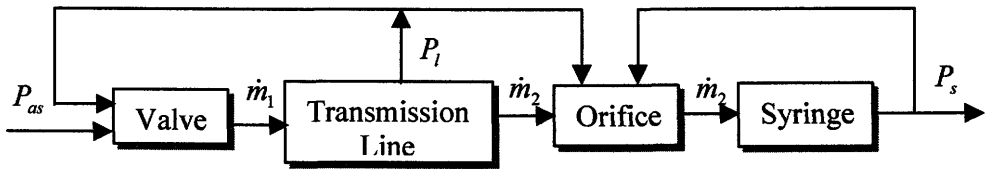

Figure 6.5 Flow chart of determining the pressure in the syringe.

It is important to note that, because of the dependence of the dynamics on the air volume in the syringe, as indicated in Equation 6.8 or 6.9, the transient response of the pressure in the syringe to the same pressure pulse from the air supply will not be the same at different air volumes in the syringe. This is considered as the main reason resulting in the inconsistency of the amount of fluid dispensed in time-pressure dispensing.

6.3 Dynamic Modeling of the Flow Rate of Fluid Dispensed

In this section, based on the pressure in the syringe established previously, the flow rate of fluid dispensed is represented taking into account fluid inertia. For this purpose, the following assumptions are made: (1) the fluid is incompressible and in fully-developed laminar flow, and (2) the internal diameter of the syringe is much larger than that of the needle, which implies that the pressure drop in the syringe can be ignored.

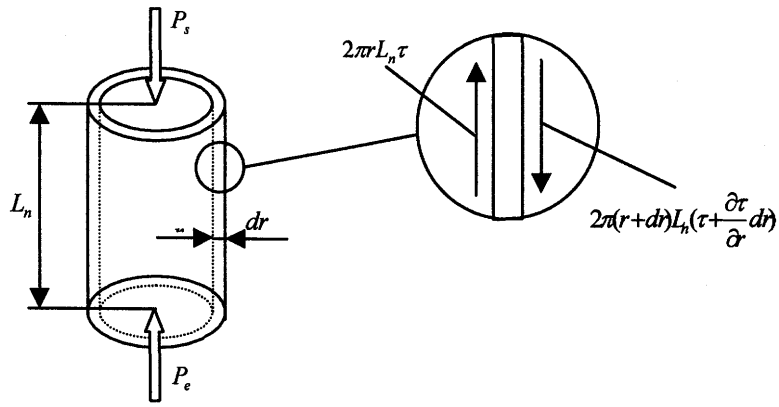

Figure 6.6 Forces acting on the vertical annular element of fluid in a needle.

Consider the fluid in a vertical annular element in the needle at the radius of r, which has a radial thickness, dr, and the same length as the needle, L_n, as shown in Figure 6.6. A summation of forces acting on the annular element of fluid leads to

$$2\pi r dr \Delta P + \sum F_{shear} = 2\pi r dr L_n \rho \frac{\partial u}{\partial t} \tag{6.10}$$

where ΔP is the pressure drop in the needle ($\Delta P = P_s - P_e$, in which P_s and P_e denote the pressures in the syringe and atmosphere, respectively), ρ the fluid density, and u the fluid flowing velocity. In the above equation, the term of the right side is the acceleration force due to fluid inertia, the first term of the left side is the force due to the pressure drop ΔP, and the second one denotes the summation of the forces acting on the inside and outside surface of the element resulting from fluid viscousness, as shown in Fig. 5, which is given by

$$\sum F_{shear} = 2\pi(r+dr)L_n(\tau + \frac{\partial \tau}{\partial r}dr) - 2\pi r L_n \tau = 2\pi dr L_n(r\frac{\partial \tau}{\partial r} + \tau) \qquad (6.11)$$

where τ is the shear stress in fluid.

Substituting Equation 6.11 into Equation 6.10 and then dividing by $2\pi r dr L_n$ yield

$$\frac{\Delta P}{L_n} + \frac{\partial \tau}{\partial r} + \frac{\tau}{r} = \rho \frac{\partial u}{\partial t} \qquad (6.12)$$

To solve the above equation, the fluid flow behaviour, i.e., relationship between shear stress and shear rate needs to be utilized. It is known in Chapter 2 that this relationship is either linear for Newtonian fluids or non-linear for non-Newtonian fluids. For Newtonian fluids, suppose the flow behaviour is given by,

$$\tau = K\dot{\gamma} \tag{6.13}$$

where K is the fluid viscosity, and $\dot{\gamma}$ is the shear rate in fluid and given by $\dot{\gamma} = -\partial u / \partial r$. Thus, Equation 6.12 can be rewritten as

$$\frac{\Delta P}{L_n} - \frac{K}{r}\frac{\partial}{\partial r}\left(r\frac{\partial u}{\partial r}\right) = \rho\frac{\partial u}{\partial t} \tag{6.14}$$

Using the assumption that the flow in the needle is fully developed laminar, the second term of the left side in the above equation can be simplified and replaced by $32Ku / D_n^2$ [Andersen 1967]. Hence, one has

$$\frac{\Delta P}{L_n} = \frac{32K}{D_n^2}u + \rho\frac{\partial u}{\partial t} \tag{6.15}$$

As the above equation is given linearly in the velocity, u, the average velocity, u_{ave}, can be used to replace it. As a result, the equation is reduced to

$$\frac{\Delta P}{L_n} = \frac{32K}{D_n^2}u_{ave} + \rho\frac{du_{ave}}{dt} \tag{6.16}$$

Thus, the transfer function for the above equation can be derived and given as

$$\frac{Q(s)}{\Delta P(s)} = \frac{A_n V_{ave}(s)}{\Delta P(s)} = \frac{A_n}{\rho L_n s + \frac{32KL_n}{D_n^2}} = \frac{Q_u}{\rho L_n \frac{Q_u}{A_n}s + 1} \tag{6.17}$$

where Q_u denotes the steady-state flow rate of the fluid under a unit pressure drop and is given by

$$Q_u = \frac{\pi D_n^4}{128 K L_n} \tag{6.18}$$

It can be seen for Newtonian fluids that the dynamics of the flow rate to the pressure drop is equivalent to a first-order system, in which the steady-state value depends upon Q_u and the time constant upon both the fluid inertia (measured by ρL_n) and the steady-state average velocity (measured by Q_u / A_n).

For non-Newtonian fluids, the flow behaviour is nonlinear as discussed in Chapter 2. It is important to note that substitution of this nonlinearity into Equation 6.12 may make it exceedingly complex and extremely difficult to solve. To avoid this dilemma, a strategy is taken in this study, in which the flow rate dynamics for non-Newtonian fluids is assumed to have the same form as Equation 6.17, and the influence of the nonlinear flow behaviour is only on the steady-state flow rate, Q_u, not the time constant. By this way, the dynamics of the flow rate for non-Newtonian fluids can also be established, in which Q_u is determined using Equation 3.14 or Equation 3.15 of Chapter 3.

6.4 Experimental Verification

As mentioned previously, one of the most important issues in time-pressure dispensing is the variability in the amount of fluid dispensed under the same pressure pulse. In this section, the model developed in the previous sections is applied to predict this variation, and the results are compared with the experimental ones to illustrate the effectiveness of the model.

6.4.1 Experimental Settings

The time-pressure dispensing system for the experimental verification is shown in Figure 6.7. It consists of the air supply controller of Σ-MX 9000 SMII provided by Musashi Engineering, Inc. [Musashi], a transmission line (internal diameter: 4 mm; length: 3270 mm), a syringe (volume: 60 cc) and a needle (internal diameter: 1.35 mm; length: 18 mm). An orifice (area: 1.2 mm^2) is located between the transmission line and the syringe. To monitor the pressure in the system, two pressure transducers with a response time of 1 ms were connected to both ends of the transmission line, and their outputs are fed to an oscilloscope for data acquisition. In addition, the ambient temperature was maintained at 25 ± 1 °C.

6.4.2 Identification of the Air Controller Dynamics and Effective Area

The air controller consists of a pressure regulator and a solenoid valve, which, respectively, control the magnitude and width of a pressure pulse applied to the dispensing system. Unfortunately, the dynamics of the pressure regulator and the air

passage effective area of the solenoid valve are not provided by the supplier, and need to be identified experimentally.

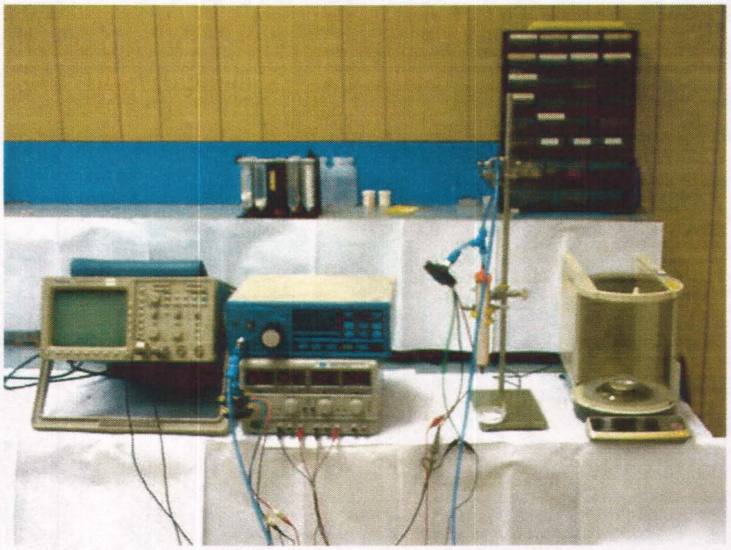

(a)

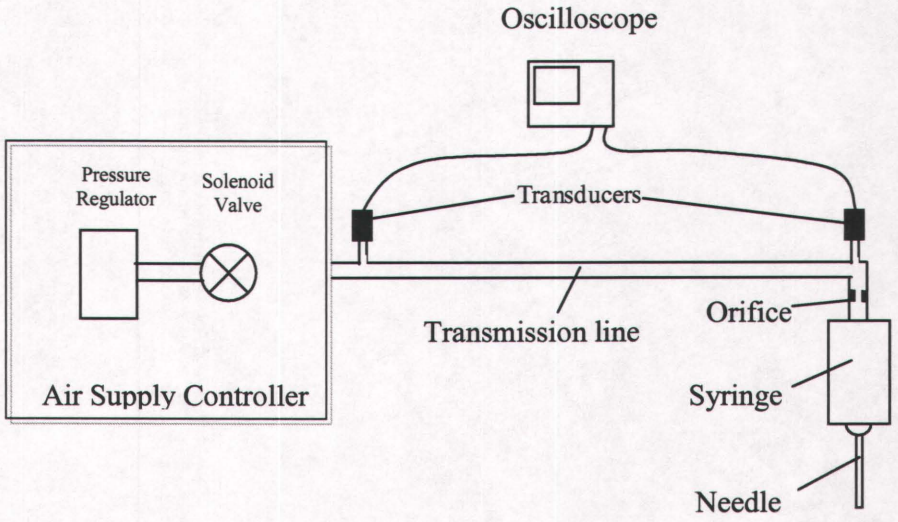

(b)

Figure 6.7 Equipment arrangement for dynamic model verification;

(a) overview and (b) schematic

For the identification of the pressure regulator dynamics, the step response just at the outlet of the controller was measured with a pressure transducer while the transmission line was disconnected. Note that in this measurement the connection between the controller outlet and the transducer should be made as short as possible in order to reduce the influence of the extra air volume introduced due to the connection. Figure 6.8 shows the measured step response. Based on the measurement, the dynamics of the pressure regulator was identified as a first-order system with the transfer function given by

$$T.F. = \frac{1}{0.011s + 1} \tag{6.19}$$

The simulation results using this identified dynamics are also shown in Figure 6.8, along with the measurement results.

For the identification of the air passage effective area of the solenoid valve, the step responses in the transmission line were measured using two pressure transducers located at the both ends of the line, while the end to syringe was closed. The measured results are shown in Figure 6.9. Since the response of a solenoid valve is usually very fast (typically the response time is smaller than 2 ms [Pawlak and Nehl 1988]), by neglecting this response time, the solenoid valve can be considered as an on-off one, i.e. either completely opened or completely closed. Thus, based on the measured results, the effective area of the valve was identified by using Equations 6.3, 6.4, 6.7, and 6.19, which is given by

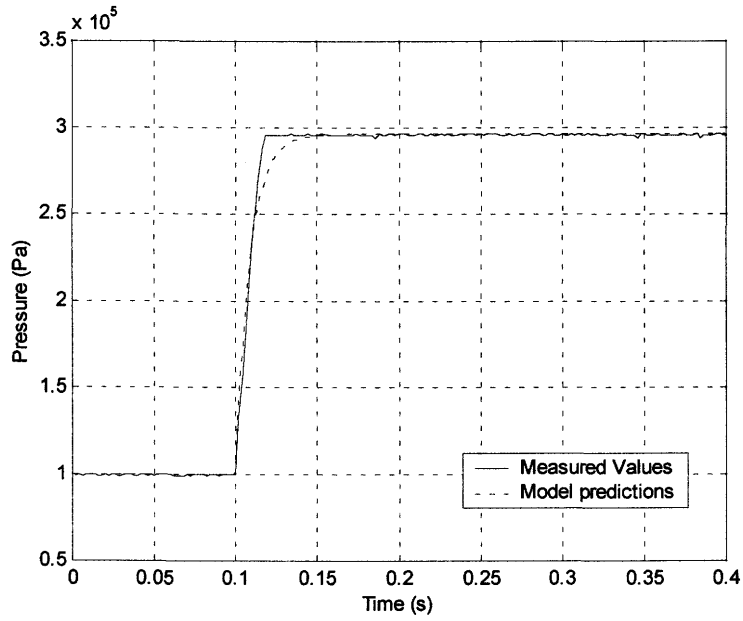

Figure 6.8 Step responses at the outlet of the air supply controller with the transmission line disconnected.

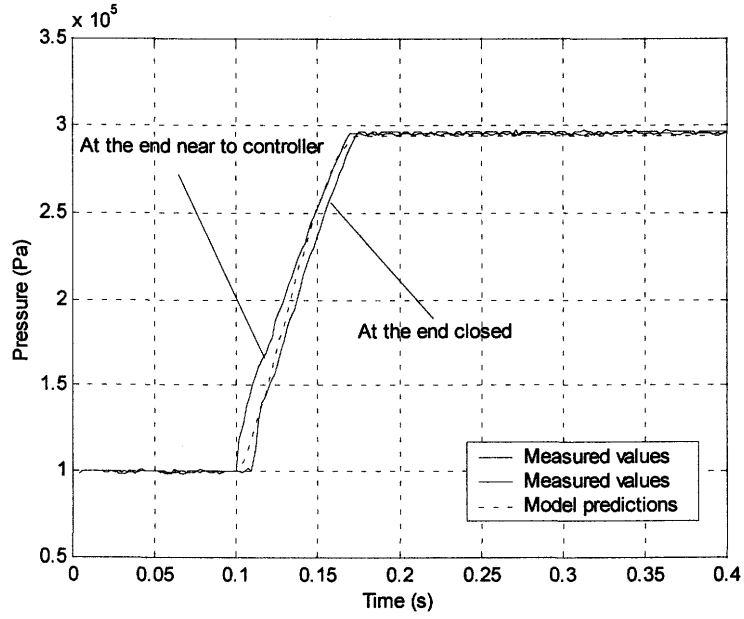

Figure 6.9 Step responses in the transmission line with the end to the syringe closed.

$$C_d A = 3.0 \text{ mm}^2 \tag{6.20}$$

The simulation results using this identified effective area are also shown in Figure 6.9, along with the measurement results.

6.4.3 Simulation and Experimental Results

Once the dynamics of the pressure regulator and the effective area of the valve have been identified, they can be used for simulating the amount of fluid dispensed under a pressure pulse. The flow chart of the prediction is shown in Figure 6.10, in which the amount of the fluid dispensed is obtained by integrating the output of *Flow Rate Model* developed in this chapter, while the variation of air volume in the syringe is determined by *Air Volume Calculation* based on the amount of the fluid dispensed, and then fed to *Flow Rate Model* for use.

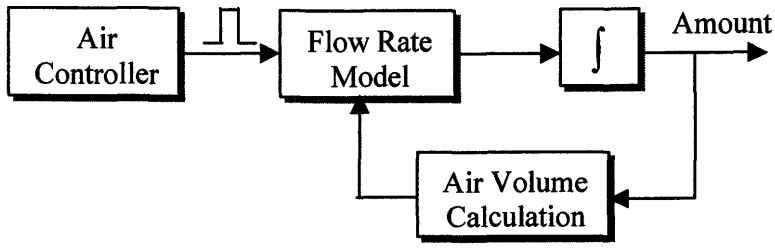

Figure 6.10 Flow chart of simulating the amount of fluid dispensed.

In the experiment, silicon oil was chosen for dispensing in order to reduce the error resulting from the time dependence associated with non-Newtonian fluids. The amount of the fluid dispensed under each pressure pulse was weighed using an

electronic balancer having a resolution of 0.01 mg. In practice, to reduce the random error, the total amount of the fluid dispensed in five pulses was weighed and averaged. This procedure was repeated at different amounts of fluid left in the syringe that also corresponds to different air volumes in the syringe. Measured amount of fluid dispensed are shown in Figures 6.11 and 6.12. In Figure 6.11, the pressure pulse with a magnitude of 3.97 bar and width of 70 ms is applied, while in Figure 6.12, the pressure pulse with a magnitude of 3.97 bar and width of 120 ms is applied.

The amount of fluid dispensed was simulated using Matlab, and the results are also shown in Figures 6.11 and 6.12. Both experimental and simulation results illustrate the amount of fluid dispensed under the same pressure pulse can change significantly due to different air volumes in the syringe. In Figure 6.11, the amount dispensed is directly proportional to the fluid amount left in the syringe or inversely proportional to the air volume in the syringe. While in Figure 6.12, the left part still illustrates the dependency of the fluid amount on the air volume in the syringe, but the right part shows the amount of fluid dispensed becoming insensitive to the air volume. The reason for this insensitivity is due to the fact that the rise time of the air pressure built in the syringe becomes shorter than the pressure pulse width due to relatively less air volume in the syringe. Meanwhile, it is also seen that the simulation results are in close agreement with the measured ones, indicating that the model developed in this paper is very promising for representing the flow rate in time-pressure dispensing processes.

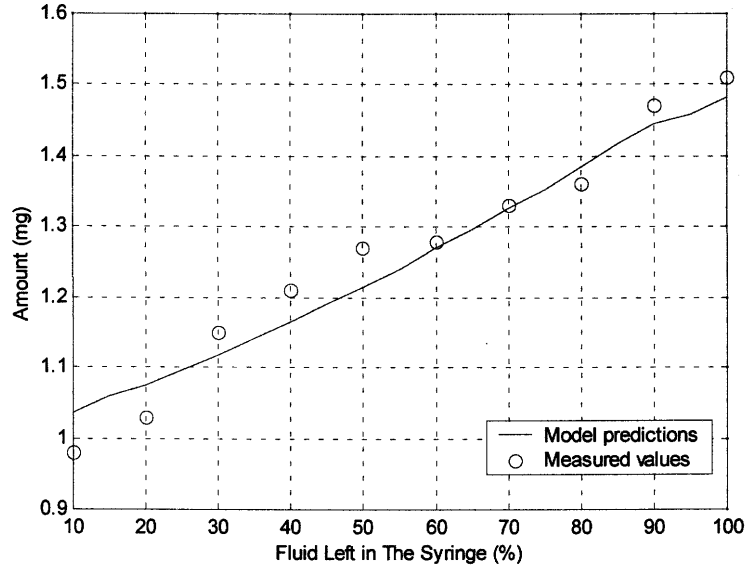

Figure 6.11 Comparison of the measured and predicted amounts of the fluid dispensed under a pulse pressure width of 70 ms.

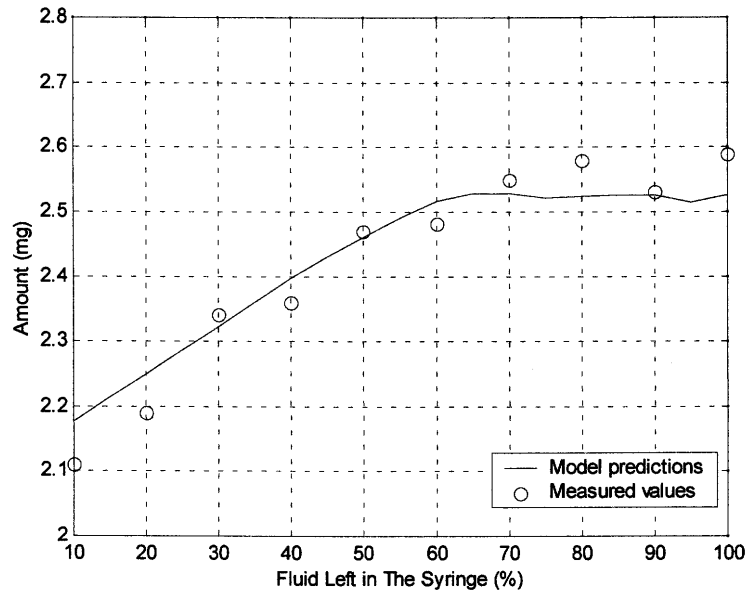

Figure 6.12 Comparison of the measured and predicted amounts of the fluid dispensed under a pulse pressure width of 120 ms.

6.5 Summary and Discussions

In time-pressure dispensing, the flow rate dynamics is a critical factor in controlling the amount of fluid dispensed, especially when a very small amount of fluid needs to be dispensed. This chapter presents the development of a model to represent the flow rate dynamics, taking into account both air compressibility and fluid inertia.

The dynamics of the pneumatic solenoid valve, the transmission line, and the air in the syringe are addressed individually, and then integrated to represent the transient response of the pressure in the syringe. By combining this transient response with the influence of fluid inertia, a model representing the flow rate dynamics in the time-pressure dispensing process is developed. Based on the model developed, experimental and simulation studies are carried out, with the objective of investigating the variability in the amount of fluid dispensed due to different air volumes in the syringe, which is the most serious problem occurring in time-pressure dispensing. Both results are in close agreement with each other, indicating the effectiveness of the model developed.

As shown, the compressibility of the air in the syringe can have a significant influence on the amount of fluid dispensed. Small-size syringes are recommended to use in practice for alleviating the inconsistency in the amount dispensed due to this influence, because small-size syringes have a relatively small difference in air volume as the fluid is dispensed. It, however, should be noted that small-size syringes can reduce the productivity due to the frequent need to re-fill the syringes.

A trade-off between the performance and the productivity has to be considered in this situation. One effective method to solve this problem is to compensate for the influence of the variation in air volume by modifying the magnitude or the width of the pressure pulse based on the models developed. This will be addressed further in the next chapter.

7. OFF-LINE CONTROL OF FLUID DISPENSING PROCESSES

7.1 Introduction

As mentioned previously, there are two basic types of fluid dispensing for electronics packaging, i.e., dispensing of lines and dispensing of dots. A fundamental requirement to control the fluid dispensing processes in electronics packaging is to maintain consistency in process performance. In the case of line dispensing, the main concern is the flow rate of fluid dispensed, while in the case of dot dispensing, the main concern is the amount of fluid dispensed. However, this consistency in practice is always broken by some unavoidable change in the dispensing process. As shown in Chapter 5, time dependency of fluid behaviour could cause a significant change in the flow rate. Also, in Chapter 6, it was shown that increasing the air volume in the syringe during the dispensing process could result in very different amounts dispensed. This variation in flow rate and/or amount of fluid dispensed under the same dispensing conditions causes the difficulty in the control of fluid dispensing in industry. Although many efforts have been made, as reviewed and discussed in Chapter 1, the results are not as good as expected.

Also, it was indicated previously that one distinct characteristic of the variation in flow rate and/or amount of fluid dispensed is that the variation is slow with

respect to time. This implies that timing is not an important factor in the design of a controller. As a result, on-line feedback control in this particular problem may be unnecessary.

In this chapter, an off-line control strategy is proposed based on a periodic but continual mode updating. The strategy is then applied for controlling the processes of both dispensing lines and dispensing dots to improve the consistency in the process performance.

7.2 Proposed Off-Line Control Strategy

From a control point of view, the fluid dispensing process is nonlinear and time-variable. The proposed control strategy is to deal with the off-line control of such a process. The basic idea of the strategy is that the model of the process is updated continuously, at least, periodically to maintain the accuracy of the model predictions. The control action is then determined based on the updated model to achieve the desired performance. In this strategy, methods used for model updating may be different, depending on the processes or systems considered. For the dispensing process, this will be discussed in the following section. This section focuses on the determination of the control action.

Let the updated model be generally expressed in terms of the manipulating parameter vector, P, as

$$Y = f(P) \tag{7.1}$$

where Y is the process performance. The sensitivity of Y to P can be obtained by

$$S = \frac{dY}{dP} = \frac{df(P)}{dP} \tag{7.2}$$

It is noted that, depending the complexity of the model developed, an analytical form of Equation 7.1 sometimes may not be obtained. In such case, a numerical finite difference approximation has to be used to determine S by perturbing P.

Let the desired performance and the actual performance be denoted by Y_d and Y_a, respectively. Then the error between them is

$$e = Y_d - Y_a \tag{7-3}$$

To eliminate this error, the manipulated parameter vector, P, can be updated according to the sensitivity, S, i.e.,

$$P(1) = P(0) + \frac{e}{S(0)} \tag{7.4}$$

where $P(1)$ is the updated value of P, and $P(0)$ is the value of P before this updating, under which the actual performance of Y_a was observed, and $S(0)$ is the sensitivity at the working point of $P = P(0)$.

Note that $P(1)$ in the above equation is established based on a linear relationship between the manipulated parameter and the process performance which is not always true. Consequently, a residual error that is the difference between the desired performance and the performance predicted from the model using $P(1)$ still exists, and it is given by

$$e(1) = Y_d - f(P(1)) \tag{7-5}$$

To eliminate this residual error, a second updating of P can be established as

$$P(2) = P(1) + \frac{e(1)}{S(1)} \tag{7-6}$$

in which $S(1)$ is the updated sensitivity using $P = P(1)$. Similarly, the residual error after the second updating is

$$e(2) = Y_d - f(P(2)) \tag{7.7}$$

In the same way, it is possible to establish a third updating of P to eliminate the above residual error. Thus, a recursive algorithm can be developed and used to iteratively update P until the residual error is smaller than an accepted or predefined value. Figure 7.1 is the flowchart of this recursive algorithm, in which Δ denotes the predefined value. Once the condition of $e \leq \Delta$ is satisfied, the finally updated value of P is outputted and used to control the process. This algorithm can also be expressed mathematically as follows.

$$\begin{cases} e(0) = Y_d - Y_a \\ P(n) = P(n-1) + \dfrac{e(n-1)}{S(n-1)} = P(0) + \sum_{i=1}^{n} \left(\dfrac{e(i-1)}{S(i-1)} \right) \\ e(n) = Y_d - f(P(n)) \end{cases} \qquad \text{n} = 1, 2, 3, \cdots \qquad (7\text{-}8)$$

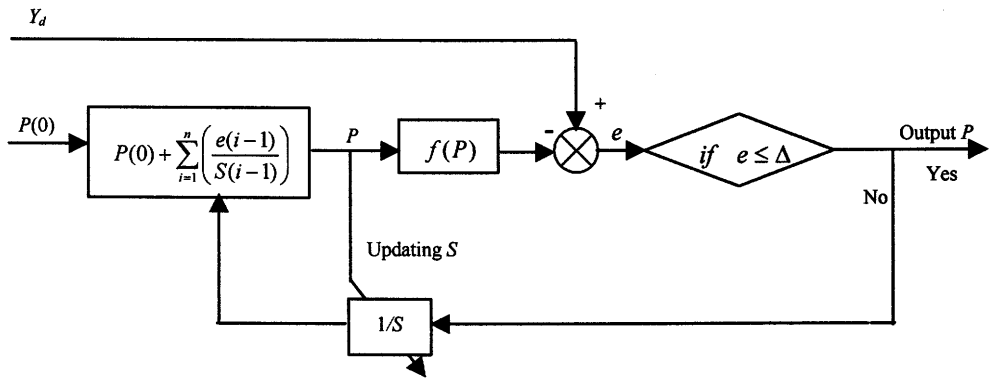

Figure 7.1 Recursive algorithm used to determine the control action.

7.3 Off-Line Control of Fluid Dispensing Processes

In this section, the off-line control strategy proposed in the preceding section is applied into the processes of dispensing lines and dispensing dots to improve the consistency of the process performance.

7.3.1 Dispensing Lines

For dispensing lines, the variation of the flow rate of fluid dispensed mainly results from the influence of time-dependent fluid behavior. As shown in Chapter 5, the influence could be identified using the model updating method. By combining

the updating method with the off-line control strategy, the control for dispensing lines is shown schematically in Figure 7.2. The actual flow rate is measured off-line periodically and fed back to update the model for identifying the influence of the time-dependent fluid behavior. Based on the updated model, a compensator uses the recursive algorithm given in Figure 7.1 to determine the manipulated parameters in order to achieve the desired flow rate.

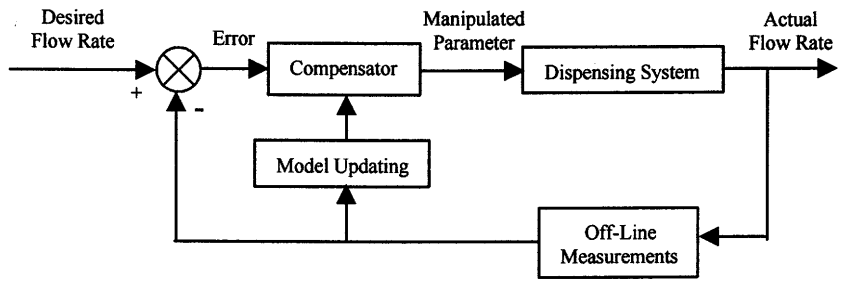

Figure 7.2 Schematic of the off-line control for dispensing lines.

In the control of dispensing lines, it should be noted that the manipulated parameter vector, P, can be either a parameter or a combination of several parameters, which can sensitively affect the flow rate, such as the pressure of the air supply, the needle temperature, etc. Determining the manipulated parameter for the realization of the control in practice is important, in which several factors, such as the cost of the realization, the resolution of the regulation of the manipulated parameters, and so on, have to be considered simultaneously. In this study, the air pressure is chosen because of its highest resolution among those manipulated parameters in the dispensing system employed in this study.

In addition, one important aspect of this control is the time interval between two measurements for model updating. Generally, the interval depends on the rate of the fluid behaviour change with time, i.e., the higher rate needs the shorter time interval and vice versa. Also, it should be noted that the change rate of the behaviour with time may be different for the same fluid, as indicated in Chapter 2 that relatively fast is in the starting of shear in comparison with a certain time period later. So in the starting period, the time interval should be set relatively small.

7.3.2 Dispensing Dots

When dispensing dots, the variation in the amounts of fluid dispensed is mainly considered as resulting from the different air volumes in the syringe. In Chapter 6, it has been shown that the variation in the dot amounts could be accurately predicted using the dynamic model developed in this study. By combining the dynamic model with the off-line control strategy proposed in the preceding section, the control for dispensing dots is schematically shown in Figure 7.2. The "actual" dot amount for feedback is predicted from the dynamic model that is updated either continuously or periodically using the air volume in the syringe. The predicted dot amount is compared with the desired one, and the error between them is fed to a compensator. The compensator uses the recursive algorithm given in Figure 7.1 to determine the air pressure pulse for achieving the desired dot amount.

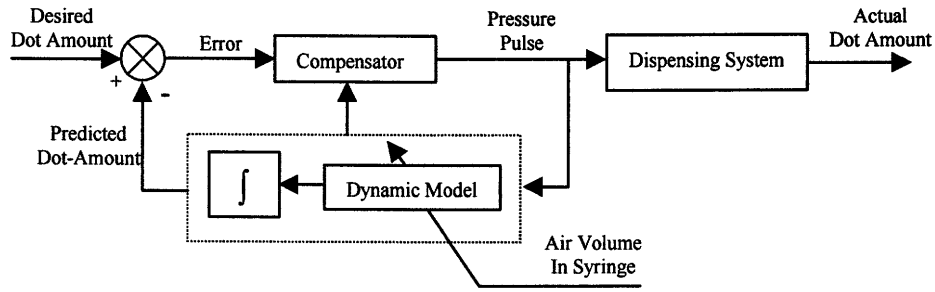

Figure 7.3 Schematic of the off-line control for dispensing dots.

In the control of dispensing dots, both the magnitude and width of the pressure pulse can be regulated to achieve the desired dot amount. But, in industry the regulation of magnitude is preferable because changing the pulse width can affect the productivity of the dispensing process. In following experiments, the regulation of magnitude is used.

7.4 Experimental Verification

Experiments have been designed and conducted to verify the effectiveness of the off-line control strategy in the fluid dispensing processes. The verification for dispensing lines is firstly presented, and then followed by the verification for dispensing dots.

7.4.1 Verification for Dispensing Lines

In the experiment, fluid FP® 4451 was again chosen for dispensing, and the dispensing system, which is shown in Figure 3.4 with a detailed system description given in Chapter 3, was used to dispense lines on PCBs. Two sets of dispensing conditions, called *Set A* and *Set B*, are designed and given in Table 7.1. Under these conditions, the flow rates of fluid dispensed are determined as 13.54 mg/sec for *Set A* and 27.17 mg/sec for *Set B*, respectively, using the model developed in Chapter 3. These flow rates are, respectively, set as the desired flow rates for the two sets of dispensing conditions. The objective of this experiment is to compensate for the influence of time-dependent fluid behaviour on the flow rate by using the off-line control strategy, thereby improving the flow rate consistency.

Table 7.1 Conditions for dispensing lines.

	Set A	*Set B*
Parameters	**Values**	
Air pressure	2.45×10^5 Pa	2.55×10^5 Pa
Needle temperature	45 °C	55 °C
PCB temperature	100 °C	
Dispenser movement velocity	3 mm/sec.	
Distance between needle and PCB	1.5 mm	
Length of needle	18 mm	
Internal diameter of needle	0.92 mm	

The experimental procedure consists of the following steps:

(1) Dispense a line on a board for a time period of 100 seconds, under *Set A* dispensing conditions.

(2) Weigh the amount of fluid dispensed, and then calculate the average flow rate during this period, i.e., flow rate = weight / 100 seconds.

(3) Determine the air pressure using the recursive algorithm shown in Fig. 7.1, based on the above measured flow rate.

(4) Update the conditions using the air pressure from Step (3), and dispense a line again for the same time period.

(5) Repeat Step (2) to determine the average flow rate. (Note this is the flow rate with the off-line control).

(6) Repeat the above steps over a working day (8 hours) randomly.

(7) Change the dispensing conditions to *Set B*, and repeat the experiment.

Air pressures and measured flow rates with and without the off-line control are shown in Table 7.2 for *Set A* dispensing conditions and Table 7.3 for *Set B* dispensing conditions. It is seen that the flow rates without the off-line control (or uncontrolled) are randomly distributed. This is because they were measured randomly over a working day and an uncertain change of fluid behaviour occurred during the time period between two measurements, as explained in Chapter 5. Depending on the measured flow rates, the updated air pressures are quite different at the measurement points.

Very importantly, it is seen from Tables 7.2 and 7.3 that a significant improvement of the consistency in flow rate has been achieved for both sets of dispensing conditions by introducing the off-line control. To measure the degree of the improvement, the standard deviation is used, which is given in the following

Table 7.2 Air pressures and measured flow rates

with and without the off-line control under *Set A* dispensing conditions

Sample No.	Desired flow rate (mg/sec)	Uncontrolled		Off-line control	
		Air pressure ($\times 10^5$ Pa)	Measured flow rate (mg/sec)	Air pressure ($\times 10^5$ Pa)	Measured flow rate (mg/sec)
1	13.54	2.45	12.09	2.67	13.41
2			12.87	2.57	13.19
3			10.92	2.85	13.63
4			11.26	2.80	12.96
5			10.48	2.93	13.31
6			11.25	2.80	13.33
7			12.16	2.67	13.94
8			11.47	2.77	13.53
9			11.77	2.73	13.35
10			10.95	2.85	13.25

Table 7.3 Air pressures and measured flow rates

with and without the off-line control under *Set B* dispensing conditions

Sample No.	Desired flow rate (mg/sec)	Uncontrolled		Off-line control	
		Air pressure ($\times 10^5$ Pa)	Measured flow rate (mg/sec)	Air pressure ($\times 10^5$ Pa)	Measured flow rate (mg/sec)
1	27.17	2.55	27.02	2.61	27.07
2			26.55	2.64	27.09
3			25.40	2.71	26.81
4			23.92	2.81	26.93
5			28.13	2.55	27.61
6			26.96	2.62	27.40
7			26.92	2.61	26.39
8			26.37	2.65	27.00
9			25.63	2.70	26.78
10			25.01	2.73	27.11

$$\bar{X} = \frac{1}{n}\sum_{i=1}^{n} X_i , \qquad S = \sqrt{\frac{\sum_{i=1}^{n}(X_i - \bar{X})^2}{n-1}} \tag{7-9}$$

where $\bar{X}$ is the mean of the sample X_i, S is the sample standard deviation, and n the sample number (n = 10 for this experiment). The calculated results for each set of data are given in Table 7.4 along with the desired flow rates. It can be seen that the sample means of the flow rate with the introduction of the off-line control is closely approaching the desired flow rates. The slight difference likely results from the experimental uncertainties, including the measurement noise, the limited resolution of the regulation of air pressure, etc. It is also observed that the sample deviations can be significantly reduced from 0.7094 to 0.2679 for *Set A* dispensing conditions, and from 1.2136 to 0.3349 for *Set B* dispensing conditions.

Table 7.4 Sample means and standard deviations of measured flow rates.

	A		B	
	Uncontrolled	Off-line control	Uncontrolled	Off-line control
Desired flow rate	13.54 mg/sec		27.17 mg/sec	
Sample mean	11.52 mg/sec	13.39 mg/sec	26.19 mg/sec	27.02
Sample standard deviation	0.7094	0.2659	1.2136	0.3349

7.4.2 Verification for Dispensing Dots

The experiment for this verification was carried out on the dispensing system shown in Figure 6.7. A detailed system description was given in Chapter 6. Dots were dispensed on PCBs with and without the presence of the off-line control.

In the experiment, two kinds of silicon oil were chosen in order to reduce the involvement of the time-dependent behavior of non-Newtonian fluids. The oil viscosities are 100,000 and 350 cSt, respectively. The experimental settings are listed in Table 7.5. Under each pressure pulse, a dot of fluid was dispensed on a PCB and its amount was then weighed using an electronic balance with a resolution of 0.01 mg. In practice, to reduce the random error, the amount of fluid dispensed in five pulses was weighed and then averaged. This procedure was repeated for different volumes of fluid in the syringe, which also corresponds to different air volumes in the syringe. The measured dot amounts are shown in Figure 7.4 (a) and (b) for dispensing the two types of silicon oils, respectively, which indicates a significant inconsistency in amount when fluid in syringe varies from full to empty.

Table 7.5 Experimental settings for dispensing dots.

	For dispensing oil with a Viscosity of 100,1000 cSt	For dispensing oil with a viscosity of 100,1000 cSt
Parameters	**Values**	
Magnitude of air pressure	2.45×10^5 Pa	
Width of air pressure	120 ms	
Syringe capacity	64 cc	
Length of needle	18 mm	
Internal diameter of needle	1.346 mm	0.508 mm

To improve the dot-amount consistency, the off-line control developed in this study was used to determine the magnitude of the compensated pressure pulse. Figure 7.5 shows these magnitudes as a function of the fluid volume in the syringe. It can be seen that the magnitude increases with decreasing in fluid volume (or increasing of air volume) in the syringe. In such a way, the influence of the air compressibility in the syringe can be compensated. It should be noted here that the compensated pressure pulses are applicable for dispensing both types of silicon oils because their determination is only based on the air volume in the syringe. Using the compensated air pressure pulses, dots of fluid were dispensed and weighed again at different fluid volumes in the syringes, similar to the procedure without the compensation. The measured dot amounts are also shown in Figure 7.4 along with the results without the off-line control.

Figure 7.4 illustrates a significant improvement of the dot-amount consistency with the introduction of the off-line control. To measure the improvement quantitatively, the sample mean and standard deviation are also calculated for each set of data using Equation 7.9, and the results are given in Table 7.6. It can be seen that the sample means of the dot amount with the introduction of the off-line control is closely approaching the desired dot amount for both types of oils. The slight difference likely results from the experimental uncertainties, including the measurement noise, the limited resolution of the regulation of air pressure, etc. It is also observed that the sample deviations can be significantly reduced, from 0.122 to 0.0154 for one dispensing case and from 0.1353 to 0.0243 for the other dispensing case.

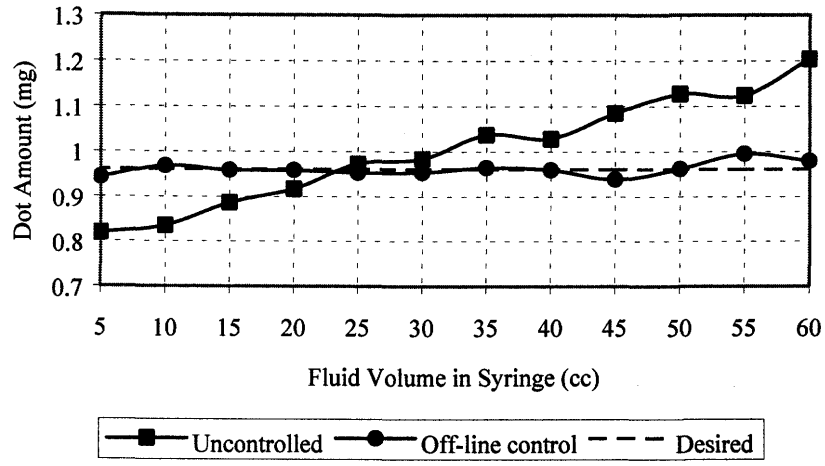

(a)

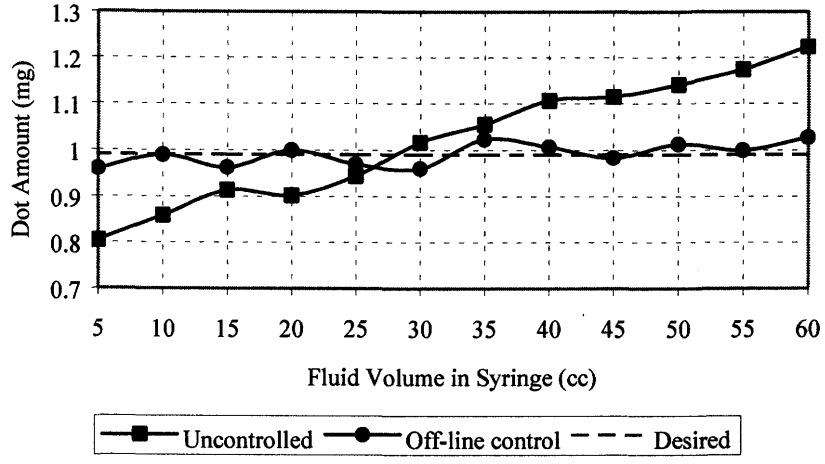

(b)

Figure 7.4 Measured dot amounts versus the fluid amounts in the syringe;
(a) dispensing the silicon oil with a viscosity of 100,000 cSt and
(b) dispensing the silicon oil with a viscosity of 350 cSt.

Table 7.6 Sample means and standard deviations of measured dot amounts.

	For dispensing oil with a viscosity of 100,1000 cSt		For dispensing oil with a viscosity of 100,1000 cSt	
	Uncontrolled	Off-line control	Uncontrolled	Off-line control
Desired dot amount	0.96 mg		0.99 mg	
Sample mean	1.001 mg	0.961 mg	1.021 mg	0.991 mg
Sample deviation	0.1220	0.0154	0.1353	0.0243

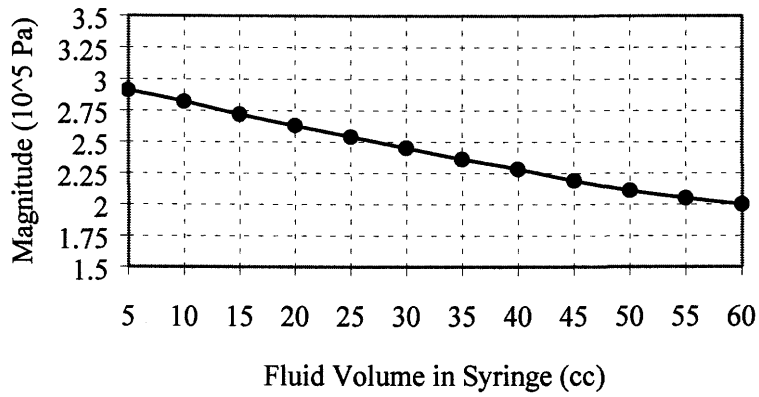

Figure 7.5 Magnitudes of compensated pressure pulses vs. fluid volume in syringe.

7.5 Summary

Fluid dispensing for electronic packaging applications consists of two types: one is to dispense lines in which the flow rate of fluid dispensed is of importance, and the other one is to dispense dots in which the dot amount is of importance. A fundamental requirement of controlling the dispensing processes is to maintain the consistency in the flow rate and amount.

To improve the consistency, an off-line control strategy is proposed. This strategy includes two major steps; one is to update the model, and the other one is to calculate the control actions based on the updated model. For the process of dispensing lines, the model is updated by using off-line measurements of the flow rate periodically; while for the process of dispensing dots, the model is updated either continuously or periodically by using the air volume in the syringe. For the calculation of the control actions, a recursive algorithm is developed, in which the manipulated parameter of the control system is calculated iteratively until the residual error between the desired performance and the "actual" performance predicted from the updated model is smaller than an predefined value, and then it is outputted to control the process.

To verify the effectiveness of the off-line control in the dispensing process, the experiments of dispensing lines and dots were conducted with and without the presence of the off-line control, respectively. The comparison of the measurements of the process performance (the flow rate for dispensing lines and the amount for dispensing dots) shows that a significant improvement of the consistency in the performance can be achieved with the off-line control.

8. CONCLUSIONS AND FUTURE WORK

8.1 Conclusions

Fluid dispensing is a very complex process. It is an interdisciplinary area involving electronics packaging, fluid mechanics, pneumatics, materials engineering, control systems, and manufacturing. The research presented in this thesis is aimed to carry out a comprehensive study on the modeling and control of the fluid dispensing process, with the objective of achieving a significant improvement of the process performance. The main contributions from this study are summarized.

1. For the characterization of the rheological behaviour of fluids for electronics packaging, some empirical models reported in the literature were examined. For the time-independent fluid behaviour, the Power Law equation and Generalized Power Law equations are effective to include the dependency of fluid behaviour on the shear rate and temperature. For the time-dependent fluid behaviour, the model using structural theory can be extended to represent the recovery of the fluid behaviour upon the removal of shear stress.

2. A new model that represents the steady-state flow rate of fluid dispensed was developed. Based on the model, the effects of factors such as the air-supply pressure, the fluid temperature, etc. on the flow rate can be well recognized.

3. The equilibrium conditions of the spreading of fluid on a board in the dispensing process were established. By applying these conditions, the general equation governing the spreading of fluid was solved. As a result, a model representative of the equilibrium shape of fluid formed on a board was developed, which had been validated experimentally.

4. To take into account the time-dependent influence in fluid dispensing, a method of applying model updating technique was developed. In this method, some parameters of the model for the dispensing process were updated based on periodic measurements of the process performance. With the updated parameters, the model is effective for tracking and representing the influence of the time-dependent fluid behaviour in fluid dispensing.

5. A model representative of the dynamics of the flow rate of fluid dispensed was developed taking into account both air compressibility and fluid inertia. Based on the model, the inconsistency of the amount of fluid dispensed due to the variation of the air volume in the syringe can be accurately predicted.

6. A control strategy was proposed to deal with the off-line control of nonlinear and time-variable processes. Based on the strategy, the off-line controls of the processes for dispensing lines and dispensing dots were developed to improve

the consistency in the process performance. Experimental results show that a significant improvement of the consistency in the process performance can be achieved with the off-line control.

8.2 Future Work

There are a number of issues that arise from the present study or from an extension of the study. The work to address each of them can contribute in some way to the understanding of the fluid dispensing process and thereby to the improvement of the process performance. Future studies on some of these issues are presented in this section.

1. Representing the amounts of fluid dispensed while taking into account air compressibility and time-dependent fluid behaviour simultaneously.

The influence of air compressibility on the amounts of fluid dispensed has been studied in Chapter 6. However, it should be noted that this study did not consider the influence of time-dependent fluid behaviour on those amounts, though this influence on the steady-state flow rate of fluid dispensed has been addressed in Chapter 5. Therefore, it would be interesting to examine how a simultaneous consideration of both air compressibility and time-dependent fluid behaviour could affect the amount of fluid dispensed.

2. Extending the present study to the rotary screw dispensing process.

The present study was carried out with the focus on the time-pressure dispensing process. Some issues addressed in this study can also apply to the rotary screw dispensing process. Therefore, the methods developed here could be extended to the rotary screw dispensing. One of the examples is the influence of time-dependent fluid behaviour on the process performance. To deal with this issue in the rotary screw dispensing, the method of applying model updating technique, presented in Chapter 5, could also be used straightforwardly. For this purpose, a model representative of the rotary screw dispensing process is required. Once the influence of time-dependent fluid behaviour is identified, the off-line control strategy, presented in Chapter 7, could be employed to improve the consistency in the performance of the rotary screw dispensing process.

3. Extending the present study to the positive displacement dispensing process.

The effects of both air compressibility and fluid inertia on the dynamics of the flow rate of fluid dispensed have been addressed in the present study. In the positive displacement dispensing, the piston movement is utilized to drive fluid out of the needle; therefore the effect of air compressibility is ruled out. However, fluid inertia is still an important factor to affect the flow rate dynamics. Meanwhile, new issues could arise in this situation, for examples, fluid compressibility. As the positive displacement method is considered as the most promising one for fluid dispensing in industry, modeling and control of the positive displacement dispensing process is of great significance.

REFERENCES

[1] Adamson, A.W. and Gast, A.P., 1997, *Physical Chemistry of Surfaces*, John Wiley & Sons, Inc.

[2] Andersen, B.W., 1967, *The Analysis and Design of Pneumatic Systems*, John Wiley & Sons.

[3] ASM Assembly Autotomaiton Ltd., 2000, *DS500 Precision Dispensing System Operation Manual.*

[4] Babiarz, A. J., 1997, "Die Encapsulation and Flip Chip Underfilling Processes for Area Array Packaging of Advanced Integrated Circuits," *Asymtek Technical Report.*

[5] Babiarz, A. J. and Huysmans, F., 1997, "Reliability and Process Control in a Variety of Dispensing Applications," *Asymtek Technical Report.*

[6] Barnes, H.A., Hutton, J.F., and Walters, K., 1989, *An Introduction to Rheology*, Elsevier Science Publishers B.V., pp. 1-37.

[7] Baron, C.N., *at al.*, 2000, *Method of Compensating for Non-Linear Characteristics in Dispensing a Coating Material*, United States Patent, no. 6139903.

[8] Ben-Hai, Y. and Natke, H.G., 1992, "Diagnosis of Changes in Elastic Boundary Conditions in Beams by Adaptive Vibrational Testing," *Archive of Applied Mechanics*, vol. 62, pp.210-221.

[9] Benezech, T, and Maingonnat, J.F., 1994, "Characterization of the Rheological Properties of Yougurt - A Review," *Journal of Food Engineering*, vol. 21, pp. 447-472.

[10] Bogue, D.C., 1959, "Entrance Effects and Prediction of Turbulence in Non-Newtonian Flow," *Ind. Eng. Chem.*, vol.51, p874.

[11] Bouras, C.E., *at al.*, 1999, *Flip Chip Underfill System and Method*, United States Patent, no. 5906682.

[12] Box, G.W., 1998, *Volume Compensating Pressure Regulated Flow Control Dispensing System*, United States Patent, no. 5847285.

[13] Bradner, M., 1949, "Pneumatic Transmission Lines," *Instruments*, vol. 22, pp. 618-625.

[14] Bretmersky, C.A., *at al.*, 1999, *Method of Compensating for Changes in Flow Characteristics of a Dispensed Fluid*, United States Patent, no. 5995909.

[15] Brian, D., *et al.*, 1996, "Application Experience of a Robotic Cell for Automated Adhesive Dispensing," *Mathematics and Computers in Simulation* 41, pp. 419-427.

[16] Brookfiled Engineering Laboratories, INC. (USA), *Brookfiled Cone/Plate Viscometer and Rheocalc for Windows: Operating Instructions.*

[17] Brown, F.T., 1962, "The Transient Response of Fluid Lines," *Journal of Basic Engineering*, pp. 547-553.

[18] Brughmans, M., Leuridan, J. and Blauwkamp, K, 1993, "The Application of FEM-EMA Correlation and Validation Techniques on a Body-in-white," *11th International Modal Analysis Conference*, Kissimmee, Florida, pp. 646-654.

[19] Bush, R., 1997, "Matching Fluid Dispensers to Materials for Electronics Applications," *Electronic Packaging & Production*, vol. 37, pp. 56-62.

[20] Byers, J. P. and Reighard, M. A., 1998, "Non-Contact Adhesive Dispensing," *Circuits Assembly*, vol. 9, pp. 68-72.

[21] Carbin, J. W., Reilly, J. W., and Hoffman, R.H., 1998, "A Total Process Module Approach to Advanced Flip-Chip Underfill Dispensing & Cure," *Asymtek Technical Report.*

[22] Cavallaro, K. J., 1991, "Dispensing Adhesives for High Throughput SMT Assembly," *Electronic Packaging & Production*, vol. 31, pp. 141-142.

[23] Cavallaro, W.A., *at al.*, 1998, *Method and Apparatus for Measuring the Size of Drops of a Viscous Material Dispensed from a Dispensing System*, United States Patent, no. 5837892.

[24] Chan Man Fong, C. F., Turcotte, G., and De Kee, D., 1996, "Modelling Steady and Transient Rheological Properties," *Journal of Food Engineering*, vol. 27, pp. 63-70.

[25] Chandraker, R., West, A. A., and Willians, D. J., 1990a, "Knowledge-Based Control of Adhesive Dispensing for Surface Mount Device Assembly," *IEEE Transactions on Components, Hybrids, and Manufacturing Technology*, vol. 13, pp. 516-520.

[26] Chandraker, R., West, A. A., and Willians, D. J., 1990b "Intelligent Control of Adhesive Dispensing," *International Journal of Computer Integrated Manufacturing*, vol. 3, pp.24-34, 1990.

[27] Chen, X.B., Schoenau, G., and Zhang, W.J., 1999, "Issues on Dispensing in Surface Mount Technology (SMT)," *Proc. International Conference on Advanced Manufacturing Technology*, China.

[28] Chen, X.B., Schoenau, G., and Zhang, W.J., 2000, "Modelling of Time-Pressure Fluid Dispensing Process," *IEEE Trans. On Electronics Packaging Manufacturing*, vol. 23, no. 4, pp. 300-305.

[29] Chen, X.B., Schoenau, G., and Zhang, W.J., 2001, "Dynamic Modelling of the Flow Rate in Time-Pressure Fluid Dispensing Processes," *The PACIFIC RIM/international, Intersociety, Electronic Packaging Technical/Business Conference& Exhibition*, Hawaii, USA.

[30] Chen, X.B., Schoenau, G., and Zhang, W.J., 2002 "On the Flow Rate Dynamics in Time-Pressure Dispensing Processes," *ASME Journal of Dynamic Systems, Measurement, and Control* (in press).

[31] Cheng, D.C.-H. and Evans, F., 1965, "Phenomenological Characterization of the Rheological Behaviour of Inelastic Reversible Thixotropics and Antithixotropic Fluids," *Brit. J. of Appl. Phys.*, vol. 16, pp. 1599-1617.

[32] Chhabra R.P. and J.F. Richardson, 1999, *Non-Newtonian Flow in the Process Industries*, Butterworth-Heinemann.

[33] Davies, B. L., Harris, S., Razban, A., and Efstathiou, J., 1996, "Application Experience of a Robotic Cell for Automated Adhesive Dispensing," *Mathematics and Computers in Simulation*, vol. 41, pp. 419-427.

[34] De Kee, D. and Turcotte, G., 1983, "Flow Properties of Time-Dependent Foodstuffs," *Journal of Rheology*, vol. 27(6), pp. 581-604.

[35] De Kee, D. and Chan Man Fong, C. F., 1993, "Letter to the Editor: A True Yield Stress?," *Journal of Rheology*, vol. 37 (4), pp. 775-776.

[36] Dilthey, U., Brandenbury, A., and Moller, M., 1998, "Optimization of the Adhesive Application by a New Control Concept for Speed-Controller Nozzles," *Welding & Cutting*, vol. 50, pp. 105-107.

[37] Dixon, D., Kazalski, J., Murch, F., and Marongelli, S., 1997, "Practical Issues Concerning Dispensing Pump Technologies," *Circuits Assembly*, August, pp. 36-40.

[38] Dussan V., E.B., 1979, "On the Spreading of Liquids on Sold Surfaces: Static and Dynamic Contact lines," *Ann. Rev. Fluid Mech.* No. 11, pp.371-400.

[39] Ehrhanrd, P. and Davis, S.H., 1991, "Non-Isothermal Spreading of Liquid Drops on Horizontal Plates," *Journal of Fluid Mechanics*, vol. 229, pp. 365-388.

[40] Foster, C.D. and Mottershead, J.E., 1990, "A Method for Improving Finite Element Models by Using Experimental Data: Application and Implications for Vibration Monitoring," *International Journal of Mechanical Science*, 32(3), 191-203.

[41] Foust, A.S., *et al.*, 1960, *Principles of Unit Operations*, John Wiley & Sons, New York,p.542.

[42] Franke, M.E., Malanowski, A.J., and Martin, P.S., 1972, "Effects of Temperature, End-Conditions, Flow, and Branching on the Frequency Response of Pneumatic Lines," *Journal of Dynamic System, Measurement, and Control*, March, 1972, pp. 15-20.

[43] Friswell, M.I. and Penny, J.E.T., 1992, "The Effect of Close or Repeated Eigenvalues on the Updating of Model Parameters from FRF Data," *Journal of Vibration and Acoustics*, 114(4), 514-520.

[44] Friswell, M.I. and Mottershead, J. E. 1995, *Finite Element Model Updating in Structural Dynamics*, Kluwer Academic Publishers.

[45] Fritzen, C.-P and Zhu, S. 1991, "Updating of Finite Element Models by Means of Measured Information," *Computers and Structures*, 40(2), 475-486.

[46] Gilleo, K., 1996, "Adhesives/Epoxies & Dispensing," *Surface Mount Technology (SMT)*, pp. 56-60.

[47] Golub, G., and Kahan, W., 1965, "Calculating the Singular Values and Pseudoinverse of a Matrix," *SIAM J. Numerical Analysis*, Ser. B., Vol. 2, No.2, pp. 205-224.

[48] Goodin, J.W., *at al.*, 2001, *Fluid Dispenser*, United States Patent, no. 6209751.

[49] Greenspan, H.P. 1978, "On the Motion of a Small Viscous Droplet that Wets a Surface," *Journal of Fluid Mechanics*, vol. 84, pp. 125-143.

[50] Haggland, T., 1992, "A Predictive PI Controller for Processes with Long Dead Times," *IEEE Control Systems Magazine*, February, pp. 57-60.

[51] Haley, P.J. and Miksis, M.J., 1991, "The Effect of the Contact Line on Droplet Spreading," *Journal of Fluid Mechanics*, vol. 223, pp. 57-81.

[52] Han, S. and Wang, K. K., 1997a, "Analysis of the Flow of Encapsulant During Underfill Encapsulation of Flip-Chips," *IEEE Trans. Components, Packaging, and Manufacturing Technology - Part B*, vol. 20, pp. 424-433.

[53] Han, S. and Wang, K. K., 1997b "Study on the Pressurized Underfill Encapsulation of Flip Chips," *IEEE Transactions on Components, Packaging, and Manufacturing Technology - Part B*, vol. 20, pp. 434-442.

[54] Kay, R.L., 2001, *System and Method for Dispensing Fluid Droplets of Known Volume and Generating Very Low Fluid Rates*, United States Patent, no. 6213354.

[55] Hocking, L.M. and Rivers, A.D., 1982, "The Spreading of a Drop by Capillary Action," *J. Fluid Mech.*, vol.121, pp.425-442.

[56] Holdsworth, S.D, 1993, "Rheological Models Used for the Prediction of the Flow Properties of Food Products: a Leterature Review," *Trans. Institution of Chemical Engineering*, Vol. 71(C3), pp. 139-179.

[57] Hougen, J.O., Martin, O.R., and Walsh, R.A., 1963, "Dynamics of Pneumatic Transmission Lines," *Control Engineering*, vol. 10, pp. 114-117.

[58] Iberall, A.S., 1951, "Attenuation of Oscillatory Pressures in Instrument Lines," *Journal of Research*, National Bureau of Standards, vol. 45, Research Paper 2115.

[59] Irvine, T.F. and Capobianchi, M., 1998, New-Newtonian Flows, *CRC Handbook of Mechanical*, Editor-in-Chief: Krieith F., CRC Press, Florida, pp. 114-127, 1998.

[60] Kolcun, J.F., *at al.*, 1997, *Dispenser and Method for Dispensing Viscous Fluids*, United States Patent, no. 5699934.

[61] Krieger, M. and Behler, S., 1998, "Stability Aspects of Volumetric Epoxy Dispense," *Test & Assembly Seminarin*, Singapore.

[62] Laplace, P.S., 1806, *Mechanique Celeste*, Supplement to Book 10.

[63] Lewis, A., *et al.*, 1998, "Best Practices in Automated Underfill Dispensing," *Asymtek Technical Report*.

[64] Li, Y. and Hsieh, F., 1996, "Modeling of Flow in a Single Screw Extruder," *Journal of Food Engineering*, 27, pp 353-375.

[65] Martinez-Padilla, L. P. and Hardy, J., 1989, "Quantifying Thixotropy of Bechamel Sauce Under Constant Shear Stress by Phenomenological and Empirical Models, " *Journal of Texture Studies*, vol. 20, pp. 71-85.

[66] McCloy, D., and Martin, H. R., 1980, *Control of Fluid Power: Analysis and Design*, 2nd Edition, John Wiley & Sons.

[67] Messom, C. H., Hinde, C. J., West, A. A., and Williams, D. J., 1992, "Designing Neural Networks for Manufacturing Process Control Systems," *The 7th IEEE Intelligent Control Symposium*, Glasgow, pp. 423-429.

[68] Mottershead, J.E. and Friswell, M.I., 1993, "Model Updating in Structural Dynamics: A Survery," *Journal of Sound and Vibration*, 167(2), pp 347-375.

[69] Murch, F., Dixon, D., and Davis, M., 1997, "Issues for the Practical Production Use of Dispensing Technologies," *NEPCON WEST'97*, pp. 245-256.

[70] Musashi Engineering, Inc., *Σ-MX 9000 SMII /8000 SMII Instruction Manual*.

[71] Ness, C. Q. and Lewis, A.R., 1997, "Best Practices in Surface Mount Adhesive Dispensing," *Asymtek Technical Report.*

[72] Ness, C. Q. and Lewis, A.R., 1998, "Adhesives/Epoxies & Dispensing," *Surface Mount Technology (SMT)*, May, pp. 114-122.

[73] Newman, S., 1968, "Kinetics of Wetting of Surfaces by Polymers; Capillary Flow," *Journal of Colloid Interface Science*, vol. 26, pp. 209-213.

[74] Nguyen, Q.D. and Boger, D.V., 1992, "Measuring the Flow Properties of Yield Stress Fluids," *Annu. Rev. Fluid Mech.*, vol. 24, pp. 47-88.

[75] Norris, M., 1996, "Dispensing Technology," *Surface Mount Technology (SMT)*, October, pp. 56-58.

[76] Pawlak, A.M., and Nehl, T.W, 1988, "Transient Finite Element Modelling of Solenoid Actuator: The Coupled Power Electronic, Mechanical, and Magnetic Field Problem," *IEEE Transaction of Magnetics*, vol. 24, no. 1. pp. 270-273.

[77] Petrellis, N.C and Flumerfelt, R.W, 1973, "Rheological Behaviour of Shear Degradable Oils: Kinetic and Equilibrium Properties," *Can. J. Chem. Eng.*, 51, 291.

[78] Prasad, R. P., 1989, *Surface Mount Technology Principle and Practice*, Van Nostrand Reinhold, New York. pp. 269-310.

[79] Quinones, H., Babiarz, A.J., and Adamson, S.J., 2000, "Flip Chip and Chip Scale Packaging Technologies: A Historical Perspective and Future Challenges," *SEMICON China 2000 Technical Symposium.*

[80] Razban, A. and Davies, B. L., 1991, "An Automated System for Dispensing Adhesives," *International Journal of Adhesion and Adhesives*, vol. 11, pp. 187-191.

[81] Razban, A., Bryant, G. F., and Davies, B. L., 1992, "Dynamic Modelling and Control Simulation of Automatically Dispensing Adhesive Beads," *Proceeding of the International Conference on Industrial Electronics, Control, Instrumentation and Automation*, San Diego, USA., pp. 891-895, 1992.

[82] Razban, A., 1993, "Intelligent Control of an Automated Adhesive Dispensing Cell," Ph.D Thesis, Imperial College, London, UK.

[83] Razban, A. and Davies, B.L., 1995, "Analytical Modelling of the Automated Dispensing of Adhesive Material," *Journal of Adhesion Science Technology*, vol. 9, pp. 1435-1450.

[84] Razban, A., Davies, B. L., Harris, S., and Efstathiou, J., 1995, "Control of an Automated Dispensing Cell with Vision Controlled Feedback," *Control Engineering Practice*, vol. 3, pp. 1217-1223, 1995.

[85] Reighard, M.A., *at al.*, 2001, *Viscous Material Dispensing System and Method with Feedback Control*, United States Patent, no. 6173864.

[86] Rohmann, C.P., and Grogan, E.C., 1957, "On the Dynamics of Pneumatic Transmission Lines," *Trans. ASME*, vol. 79, pp. 853-867.

[87] Schonhorn, H., Frisch, H.L., and Kwei, T.K., 1966, "Kinetics of Wetting of Surfaces by Polymer Melts," *Journal of Applies Physics*, vol.37, no.13, pp.4967-4973.

[88] Schuder, C.B., and Binder, R.C., 1959, "The Response of Pneumatic Transmission Lines to Step Inputs," *Journal of Basic Engineering*, pp.578-584.

[89] Skelland, A.H.P., 1967, *Non-Newtonian Flow and Heat Transfer*, John Wiley & Sons, New Youk, pp.1-14.

[90] Stokes, P., 1996, "Automated Dispensing in Surface Mount Assembly," Assembly Automation, Vol. 16, no. 4, pp. 30-33.

[91] Summ, B.D., 1997, *Chapter 14: Surface Tension, Handbook of Physical Quantities*, edited by Grigoriev, I.S. and Meilikhov, E.Z., CRC Press.

[92] Tiu, C. and Boger, D.V., 1974, "Complete Rheological Characterization of Time-Dependent Food Products," *Journal of Texture Studies*, vol. 5, pp. 329-338.

[93] Tummala, R.R, and Rymaszewski, E.J., 1989, *Microelectronics Packaging Handbook*, New York: Van Nostrand-Reinhold, pp. 604-621.

[94] Weltmann, R.N. and Keller, T.A., 1957, "N.A.C.A.", Tech. Mem..

[95] West, A. A., Williams, D. J., Hinde, C. J., and Messom, C. H., 1993, "A Benchmark of Intelligent Control Techniques for Surface Mount Technology (SMT) Adhesive Dispensing: Process Overview and the Application of a

Structured Neural Network Controller," *ASME Winter Meeting, Manufacturing Aspects of Electronic Packaging*, PED-vol. 65/EEP-vol.5, pp. 107-118, 1993.

[96] West, A. A., Williams, D. J., and Hinde, C. J., 1995, "Experience of the Application of Intelligent Control Paradigms to Real Manufacturing Processes," *Proc. Instn. Mech. Engrs.* vol. 209, pp. 293-308.

[97] Wun, K. B. and Margaritis, G., 1998, "The Evaluation of Fast-Flow, Fast-Cure Underfills for Flip Chip on Organic Substrate," *IEEE Transaction on Components, Packaging, and Manufacturing Technology*, Part A, Vol. 21, No. 1, pp. 13-17.

[98] Ye, N., Scavarda, S., Betemps, M., and Jutard, A., 1992, "Models of a Pneumatic PWM Solenoid Valve for Engineering Applications," *Journal of Dynamics Systems, Measurement, and Control*, vol. 114, pp. 680-688.

[99] Young, T. 1805, "An Essay on the Cohesion of Fluids," *Philos. Trans. R. Soc.* London 95:65-87.